

47397

**THE PRODUCTION, CHARACTERIZATION AND  
BURNUP OF URANIUM DIOXIDE-  
GADOLINIUM OXIDE FUEL AND BORON NITRIDE COATED  
URANIUM DIOXIDE-GADOLINIUM OXIDE FUEL**

**A THESIS SUBMITTED TO  
THE GRADUATE SCHOOL OF NATURAL AND APPLIED SCIENCES  
OF  
THE MIDDLE EAST TECHNICAL UNIVERSITY**

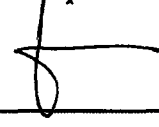
**BY**

**İBRAHİM TİSTİ**

**IN PARTIAL FULFILLMENT OF THE REQUIREMENTS FOR THE  
DEGREE OF  
DOCTOR OF PHILOSOPHY  
IN  
THE DEPARTMENT OF CHEMICAL ENGINEERING**

**JUNE 1995**

Approval of the Graduate School of Natural and Applied Sciences.



Prof. Dr. İsmail TOSUN

Director

I certify that this thesis satisfies all the requirements as a thesis for the degree of Doctor of Philosophy.



Prof. Dr. Canan ÖZGEN

Head of the Department

This is to certify that we have read this thesis and that in our opinion it is fully adequate, in scope and quality, as a thesis for the degree of Doctor of Philosophy.



Prof. Dr. GÜNGÖR GÜNDÜZ

Supervisor

Examining Committee Members

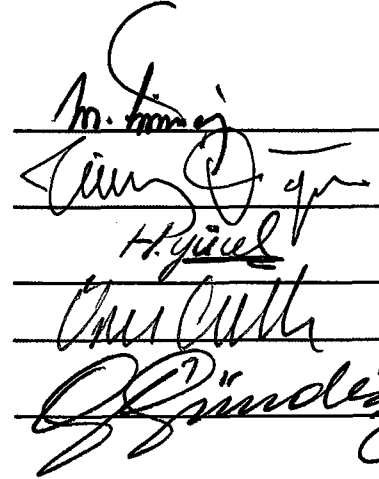
Prof. Dr. Muharrem TİMUÇİN

Prof. Dr. Timur DOĞU

Prof. Dr. Hayrettin YÜCEL

Prof. Dr. Üner ÇOLAK

Prof. Dr. GÜNGÖR GÜNDÜZ



## **ABSTRACT**

### **THE PRODUCTION, CHARACTERIZATION AND BURNUP OF URANIUM DIOXIDE- GADOLINIUM OXIDE FUEL AND BORON NITRIDE COATED URANIUM DIOXIDE-GADOLINIUM OXIDE FUEL**

**İbrahim USLU**

**Ph.D., Department of Chemical Engineering**

**Supervisor: Güngör GÜNDÜZ, Prof. Dr.**

**June 1995, 154 pages**

In this research work pure urania and urania-gadolinia (5 and 10%) fuels were first produced by sol-gel technique. The effects of some operational parameters such as grinding, use of binder, compaction pressure, and reduction temperature on the porosity of the sintered fuels were investigated. The sintered fuel pellets were then coated with boron nitride (BN). This is achieved through chemical vapor deposition (CVD) using boron trichloride and ammonia. The coated samples were sintered at 1600 K. The analyses under scanning electron microscope (SEM) showed a variety of BN structures, but mainly platelike and rodlike BN structures were observed. The burnup calculations by using WIMS-D/4 showed that BN

coated and gadolinia containing fuels had larger burnups than other fuels. The calculations were repeated at different pitch distances. The change of the radius of the fuel pellet or the moderator/fuel ratio did not introduce an improvement in the performance of fuel and all fuel gives the highest burnup at the present design values of a PWR .

Keywords: Uranium dioxide, gadolinium oxide, boron nitride, chemical vapor deposition, nuclear fuel, burnup



## ÖZ

### URANYUM DİOKSİT - GADOLONYUM OKSİT YAKITLARININ VE BOR NİTRÜR KAPLI URANYUM DİOKSİT - GADOLONYUM OKSİT YAKITLARININ ÜRETİMİ, FİZİKSEL ÖZELLİKLERİ VE NÜKLEER YANMA ÖZELLİKLERİ

İbrahim USLU

Doktora, Kimya Mühendisliği Bölümü

Tez yöneticisi: Güngör GÜNDÜZ, Prof. Dr.

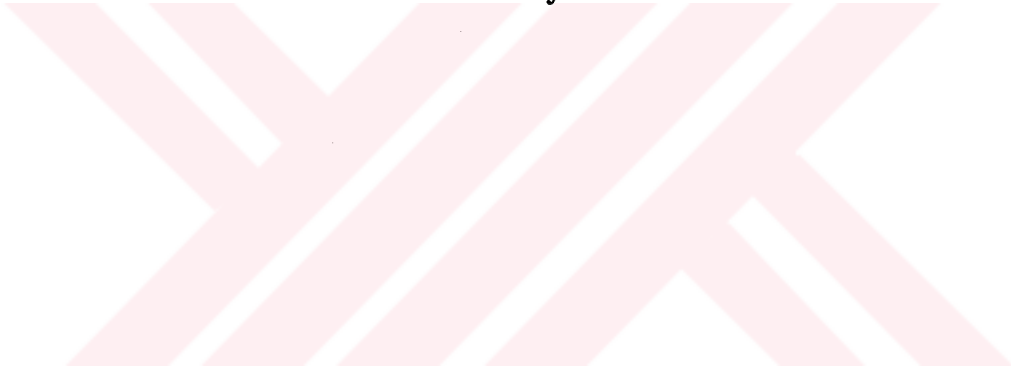
Haziran 1995, 154 sayfa

Bu araştırmada saf uranyum dioksit ile uranyum-gadolonyum (%5-10) yakıtları çöz-pel tekniğiyle üretilmiştir. Öğütme, bağlayıcı kullanımı, sıkıştırma basıncı ve indirgeme sıcaklığı gibi işletim değişkenlerinin sinterlenmiş yakıtın gözenekliliğine olan etkisi incelenmiştir. Yakıtlar sinterlendikten sonra bor nitrür (BN) ile kaplanmıştır. Kaplama, bor triklorür ve amonyak gazı kullanılarak gaz fazında kimyasal çökeltme yöntemiyle gerçekleştirilmiştir. Kaplanmış yakıtlar,

tekrar 1600 K de sinterlenmiştir. Taramalı elektron mikroskopla örnekler incelendiğinde tabaka ve çubuk şeklinde BN yapıları gözlenmiştir. WIMS-D/4 bilgisayar programı kullanılarak yapılan hesaplamalarda, BN kaplı ve gadolonyum içeren yakıtların, diğer yakıtlara oranla daha verimli yanma özelliği olduğu görülmüştür. Hesaplamalar değişik yakıt çubuğu aralıklarında tekrar edilmiştir. Yakıtın yarıçapı veya yavaşlatıcı/yakıt oranlarını değiştirerek yapılan hesaplamalar, yakıtların yanma verimlerinde bir artış göstermemiş ve bütün yakıtların basınçlı su reaktörlerin şimdiki tasarım değerlerinde en iyi yanma özelliklerine sahip olduğunu göstermiştir.

Anahtar kelimeler: Uranyum dioksit, gadolonyum oksit, bor nitrür, gaz fazında kimyasal çökeltme, nükleer yakıt, yanma

**To My Parents**



## ACKNOWLEDGMENT

This work was partly supported by the International Atomic Energy Agency (IAEA) by the contract IAEA:5977 RB2. We realize that this work could not be accomplished without this very valuable support, and we appreciate it.

I am deeply indebted to my supervisor Gngr Gndz, Prof. Dr. who helped me throughout my study with his advice, guidance and encouragement. I appreciate Prof.Dr. Hayrettin Ycel who helped in the evaluation of porosimeter data and Prof.Dr. Macit zenba who helped with SEM pictures.

I am also grateful to some of the staff and the technicians of the Chemical Engineering Department, the Food Engineering Department and the Metallurgical Engineering Department for their kind assistance.

I wish to express my thanks to Candan Tre, Dr. Ediz Tanker, Ouzhan Aliefendiolu, Nazım Bayraktar and all the other friends in the Nuclear Computing and Design Group in the Turkish Atomic Energy Authority for their kind help, during the preparation of this thesis.

Special thanks to Dr. Bayram Kopuz and all the other friends in the Nuclear Fuel Department of the ekmece Nuclear Research and Training Center for the sintering and processing the fuel pellets.



## TABLE OF CONTENTS

<b>ABSTRACT</b> .....	<b>ii</b>
<b>ÖZ</b> .....	<b>iv</b>
<b>ACKNOWLEDGMENTS</b> .....	<b>vii</b>
<b>TABLE OF CONTENTS</b> .....	<b>viii</b>
<b>LIST OF TABLES</b> .....	<b>xii</b>
<b>LIST OF FIGURES</b> .....	<b>xiii</b>
<b>CHAPTER</b> .....	
<b>1. INTRODUCTION</b> .....	<b>1</b>
<b>1.1 Nuclear Energy Situation in the World</b> .....	<b>1</b>
<b>1.2 Waste arising (coal energy vs. nuclear energy)</b> .....	<b>3</b>
<b>1.3 Economic Competitiveness of Nuclear Power Plants</b> .....	<b>4</b>
<b>1.4 Situation in Turkey</b> .....	<b>5</b>
<b>1.5 Scope of This Research Work</b> .....	<b>6</b>
<b>2. NUCLEAR REACTOR TECHNOLOGY</b> .....	<b>7</b>
<b>2.1 History of Nuclear Energy</b> .....	<b>7</b>
<b>2.2 Reactor System</b> .....	<b>8</b>
<b>2.3 Fundamental Principles</b> .....	<b>9</b>
<b>2.3.1 The Multiplication Factor</b> .....	<b>10</b>
<b>2.4 Thermal and Fast Reactors</b> .....	<b>11</b>
<b>2.5 Nuclear Fuels</b> .....	<b>12</b>
<b>2.6 Desired Properties of the Fuel Material</b> .....	<b>13</b>
<b>2.7 Fuel Utilization Economy</b> .....	<b>14</b>
<b>3. URANIUM DIOXIDE</b> .....	<b>16</b>
<b>3.1 Uranium Resources of Turkey</b> .....	<b>16</b>
<b>3.2 Conventional Preparation of Uranium Dioxide</b> .....	<b>17</b>
<b>3.3 Sol-Gel Method</b> .....	<b>18</b>
<b>3.3.1 Advantages of Sol-Gel Method</b> .....	<b>19</b>

<b>4. BURNABLE ABSORBERS .....</b>	<b>20</b>
<b>4.1 Importance .....</b>	<b>20</b>
<b>4.2 General Overview .....</b>	<b>22</b>
<b>4.2.1 Soluble Burnable Absorbers .....</b>	<b>22</b>
<b>4.2.2 Gaseous Burnable Absorbers .....</b>	<b>22</b>
<b>4.2.3 Discrete Burnable Absorber .....</b>	<b>23</b>
<b>4.2.4 Burnable Absorbers Used in Fuel .....</b>	<b>23</b>
<b>4.2.4.1 Burnable Absorbers Mixed with Fuel .....</b>	<b>24</b>
<b>4.2.4.2 Burnable Absorbers Coated with Fuel .....</b>	<b>25</b>
<b>5. BORON NITRIDE .....</b>	<b>27</b>
<b>5.1 Chemical Vapor Deposition of Boron Nitride .....</b>	<b>27</b>
<b>5.1.1 History .....</b>	<b>28</b>
<b>5.2 Properties of Boron Nitride .....</b>	<b>31</b>
<b>5.3 Chemical Reaction of BN Film Deposition .....</b>	<b>32</b>
<b>6. FISSION REACTION AND NEUTRON TRANSPORT .....</b>	<b>33</b>
<b>6.1 Comparison of Nuclear and Chemical Reactions .....</b>	<b>33</b>
<b>6.2 Equation of Continuity .....</b>	<b>37</b>
<b>6.2.1 Rate of Change in Number of Neutrons in V .....</b>	<b>38</b>
<b>6.2.2 Gain Mechanism .....</b>	<b>39</b>
<b>6.2.2.1 Neutron Sources in the Volume (e.g. fission) .....</b>	<b>39</b>
<b>6.2.2.2 Scattering of Neutrons from other Energies and                     Directions .....</b>	<b>40</b>
<b>6.2.3 Loss Mechanism .....</b>	<b>41</b>
<b>6.2.3.1 Neutrons in the Volume Suffering Collision .....</b>	<b>41</b>
<b>6.2.3.2 Leakage into or Diffusion from the Volume .....</b>	<b>41</b>
<b>6.2.4 Combination of all the Terms .....</b>	<b>42</b>
<b>6.3 One Group Model .....</b>	<b>44</b>
<b>6.4 Two Group Model .....</b>	<b>44</b>
<b>6.5 Multi Group Model .....</b>	<b>44</b>
<b>7. EXPERIMENTS .....</b>	<b>46</b>
<b>7.1 Objective .....</b>	<b>46</b>
<b>7.2 Experimental Methods .....</b>	<b>47</b>
<b>7.2.1 Sol-Gel Fuel Preparation .....</b>	<b>48</b>
<b>7.2.1.1. Sol Preparation .....</b>	<b>48</b>
<b>7.2.1.2 Dropping and Gelation .....</b>	<b>49</b>
<b>7.2.1.3. Washing, Aging and Drying .....</b>	<b>50</b>
<b>7.2.1.4 Calcination and Reduction .....</b>	<b>53</b>
<b>7.2.1.5 Pellet Production .....</b>	<b>54</b>
<b>7.2.1.6 Sintering .....</b>	<b>55</b>
<b>7.3 Boron Nitride Film Deposition and Sintering Experiments .....</b>	<b>56</b>
<b>8. FRACTAL ANALYSIS OF FUEL GRAINS .....</b>	<b>60</b>

<b>8.1 Models of Surfaces</b> .....	<b>60</b>
<b>8.1.1 Euclidean Geometry: Man Made Surfaces</b> .....	<b>60</b>
<b>8.1.2 Fractal Geometry</b> .....	<b>61</b>
<b>8.2 Principles of Fractal Geometry</b> .....	<b>61</b>
<b>8.3 Fractal Exponent</b> .....	<b>63</b>
<b>8.3.1. Structured Walk Method</b> .....	<b>63</b>
<b>8.4 Limited Self Similarity</b> .....	<b>65</b>
<b>9. PERFORMANCE CALCULATIONS OF THE FUEL USING WIMS-D/4</b> .....	<b>68</b>
<b>10.RESULTS AND DISCUSSIONS</b> .....	<b>72</b>
<b>10.1 Properties of Uranium Dioxide</b> .....	<b>72</b>
<b>10.1.1 Properties of yellow cake</b> .....	<b>73</b>
<b>10.1.2 Properties of calcined and reduced Powder</b> .....	<b>73</b>
<b>10.1.1.1 Color</b> .....	<b>73</b>
<b>10.1.2.2 Stoichiometry</b> .....	<b>73</b>
<b>10.1.2.3 BET Surface Area of the Powder</b> .....	<b>75</b>
<b>10.1.2.4 Powder Flowability</b> .....	<b>77</b>
<b>10.1.3 Green Pellet Density and Porosity</b> .....	<b>77</b>
<b>10.1.4 Properties of Sintered Pellet</b> .....	<b>79</b>
<b>10.1.4.1 Density</b> .....	<b>79</b>
<b>10.1.4.2 Microstructure of Sintered Pellets</b> .....	<b>80</b>
<b>10.1.4.3 Production of Vacancies in the Crystal Structure</b> .....	<b>83</b>
<b>10.1.4.4 Production of Oxygen Interstitials</b> .....	<b>84</b>
<b>10.1.4.5 Effect of Grinding on Density</b> .....	<b>85</b>
<b>10.1.4.6 Effect of Binder on Pore Size Distribution</b> .....	<b>86</b>
<b>10.1.4.7 Effect of Compaction Pressure on Density</b> .....	<b>89</b>
<b>10.1.4.8 Effect of Reduction Temperature on Density</b> ..	<b>89</b>
<b>10.1.4.9 Crystalline Size</b> .....	<b>90</b>
<b>10.1.4.10 Scanning Electron Microscope(SEM)</b> .....	<b>94</b>
<b>10.1.4.11 Fractal Analysis of Grains</b> .....	<b>95</b>
<b>10.1.4.11.1 Structure Walk Method to Determine the Fractal Dimension of Grain Ruggedness</b> .....	<b>95</b>
<b>10.1.4.11.2 Limited Self Similarity Method to Determine the Fractal Dimension of Grain Size Distribution</b> .....	<b>97</b>
<b>10.2 Characterization of Boron Nitride Coating</b> .....	<b>99</b>
<b>10.2.1 Color</b> .....	<b>99</b>
<b>10.2.2. Porosity</b> .....	<b>99</b>
<b>10.2.3 Infrared Spectrum of BN</b> .....	<b>99</b>
<b>10.2.4 X-ray Diffraction (XRD)</b> .....	<b>101</b>
<b>10.2.5 Scanning Electron Microscope (SEM)</b> .....	<b>105</b>

<b>10.3 Neutronic Calculations .....</b>	<b>114</b>
<b>11.CONCLUSIONS .....</b>	<b>132</b>
<b>12.RECOMMENDATIONS .....</b>	<b>134</b>
<b>REFERENCES .....</b>	<b>136</b>
<b>APPENDICES</b>	
<b>A. ELECTRICAL ENERGY DEMAND OF TURKEY .....</b>	<b>147</b>
<b>B. SCHEMATIC OF PWR REACTOR VESSEL .....</b>	
<b>INTERNAL STRUCTURE .....</b>	<b>148</b>
<b>C. THE NEUTRON SPECTRUM .....</b>	<b>149</b>
<b>VITA .....</b>	<b>150</b>



## LIST OF TABLES

### TABLE

1.	Global Fossil Energy Reserves, Resources, in TW-yr. ....	2
2.	Waste Arisings: Nuclear Power Plant Comparedto Coal Fired Plant	4
3.	Atomic Weights and Abundances of the Uranium Isotopes .....	7
4.	Gadolinium and Boron Cross-Section Characteristics .....	23
5.	Preparation Techniques of BN Thin Films .....	28
6.	Reactions of Neutron with Matter .....	34
7.	Microscopic Cross Section Data .....	35
8.	Macroscopic Cross Section data .....	36
9.	Compositions of Solutions .....	48
10.	Sample Data Input .....	69
11.	BET Results of the Powder .....	77
12.	Green Pellet Densities .....	77
13.	BET Results of the Green Pellets .....	78
14.	The Effect of Compaction Pressure on Density (powder reduced at 1000 K, pellets sintered at 1900 K) .....	89
15.	The Effect of Powder Reduction Temperature on Pellet Density (pellets sintered at 1900K) .....	90

## LIST OF FIGURES

### FIGURES

1.	Historical trends in energy substitution .....	3
2.	Schematic diagram of a nuclear power plant .....	9
3.	Fission cross-section of U-235 vs. neutron energy .....	11
4.	Fuel assembly .....	12
5.	The neutron direction vector in spherical coordinates .....	38
6.	Schematic summary of the experimental steps .....	47
7.	Sol-gel apparatus .....	51
8 a.	Pure $\text{UO}_2$ microspheres (yellow cake) .....	52
8 b.	$\text{UO}_2$ -5% $\text{Gd}_2\text{O}_3$ mixture .....	52
8 c.	$\text{UO}_2$ -10% $\text{Gd}_2\text{O}_3$ mixture .....	53
9.	Reduction and sintering furnace .....	54
10.	The calcined (green pellet, on the left) and the sintered fuel pellet (on the right) .....	55
11.	Tube furnace for CVD .....	56
12.	White powder at the outlet of the furnace .....	57
13.	Plain quartz plate (on the left) and BN deposited quartz plate (on the right) .....	58
14.	CVD furnace .....	58
15.	BN deposited fuel pellets .....	59
16.	Example of a fractal object: the Sierpinski gasket .....	61
17.	Application of the structured walk method to Britain Island	65

18.	The size distribution of the Aegean Islands and log-log plots of the size distribution of the Islands .....	66
19.	1000 MWe PWR core cross section .....	70
20.	1000 MWe PWR fuel assembly cross section .....	71
21.	TGA of $\text{UO}_2$ .....	74
22.	TGA of $\text{UO}_2\text{-5\%Gd}_2\text{O}_3$ .....	74
23.	TGA of $\text{UO}_2\text{-Gd}_2\text{O}_3(10\%)$ .....	75
24.	Pore size distributions of calcined and reduced powders.....	76
25.	Pore size distributions of green pellets .....	78
26.	Pore size distributions of the sintered pellets .....	82
27.	Frenkel defect .....	83
28.	Effect of Binder on pore size distribution (sample: $\text{UO}_2$ reduced at 1000 K, sintered at 1900 K) .....	87
29.	Effect of binder on pore size distribution (sample: $\text{UO}_2\text{-Gd}_2\text{O}_3$ reduced at 1000 K, sintered at 1900 K) .....	88
30.	XRD pattern of the uranium dioxide powder .....	91
31.	XRD pattern of the uranium dioxide - 5% gadolinium oxide powder .....	92
32.	XRD pattern of the uranium dioxide - 10% gadolinium oxide powder .....	93
33.	SEM picture of $\text{UO}_2$ .....	94
34.	SEM picture of $\text{UO}_2\text{-Gd}_2\text{O}_3(5\%)$ .....	94
35.	SEM picture of $\text{UO}_2\text{-Gd}_2\text{O}_3(10\%)$ .....	94
36.	Fractal analysis of grains using structured walk technique .....	96
37.	Log-log plots of the size distributions versus area of the sintered grains using limited self similarity method .....	98
38.	IR spectrum of BN powder .....	100
39.	XRD pattern of BN powder .....	102

40 a. XRD pattern of sintered BN ( $2\theta < 50^\circ$ ) .....	103
40 b. XRD pattern of sintered BN ( $2\theta > 50^\circ$ ) .....	104
41. BN coating on $\text{UO}_2$ .....	105
42. Magnified view of Fig.41 .....	105
43. Thin BN coating .....	105
44. BN formation on cracks .....	106
45. Magnified view of Fig44 .....	106
46. BN formation on grain boundary .....	106
47. Fibrous BN formation .....	107
48. Leaflike BN formation of $\text{UO}_2$ .....	108
49. BN formation on $\text{UO}_2\text{-Gd}_2\text{O}_3(5\%)$ .....	108
50. Rodlike BN formation of $\text{UO}_2\text{-Gd}_2\text{O}_3(10\%)$ with different magnifications .....	109
51. Cracks on BN coating of $\text{UO}_2\text{-Gd}_2\text{O}_3(10\%)$ .....	110
52. Partially coated BN formation .....	111
53. Side view of BN coating on $\text{UO}_2$ .....	111
54. Side view of BN coating on $\text{UO}_2\text{-Gd}_2\text{O}_3(5\%)$ .....	112
55. Side view of BN coating with backscattering technique .....	112
56. Side view of BN coating of $\text{UO}_2\text{-Gd}_2\text{O}_3(10\%)$ .....	113
57 a. $k_{\text{eff}}$ values for uraniumdioxide-gadolinium oxide fuel coated by BN (enrichment:5%, assembly:25 rods) .....	116
57 b. $k_{\text{eff}}$ values for uraniumdioxide-gadolinium oxide fuel coated by BN (enrichment:5%, assembly:25 rods) .....	117
58. $k_{\text{eff}}$ values for uraniumdioxide-gadolinium oxide fuel coated by BN (enrichment:5%, assembly:25 rods) .....	118
59. Boron depletion with different pitch distances (pure urania with 30 mm BN, 5 % enriched fuel) .....	120



<b>60. Gadolinium depletion for different types of fuels .....</b>	<b>121</b>
<b>61. Burnup values when <math>k_{eff} = 1</math> for different types of fuels .....</b>	<b>122</b>
<b>62. The effect of BN thickness on burnups (pitch distance: 1.27 cm) ..</b>	<b>123</b>
<b>63. Gadolinium effect on plutonium production (enrichment: 5%,pitch distance:1.27 cm) .....</b>	<b>125</b>
<b>64. Boron effect of plutonium production in different fuels (enrichment: 5%, pitch distance: 1.27 cm) .....</b>	<b>126</b>
<b>65. Production of plutonium isotopes (Gd: 0%, BN: 0 <math>\mu</math>m, enrichment: 5%, pitch distance: 1.27 cm) .....</b>	<b>127</b>
<b>66. Production of plutonium isotopes (Gd: 0%, BN: 70 <math>\mu</math>m, enrichment:5%, pitch distance: 1.27 cm) .....</b>	<b>128</b>
<b>67. Production of plutonium isotopes (Gd: 10%, BN: 70 <math>\mu</math>m, enrichment: 5%, pitch distance: 1.27 cm) .....</b>	<b>129</b>
<b>68. Depletion of U-235 in different fuels (enrichment: 5%, pitch distance: 1.27 cm) .....</b>	<b>130</b>

## ABBREVIATIONS

ADU Ammonium diuranate

APWR Advanced Pressurized Water Reactor

BOC Beginning of Cycle

BWR Boiling Water Reactor

CFP Coal Fired Plant

CVD Chemical Vapor Deposition

ÇNAEM Çekmece Nuclear Research and Training Center

DTA Differential Thermal Analyses

EOC End of Cycle

GCFBR Gas Cooled Fast Breeder Reactor

GDP Gross Domestic Product

IAEA International Atomic Energy Agency

IFBA Integral Fuel Burnable Absorber

IR Infrared Absorption

LMFBR Liquid Metal Fast Breeder Reactor

LPCVD Low Pressure Chemical Vapor Deposition

MFCVD Molecular Flow Chemical Vapor Deposition

MTA Mining Research and Exploration Institute

NPP Nuclear Power Plant

**ORNL Oak Ridge National Laboratory**

**PECVD Plasma Enhanced Chemical Vapor Deposition**

**PHWR Pressurized Heavy Water Reactor**

**PVA Polyvinyl alcohol**

**PWR Pressurized Water Reactor**

**SEM Scanning Electron Microscope**

**TAEK Turkish Atomic Energy Authority**

**TGA Thermogravimetric analysis**

**WIMS Winfrith Improved Multi-group Scheme**

**XRD X-ray Diffraction**



## CHAPTER 1

### INTRODUCTION

The energy problems have naturally the first priority of importance in human life. The main energy sources can be classified as conventional and alternative energy sources. Conventional energy sources are the fossil fuels (coal, natural gas, oil), hydroelectric power, and nuclear energy. Alternative energy sources are solar, wind, geothermal, biomass, and hydrogen produced by the chemical reactions and nuclear fusion. Alternative energy sources are generally more suitable in resulting low pollution problems. However, their most severe disadvantages are relating with the characters of irregularity, low power density, and site dependency. A self sustaining fusion reactor has not yet been physically realized. It is not much promising for the time being to meet large energy demands. The commercial utilization of fusion reactor would be unlikely before the year 2020[1]. The idea of making use of the solar energy requires considerable research. Therefore they would not be for the energy supply to big social community or to industrial facilities till the middle of the next century.

#### **1.1 Nuclear Energy Situation in the World**

Growing world population with rising standards of living has brought a tremendous demand for energy and electricity that fossil fuels and hydropower together will not be able to meet it. World energy demand was approximately 15

TW-yr (15 billion Megawatt-year) in 1990 it is expected to increase to 50 TW-yr in 2050's. The world fossil energy reserves, resources and occurrences are presented in Table 1. According to this table the increase in demand will not sufficiently be compensated by the fossil fuels in spite of forecasts of large reserves; these natural resources are limited and will be expensive to get the unconventional resources[2].

The historical trend of the uses of different energy resources was shown in Fig.1[3]. According to this figure nuclear energy share of the total energy sources will be approximately 30% in the year of 2050. Today about 17% of the electricity produced around the world is produced by the 430 nuclear power plants[4]. In some industrialized countries nuclear energy has a large share in meeting the energy requirements. In France 75% of electricity is produced from nuclear power plants. The percentage of electricity is produced from nuclear power plants is 21.2% in the USA, 26.3% in Great Britain, and 30.9 % in Japan.

**Table 1. Global Fossil Energy Reserves, Resources, in TW-yr.**

	<u>Consumption</u> 1860-1990 1990		<u>Reserves:</u> Identified Remaining to be discovered		<u>Resources:</u> Recoverable with foreseen technological progress
	Oil				
Conventional	106	4.4	194	79	
Unconventional	-	-	240		285
Gas					
Conventional	54	2.5	144	136	
Unconventional					565
Coal	165	3.1	701		2740
Total	325	10.0	1279	215	3590

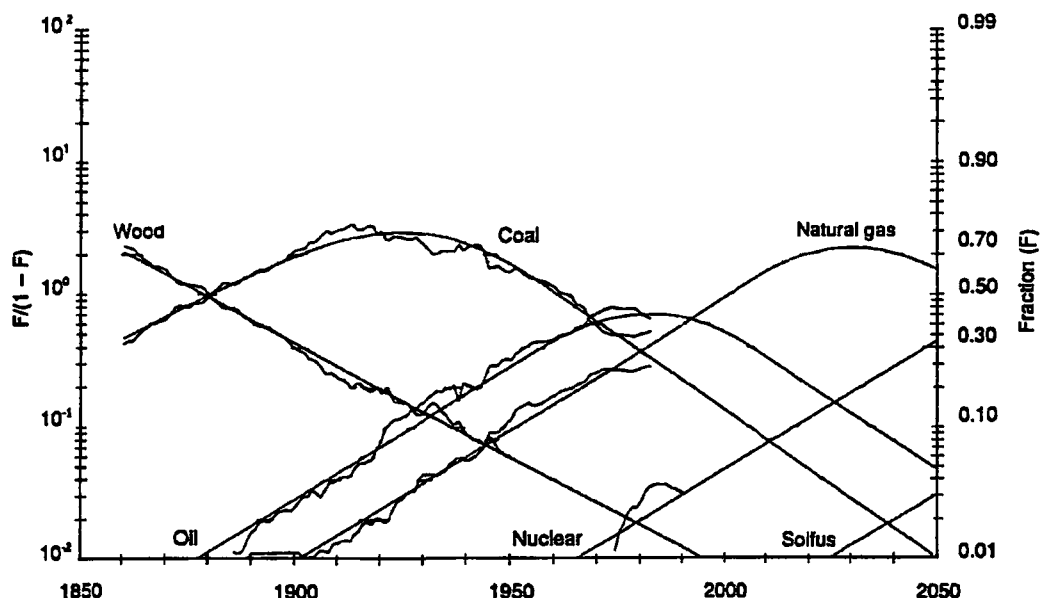


**Figure 1. Historical trends in energy substitution (the amount of primary energy (in coal-tons equivalent) from each primary source is plotted as fraction F of the total energy market)**

The burning of fossil fuel leads to huge emissions of carbondioxide, and sulfur and nitrogen oxides. Roughly 80% of carbondioxide is emitted from energy production and use. The release of these oxides causes serious pollution. The acid rains threaten the forests and the greenhouse effect increases atmospheric temperature which in turn results in anomalies in meteorological activities. It is imperative to gradually reduce the share of fossil fuels and to adopt clean technologies for power generation. Nuclear power is one of the energy sources that has contributed substantially, and could contribute even more in the future, to the lowering of greenhouse gas emissions into the atmosphere.

### **1.2 Waste Arisings (Coal Energy vs. Nuclear Energy)**

Compared to most types of industrial waste, the radioactive wastes from nuclear power use are significantly smaller in volume and have been managed with minimal effects on public health and safety. In Table 2 waste arisings of 1300 MWe nuclear power plant (NPP) and the same power coal fired plant (CFP) were compared[5].

**Table 2. Waste Arisings: Nuclear Power Plant Compared to Coal Fired Plant**  
(waste in tones)

	NPP	CFP
NO <sub>x</sub>		28,000
CO <sub>2</sub>		6,600,000
SO <sub>2</sub>		57,000
Other gases	negligible	2,000
Solid waste		415,000
High level waste	10	
Medium level waste	400	
Low level waste	600	considerable amounts of U and Th

Although significant quantities of ash is retained by precipitators (many coal fired power plants don't have precipitators), heavy metals and also trace radioactive elements such as uranium and thorium tend to concentrate on tiny glass spheres that make up the bulk of fly ash. The fly ash contains the following elements and some of them have toxic effects[6-7].

Aluminum	Chromium	Magnesium	Silver
Antimony	Cobalt	Manganese	Sulfur
Arsenic	Copper	Mercury	Thorium
Barium	Fluorine	Molybdenum	Uranium
Boron	Iron	Nickel	Vanadium
Cadmium	Lead	Selenium	Zinc

The uranium content of Turkish coals is 3-15 ppm and is released to the atmosphere with the escaping fly ash.

### 1.3 Economic Competitiveness of Nuclear Power Plants

The economic competitiveness of nuclear power depends on a number of country's specific and local conditions. These include the local prices of fuels, environmental protection and other regulatory requirements. Nuclear power

developments promote the technological development of national nonnuclear industries. Developing the industrial infrastructure for a nuclear program involves the strengthening of a number of industries in the country to achieve maximum domestic participation. They include industries for construction, fabrication of equipment, and materials and service supplies[8].

#### **1.4 Situation in Turkey**

The energy consumption in Turkey is increasing steadily as a result of high industrialization rate and high population growth. Until the end of the century, the electricity energy production is expected to increase from 80 TWh to approximately 130 TWh [9-10]. The main challenges of the energy policy since the beginning of 1980's have been to reduce the country's strong dependence on imported oil, to expand the domestic energy resources (coal, lignite and hydro), to develop new energy supplies, to promote energy conservation and to create financial resources for energy capital investments. In 1990's, Turkey's energy supply continued to be boosted by the fast-developing economy, which grew on average 5.5% annually between 1983 and 1990. Gross Domestic Product (GDP) growth was 8.18% in 1990, 1.11% in 1991 5.65% in 1992 and 8.2% in 1993. Electricity consumption per capita increased from 205 kWh in 1970 to over 1000 kWh in 1993.

The main domestic energy sources of Turkey are hydro power and lignite; some deposits of oil, natural gas and coal and significant geothermal potential also exist in the country. The sources of generated electricity in Turkey for 1993 were hydro power 40%, coal 35%, oil 7% and natural gas 18%. Turkey's hydro potential is almost 122 TWh and lignite potential is 100 TWh. Only 20% of this potential is utilized currently. By the year of 2010 approximately 60% (75 TWh) of hydro potential and approximately 90% (90 TWh) of lignite potential may be utilized. According to the long-term electric energy demand and supply projections of Planning and Coordination Department of TEK, the production will be 130 TWh in the year 2000 and increase to 271 TWh in the year of 2010 (See App. A). Total



domestic energy resources in 2010 is approximately 165 TWh (75 TWh from hydropower + 90 TWh from lignite) and therefore the demand and supply planning studies show that total resources are not sufficient to meet the demand after the year 2000. Other energy resources are also necessary to satisfy the rapidly growing demand in future. Besides the imported coal and the imported natural gas, the use of nuclear energy is necessary for diversification of the energy resources of the country. This is also necessary to cope with all aspects of nuclear technology and future fusion reactors, and also to grow additional industrial fields around this technology.

Following a comprehensive site survey studies, Akkuyu Bay has been selected as the first nuclear power plant site of Turkey. It is on the Mediterranean Sea Coast about 43 km southwest of Silifke. Sinop is planned to be the next site[11].

The financing constraints and public opinion are the most important factors influencing the final decision for the construction of the first nuclear power plant in Turkey.

### **1.5 Scope of This Research Work**

The current policy in nuclear technology is to increase the burning efficiency of fuel and thus to increase the fuel reloading time. To achieve this some special compounds, so called burnable absorbers are used. The well known burnable absorbers are gadolinium and boron. The new fuels to be used in reactors will contain either of this compounds. Turkey does have a technology of producing her own nuclear fuel. The aim of this study therefore has been to make nuclear fuels with burnable absorbers and thus to cope with the fuel technology in the world. This will naturally take us to a better position in this branch of nuclear reactor technology. The fuel developed in this study has a unique property that it combines two burnable absorbers in the same fuel pellet while usually one is used present technology.

## CHAPTER 2

### NUCLEAR REACTOR TECHNOLOGY

#### 2.1. History of Nuclear Energy

Uranium is the basic material for nuclear energy and the heaviest elements occurring in nature. Table 3 gives the atomic weights and abundances of the most common uranium isotopes.

**Table 3. Atomic Weights and Abundances of the Uranium Isotopes.**

Nuclide	Atomic weight	Abundance (Atomic %)
U-238	238.054	99.275
U-235	235.044	0.72
U-234	234.041	0.0007
Natural uranium	238.033	

Uranium was discovered by the German scientist Klaproth in 1789. Hahn, Meitner and Strassmann reported fission of uranium (U-235 ) in 1939. This was soon followed by the discovery of the manmade element plutonium and two additional isotopes, namely Pu-239 and U-233 which produce energy when fissioned during 1941-42 by Seaborg and his colleagues in Berkeley, USA.

Finally, Fermi and coworkers in Chicago had demonstrated the first self sustained "nuclear chain reaction" in December 1942 and laid the foundation for nuclear

reactors[13]. The first energy producing nuclear power plant was built in 1954 at Obninsk (APS-1) in Russia. Nuclear reactors are classified as i) the pressurized water reactor (PWR), ii) the boiling water reactor (BWR), iii) the pressurized heavy water reactor (PHWR), iv) the gas cooled reactor (GCR), v) the liquid metal or gas cooled fast breeder reactor, (LMFBR, GCFBR). This classification is based on the energy removal mechanism. Energy share of these reactors are as follows; PWR dominates the market, providing 57% of existing nuclear reactor capacity, BWRs provide 21%, PHWRs 8%, GCR 5%, and the others 9% [12]. Liquid metal or gas cooled fast breeder reactors which have the potential to breed its own fuel from useless depleted uranium has been brought to the prototype stage in several countries.

Today research studies in nuclear reactor technology has aimed in reduction of the capital cost, reducing unplanned shutdown, improving plant availability and output, overcoming the problems caused by materials of the reactor core and other auxiliary equipments, uranium demand and utilization, and reducing radiation exposures to the public and workers. Designers are developing advanced reactors, building upon the extensive experience accumulated through the operation of the reactors of the present generation.

## **2.2. Reactor System**

A nuclear power generating system basically contains a cylindrical containment, boiler, and a turbine-generator system. The fuel rods are loaded in the containment in the form of bundles so called fuel assembly. The moderator-coolant water runs through the rods removing the heat generated meanwhile slowing down neutrons. The excess neutrons are absorbed by control rods. The fuel elements, control rods, instrumental thimbles make the reactor core. A detailed picture of a PWR containment is given in Appendix B. In PWR the hot water circulates through a steam generator and leaves its heat there. The steam generated goes to turbine. In BWR the steam generated in the reactor directly goes to turbine. Figure 2 shows the schematic diagram of the basic operation of a nuclear power plants.

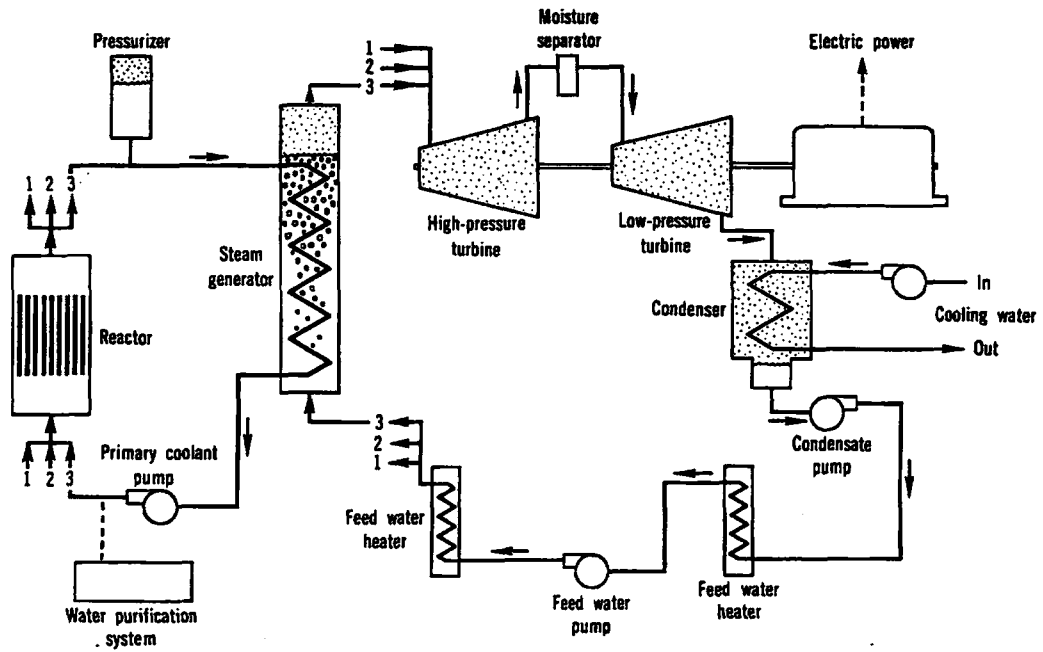
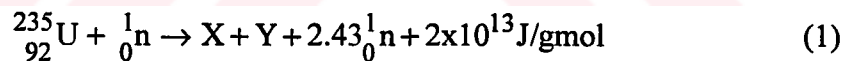


**Figure 2. Schematic diagram of a nuclear power plant**

### 2.3. Fundamental Principles

A nuclear reactor is a device in which atoms of nuclear fuel are split (fissioned) by neutrons yielding about two lighter highly radioactive atoms (fission products) and about two to three new neutrons. The resulting mass of the products is less than that of the original nucleus plus a neutron. The difference in masses appears as energy according to Einstein's  $E = mc^2$ . The reaction can be expressed as:



X and Y are isotopes mostly produced with masses in two different ranges of 85-110 and 125-150. The neutrons produced can react with other nuclei of fuel (this phenomena is termed as chain reaction), or they may be captured without producing fission by fuel atoms or they react with the structural materials of the reactor[13].

### 2.3.1. The Multiplication Factor

The neutrons play the central role in maintaining the fission chain reaction. Therefore one of the primary task of the nuclear engineer is to follow the neutron economy in a nuclear reactor in order to monitor and control the behavior of the chain reaction. Multiplication factor, “k” is used to characterize the chain reaction in a nuclear reactor, which is defined as,

$$k = \frac{\text{rate of neutron production in reactor}}{\text{rate of neutron loss in reactor}}$$

It is necessary to balance the rate at which neutrons are produced within the reactor with the rate at which they disappear. Neutrons can disappear in two ways, as a result of absorption in some type of nuclear reaction or by escaping from the surface of the reactor. When the sum of neutron absorption and leakage rates is exactly equal to the neutron production rate, the reactor is said to be critical. If the production rate is greater than the sum of the absorption and leakage rates, the reactor is supercritical and, conversely if it is smaller, the reactor is subcritical. In summary,

$k < 1$  subcritical

$k = 1$  critical

$k > 1$  supercritical

The primary objective of the reactor engineer is to design the nuclear reactor so that it is critical. The reactor is naturally loaded with fissile material which makes the reactor supercritical. The criticality is achieved by absorbing the excess neutrons by control rods. The ratio,

$$\rho = \frac{k-1}{k} \quad (2)$$

is called reactivity. When  $\rho=0$  we have criticality. Positive or negative reactivities refers the increase or decrease of the rate of neutron productions, respectively. The

rate constant for nuclear fission reaction (i.e., cross section for fission) decreases with the speed of neutrons as seen in Fig. 3.

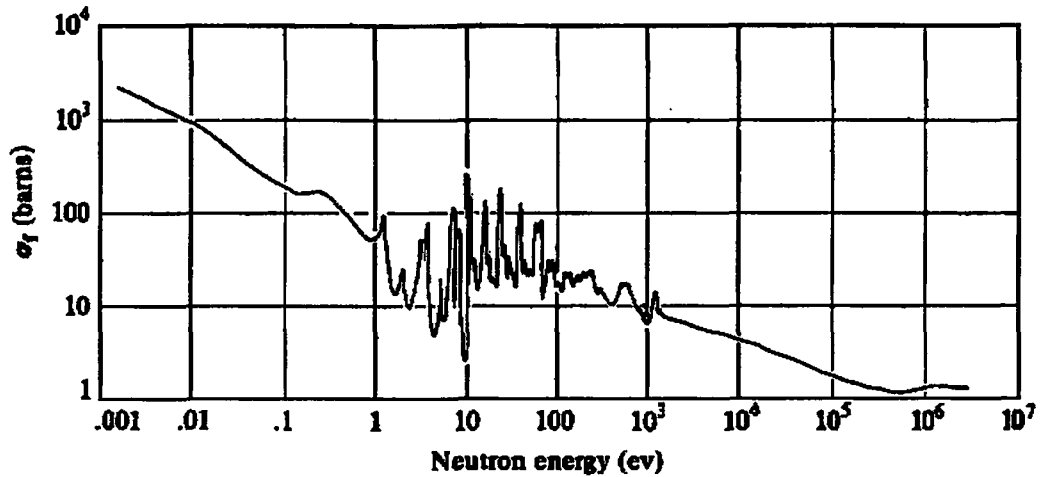


**Figure 3. Fission cross-section of U-235**

#### **2.4. Thermal and Fast Reactors**

The neutrons released in the fission process have high speeds (fast neutrons) and are relatively inefficient at fissioning the normal reactor fuel (uranium). Therefore, neutrons are slowed down by using materials called moderators, to low speeds with a possible Maxwellian distribution, and these neutrons are called thermal neutrons. Reactors relying on uranium fuels and employing moderators to slow down neutrons are known as thermal reactors. Some reactors do not contain moderators and rely on fast neutrons to produce fissions in the fuel. These are called fast reactors. Fast reactors normally rely on plutonium fuels; plutonium being a material produced when neutrons are captured by uranium atoms in the fuel without inducing fission. Reactors of either type (i.e., thermal or fast) employ a coolant to remove heat from the fuel. The coolant provides the means by which the heat generated in the nuclear fission process be utilized for power production or for other heating purposes.

## 2.5. Nuclear Fuels

Today uranium in the form of uranium dioxide is the principal nuclear fuel in wide use. In the next chapter uranium dioxide preparation technique will be explained and the importance of the sol-gel technique which is used in this study will be given. Other nuclear fuels such as thorium, recycled uranium, and plutonium may be important in the future as they become commercially available.

Uranium dioxide pellets are inserted into a Zircaloy tube, and each end of the tube is sealed by welding to form a fuel rod. A square array of fuel rods structurally bound together constitutes a fuel assembly as shown in Figure 4.

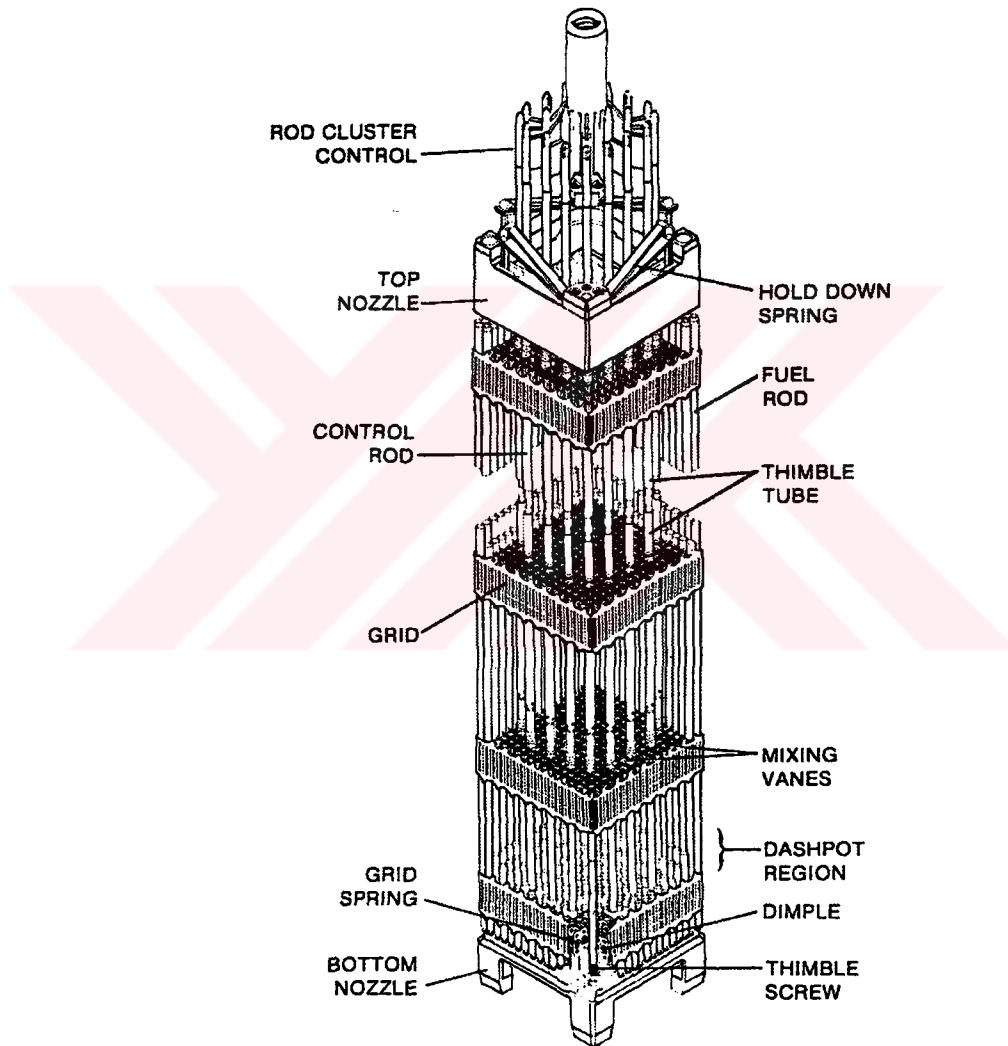
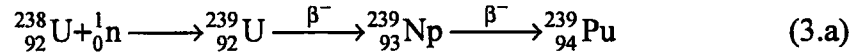


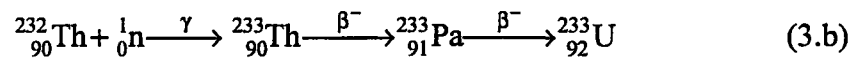
Figure 4. Fuel assembly

Plutonium is not found in nature except in trace quantities. There are fourteen isotopes of plutonium with mass numbers between 232 and 246; the isotope of greatest interest is plutonium-239. Plutonium is formed in nuclear reactors as follows,



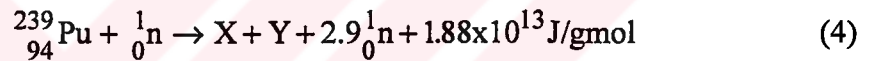
The half lives for the beta decay of U-239 and Np-239 are very short so Pu-239 is easily formed.

Similarly Th-232 produces fissile U-233 isotope as follows



Th-232 is a potential fuel and it cannot be directly used in thermal reactors.

Plutonium 239 is a fissile material and reacts with neutron as follows,



in any nuclear reactor using uranium as fuel, some U-238 is converted to Pu-239. Some of this plutonium will react with neutrons and produce U-235, so the fissile nature of plutonium makes it a benefit in nuclear reactors. The presence of plutonium enhances the economics of the fuel cycle.

## 2.6 Desired Properties of the Fuel Material

Fuel element is expected to retain physical, mechanical, and chemical stability in spite of the irradiation damage caused by neutrons and fission fragments during its lifetime in a reactor core. In order to meet these requirements nuclear fuel should have the following properties:

- a) high thermal conductivity,
- b) resistant to radiation damage,



- c) chemical stability,
- d) high melting point,
- e) low coefficient of thermal expansion,
- f) nuclear purity.

## **2.7. Fuel Utilization Economy**

Reactor operation in a nuclear reactor includes a number of stages as loading of the uranium fuel into the reactor core (beginning of cycle, BOC), period of routine operation stages, end of cycle (EOC), and the final shutdown of the reactor when it is taken out of service. During the period of routine operation the heat output of the reactor core is managed in a way to get the maximum energy. This can be achieved basically by burning the fuel efficiently.

The need to improve reactor performance through longer cycle lengths or improved fuel utilization has been apparent since the beginning of the commercial power generation. Using enriched fuel is one way to achieve this goal but additional amount of fissile material has had to be compensated for by the introduction of additional neutron absorber material in the core. For this purpose boric acid can be injected into the primary coolant system for absorbing the excess reactivity, and flatten the flux. then we may introduce highly enriched fuel into the reactor core. This increases the reactor power output. However, it also increases excess neutron generation which must be controlled by introducing new control rods into the reactor. Control rods decrease power density and introduce nonuniform burning, and thus indirectly decrease the reactor core life. The need for more control rods can be diminished by introducing neutron absorbing materials into the coolant of the reactor. Such chemicals are called soluble poison or chemical shim. The burnable poisons have high absorption cross sections for thermal neutrons. They are converted into products which have very low absorption cross sections after interacting with neutrons.

When thermal neutrons are partially absorbed by poisons, the neutron spectrum is hardened. Relatively fast neutrons yield more than 2.43 neutrons per fission (see Eq.4). This increases the conversion of U-238 into Pu-239 (see Eq.3a). Therefore burnable poison increases the production of Pu-239 and thus increase the core life of the reactor.

In the last decade soluble burnable absorbers were substituted by gadolinia which is mixed with the fuel. The advantage of using gadolinia will be explained later.



## CHAPTER 3

### URANIUM DIOXIDE

Uranium dioxide ( $\text{UO}_2$ ), a ceramic which is the most common fuel material in commercial power reactors, has the advantage of high temperature stability and adequate resistance to radiation. It has also a high melting point ( $2685^\circ\text{C}$ ). In addition,  $\text{UO}_2$  is chemically inert to attack by hot water. It is this property which makes it attractive for use in water-cooled reactors, where the consequences of a cladding failure could be catastrophic if the fuel material reacted readily with water at the existing high temperature. Another beneficial property of uranium dioxide is its ability to retain a large proportion of the fission gases especially below  $1000^\circ\text{C}$ . However, the average temperature of the fuel is around  $1200^\circ\text{C}$ . The major disadvantage of uranium dioxide as a fuel material is its low thermal conductivity, although this is partially offset by the fact that very high temperatures are permissible in the center of the fuel element due to its high melting point.

#### 3.1. Uranium Resources of Turkey

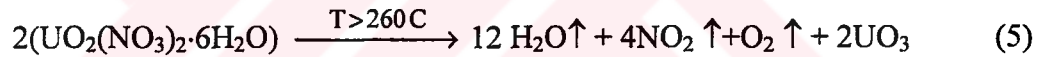
Uranium exploration in Turkey began in 1956-1957. In mid 1970's the first uranium deposit was found in the Köprübaşı area (2852 tons U). The other main uranium reserve is Demirtepe area (1729 tons U). As a result of recent exploration activities, new uranium deposit has been found in the Yozgat-Sorgun region of Central Anatolia (3850 tons U)[15].

The pilot plant established in Köprübaşı was run by MTA (Mining Research and Exploration Institute) for years. The yellow cake produced was further treated in the Çekmece Nuclear Research and Training Center (ÇNAEM) of the Turkish Atomic Energy Authority (TAEK). A pilot plant for the uranium dioxide production has already been established and started production in ÇNAEM and it is still in operation.

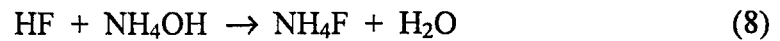
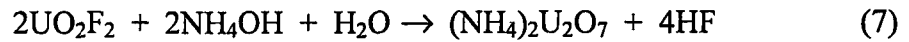
### 3.2. Conventional Preparation of Uranium Dioxide

Two main types of large scale industrial methods have been used to prepare  $UO_2$ [16]. Denitration of uranyl nitrate hexahydrate,  $UO_2(NO_3)_2 \cdot 6H_2O$ , and decomposition  $(NH_4)_2U_2O_7$  (ammonium diuranate, ADU) yield  $UO_2$ .  $UO_2$  may also be obtained by thermal decomposition of uranium salts in the absence of air. In nearly all cases, the final stage of preparation of  $UO_2$  had been the simple  $H_2$  or  $NH_3$  reduction of  $UO_3$  or  $U_3O_8$  at an elevated temperature.

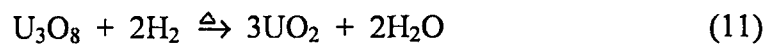
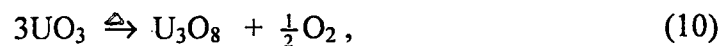
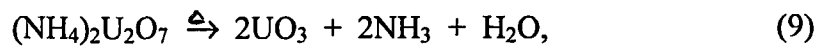
The most common method used in the past to make  $UO_2$  was the denitration of uranyl nitrate hexahydrate,  $UO_2(NO_3)_2 \cdot 6H_2O$ , to  $UO_3$  followed by hydrogen reduction. The course of reaction is as follows,



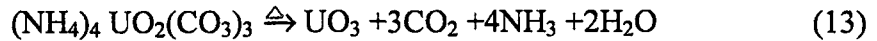
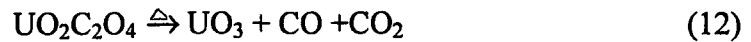
The second conventional method for  $UO_2$  production is the preparation of ADU from uranium hexafluoride as follows,



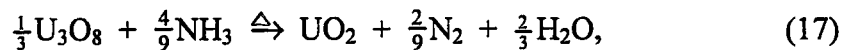
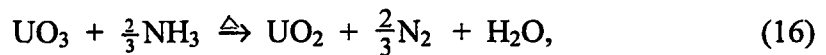
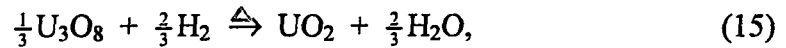
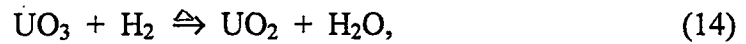
The ADU crystals are crushed to obtain small particles, and decomposed into  $UO_3$  according to the following reaction,



Uranium dioxide may also be obtained by thermal decomposition of uranium salts in the absence of air. Some common reactions are as follows,



$\text{UO}_2$  is prepared by the reduction of  $\text{UO}_3$  or  $\text{U}_3\text{O}_8$  by gaseous reducing agents at elevated temperature as,



Nearly all these methods for the preparation of  $\text{UO}_2$  create dust problems, wide size distribution of particulates, and uncontrolled moisture pick up. These particles are turned into powder form after reduction and calcination and then are pressed to make pellets. These pellets are sintered to obtain high density fuel. To produce fuels with much more uniform structure, and minimized radioactive dust problems a new technique so called sol-gel technique has been introduced in making fuel pellets.

### 3.3. Sol-Gel Method

The sol-gel method was developed to make glass and special ceramic products at low temperatures [17,18]. The first application of this method to make nuclear fuels was seen at Oak Ridge National Laboratory (ORNL) [19]. The scientific development of sol-gel (solution-gelation) or wet chemical processes for the fabrication of spherical particles or microspheres of fuel began in 1960s in USA[20-22]. In the last decade some important technical developments have been achieved to use gadolinia in urania fuel [23-33]. Gadolinia can be introduced into fuel either by powder mixing or by sol-gel and coprecipitation methods [34-40].

The basic principle is that a solution (sol) of the heavy metals (uranium, thorium or plutonium) is dispersed into droplets and solidified (gelled) by a chemical precipitation reaction. Finally, the gelled particles are calcined, reduced, pelletized, and sintered.

### 3.3.1. Advantages of Sol-Gel Method

Advantages of this process are [41-43]:

- a) generation and handling of fine powder is avoided, thus lowering radiotoxic dust hazard and associated problems,
- b) the free-flowing nature of microspheres facilitates remote and automated fabrication, thus reducing significantly exposure of personnel to radiation,
- c) better homogeneity, improved density and microstructure of pellet,
- d) excellent microhomogeneity in mixed oxide pellets (i.e.,  $\text{UO}_2\text{-Gd}_2\text{O}_3$ ,  $(\text{U-Pu})\text{O}_2$ ,  $(\text{U-Pu})\text{C}$ ,  $(\text{U-Pu})\text{N}$ ),
- e) significant reduction in the number of process steps and in turn fabrication cost,
- f) the high chemical activity and specific surface area of gel,
- g) direct preparation of the various size fractions with a narrow size distribution, and hence elimination of grinding or milling of large particles.

The end product of sol-gel process is dust-free spherical gel particles (100-1000 micrometer in diameter) of the oxide fuel with high specific surface area, and with high sinterability and excellent microhomogeneity.

In this study uranyl nitrate or uranyl nitrate-gadolinium nitrate solution was first prepared by sol-gel process and uranium dioxide and uranium dioxide-gadolinium dioxide fuels have been prepared.

## CHAPTER 4

### BURNABLE ABSORBERS

#### 4.1. Importance

The rate at which fission takes place in a reactor can be controlled by introducing neutron-absorbing materials in the form of rods (i.e., control rods), which can be raised or lowered within the core of the reactor. Fine tuning can also be affected by controlling the temperature of the coolant within the reactor core. The control rods can also be used to stop the fission process completely and thus shut the reactor down for maintenance, for refueling, or in the event of an emergency. The nuclear reactor is so designed that it cannot explode like an atomic bomb; however, the energy release can be slow that the fuel materials in the core can melt, resulting in rapid and violent chemical reactions. The irradiated fuel in the core continues to produce large amounts of heat from the decay of the highly radioactive fission products. Therefore it is essential for reactor safety that coolant flows are maintained to prevent the fuel from melting and damaging the reactor even when the reactor is shut down. Nuclear reactors have excellence in the safety and environmental performance. For example Advanced Pressurized Water Reactor (APWR) safety goals have been established to limit the core damage frequency to less than  $10^{-5}$  per reactor year[44].

After the fuel has been depleted, the spent fuel is removed from the reactor core and stored under water in cooling ponds at the reactor site for 2-4 years. Later, the plutonium is recovered from reprocessing of the spent fuel.

#### **4.2. General Overview**

Early nuclear reactors were controlled by using strong neutron absorbers. Strong flux depressions at certain locations of reactors caused unsmooth power production, and inefficient burning of fuel, while thermal stresses caused early material failure problems. The new generation control rods have been made from relatively weak neutron absorbers.

The amount of burnable absorbers are so adjusted that their consumption and the build up of fission products more or less compensate each other to minimize the need for the control rods. The loading of fuel with high amount poisons diminishes the number of control rods needed. Since burnable poisons yield products with very low neutron absorption cross sections, it is possible to load the core with high amounts of burnable poison and also with highly enriched fuel to compensate the poison. In other words the negative reactivity introduced by the poison is compensated by the positive reactivity introduced by the fuel. Otherwise high amount of poison can take the reactor to subcriticality. The use of highly enriched fuel naturally means high energy production with prolonged cycle time. This is actually the desired aim in nuclear power engineering. The use of highly enriched fuel was not possible in the past. Because the control of highly excess positive reactivity introduced by the fuel could not be smoothly controlled by control rods. Therefore severe thermal spikes and material failure problems could arise under these conditions.

Any poison represents a negative reactivity and it is good for reactor control. When it is burned or lost or decreased (i.e., due to thermal expansion of coolant water which contains boric acid) positive reactivity is introduced. It must be compensated by inserting control rods further if needed. As the burnable absorbers are consumed, fission products build up in the fuel. The fission products are also



poisons. In other words the consumed burnable poison is compensated by the build up of fission products.

The recent increased focus on more efficient fuel management schemes and longer operating cycles imposes a requirement to utilize some form of burnable absorber for power distribution and reactivity control. The burnable absorbers fall into four basic categories. These are soluble burnable absorbers, gaseous burnable absorbers, discrete burnable absorbers and burnable absorbers used in fuel .

#### **4.2.1. Soluble Burnable Absorbers**

Boric acid which is dissolved in the moderator is an example to the soluble burnable absorbers. The principal disadvantage of the soluble burnable absorber lies in the fact that the decrease of the moderator density (void formation) might lead to a positive reactivity insertion. In addition the loss of coolant may cause the removal of the soluble poison and, thereby positive reactivity insertion [45].

#### **4.2.2. Gaseous Burnable Absorbers**

The introduction of neutron absorber gas for example He-3 into the reactor core is an example to gaseous burnable absorbers. The advantage of this method is the possibility of controlling the reactor during burnup without affecting the moderator reactivity coefficient, and without distorting the reactor axial power distribution. However the proposed method also presents some disadvantages. First, He-3 is an expensive material due to the fact that natural He contains only  $1.3 \times 10^{-4}$  parts He-3. Second, the introduction of the poisonous control will require an additional system of tubes. The complexity of such an additional system would probably increase due to the fact that He-3 is transformed to H-3 by neutron capture. The creation of radioactive tritium will necessitate a leak proof system.

### **4.2.3. Discrete Burnable Absorber**

In discrete assemblies some of the fuel tubes (i.e., elements) are filled with neutron absorbing materials. They behave somehow like fixed control rods. The materials used are;

- a) ceramics- $\text{Al}_2\text{O}_3$ - $\text{B}_4\text{C}$  mixtures,
- b) glasses-borosilicate glasses such as Pyrex,
- c) graphite-boronated graphite,
- d) cermet-mixture of Zircaloy and  $\text{B}_4\text{C}$ ,
- e) alloys-zirconium boron and boronated stainless.

High swelling behavior, gas release and high cost are some disadvantages of these burnable absorbers. Discrete burnable absorbers displace water in the fuel assembly; therefore, less hydrogen (i.e., water) is present. This in turn, decreases the efficiency of neutron moderation and fuel utilization.

### **4.2.4. Burnable Absorbers Used in Fuel**

These burnable absorbers have been developed recently and they do not displace water because they exist in fuel. Since they are a part of the fuel rod, separate handling of the absorbers is eliminated. Although discrete burnable absorbers reliably control core reactivity, they carry with them a residual negative reactivity effect: discrete burnable absorbers continue to absorb neutrons later in the cycle when neutron absorption is no longer desired. They can be used in such quantities that no burnable absorber exists toward the end of cycle. They can be classified in two categories, as:

- a) burnable absorber mixed with fuel (gadolinium oxide mixed with fuel),
- b) burnable absorber coated with fuel (zirconium diboride, ( $\text{ZrB}_2$ )).

These are commercially available.

#### 4.2.4.1. Burnable Absorber Mixed with Fuel

Gadolinium oxide is an important example for this type of burnable absorber. Gadolinium is a rare earth metal and has a very high absorption cross section for neutrons. A summary of cross sections of gadolinium and boron is given in Table 4.

**Table 4. Gadolinium and Boron Cross-Section Characteristics**

Element	Isotope	Abundance (atomic, %)	Thermal CrossSection, b)*
Gadolinium	natural		49000
	Gd-152	0.2	10
	Gd-154	2.1	80
	Gd-155	14.8	61000
	Gd-156	20.6	2
	Gd-157	15.7	255000
	Gd-158	24.8	2.4
	Gd-160	21.8	0.8
Boron	natural		760
	B-10	20	3837
	B-11	80	0.005

\*1b =  $10^{-24}$  cm<sup>2</sup>

Recent trends in ceramic fuel fabrication are directed towards the use of gadolinium as burnable poison instead of soluble burnable absorbers. Potential advantages of gadolinia relative to soluble burnable absorbers are as follows:

- a) Gadolinium has higher thermal cross section than boron. Therefore, it can introduce significant control of reactivity at the very beginning of cycle when the fuel is very fresh. In addition it does not cause residual reactivity at the EOC,

- b) Boric acid changes the properties of the moderator (water) (thermal conductivity, pH, corrosivity, density),
- c) Filtering of coolant before recycling to the system creates additional waste (ion exchange resins) and necessitates additional storage and disposal. Lithium formed due to reactions,  $^{10}_5\text{B} + ^1_0\text{n} \rightarrow ^7_3\text{Li} + ^4_2\alpha$ , must be removed in the ion exchangers. Otherwise it tends to deposit inside the system.

However, the use of excessive amounts of gadolinia creates some problems. It deteriorates some physical properties of  $\text{UO}_2$ . In particular, the thermal conductivity of gadolinium oxide fuel decreases when gadolinium content increases. Gadolinia retards sintering and so results in higher porosity. This in turn lowers the thermal conductivity and increases the temperature at the very center of fuel. About 5 to 10 wt% have been considered useful for nuclear reactors to attain extended burnup. Beyond this it causes solid solution formation. The  $\text{UO}_2$ - $\text{Gd}_2\text{O}_3$  fuel pellets are generally fabricated by sintering a mixture of mechanically blended powders of  $\text{UO}_2$  and  $\text{Gd}_2\text{O}_3$ .

The sol-gel microsphere pelletization technique is a recent and advanced concept of fabrication of fuel pellets because it ensures excellent microhomogeneity in pellets.

#### **4.2.4.2. Burnable Absorber Coated Fuel**

Another method of introducing burnable absorber is to coat the fuel pellets by a thin layer of burnable absorber so called integral fuel burnable absorber (IFBA). In this method the fuel is coated with zirconium diboride ( $\text{ZrB}_2$ ) [46-47]. Boron (B) has a low neutron absorption cross section compared to gadolinium. Therefore B does not totally burn out when it is mixed with fuel and introduces residual negative reactivity at EOC. However as it exists on the surface of fuel, it interacts with the thermalized neutrons on their return from moderator before the fuel does. As the thermal neutrons are partially absorbed by boron the spectrum becomes hardened. So the burning of B is achieved at high rate while sufficiently hardened

neutrons go inside the fuel. This naturally increases the conversion efficiency of U-238 into Pu-239.

The fabrication technique of ZrB<sub>2</sub> technology is quite complicated and the dissolution of unburned ZrB<sub>2</sub> creates problems[48]. The difficulties in the sputtering of ZrB<sub>2</sub> can be overcome by the utilization of some other deposition techniques. In this study a new method, boron nitride coating of the fuel by chemical vapor deposition (CVD) technique is used. The difficulties of the coating by sputtering technology and the solubility problems of ZrB<sub>2</sub> can be overcome by BN coating. The CVD method which is encountered in BN coating is very simple. But coating technology of BN is not the only advantage of this method. It has the following additional advantages;

- a) has high thermal stability,
- b) is chemically inert,
- c) withstands high pressures and temperatures,
- d) has excellent corrosion resistance,
- e) withstands rapid heating and quenching at 1500°C,
- f) has a thermal conductivity comparable to that of stainless steel.

## CHAPTER 5

### BORON NITRIDE

There has been increasing interest in ceramic structural materials that can withstand severe conditions. Nonoxide ceramic materials, such as nitrides, carbides and borides, are extremely hard and exhibit high mechanical strength, as well as erosion, oxidation, corrosion, and thermal shock resistance at elevated temperatures.

Boron nitride prepared by CVD has been extensively investigated in the last ten years. Due to its unusual structure and properties, it has caused a great deal of scientific and technological interest in many applications such as crucibles for metal evaporation, transistor heat sinks, nuclear reactor control rods, and neutron absorbers.

#### **5.1. Chemical Vapor Deposition of Boron Nitride**

Vapor deposition consists essentially of reducing or decomposing a volatile compound of coating material upon a heated surface. For the practical employment of this method, the material must form a volatile compound which can be readily dissociated or reduced at temperatures below the melting points of the coating or of the base material, and must be sufficiently stable to prevent decomposition or reduction before reaching the deposition surface.

### 5.1.1. History

Boron nitride prepared by CVD is also known as pyrolytic boron nitride. BN films can be grown by different chemical processes including chemical vapor deposition (CVD), low pressure chemical vapor deposition (LPCVD), plasma enhanced chemical vapor deposition (PECVD), and molecular flow chemical vapor deposition (MFCVD). CVD techniques are more suitable than other techniques for obtaining BN thin films with desirable properties. However PECVD seems to be the more promising technique and it may find significant application in future. Table 5 gives the preparation techniques of BN thin films [49-50].

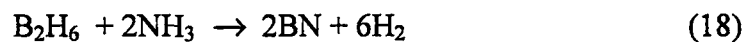
**Table 5. Preparation Techniques of BN Thin Films**

Technique	Reactants	Remarks	References
CVD	B <sub>2</sub> H <sub>6</sub> , NH <sub>3</sub>	Deposition temperature ranging from 400-1250°C. Clear vitreous film	51-54
CVD	BCl <sub>3</sub> , NH <sub>3</sub>	Deposition temperature ranging from 250-1250°C. Transparent BN films.	55-67
CVD	BF <sub>3</sub> , NH <sub>3</sub>		68-69
CVD	B <sub>3</sub> N <sub>3</sub> Cl <sub>6</sub>	Deposition temperature ranging from 900-950°C. Good adhesion	70
PECVD	B <sub>2</sub> H <sub>6</sub> , NH <sub>3</sub> , N <sub>2</sub>	Deposition temperature of about 1000°C. Polycrystalline structure.	71,72
PECVD	B <sub>2</sub> H <sub>6</sub> , NH <sub>3</sub>	Deposition temperature of about 300°C. Amorphous structure	73-75
PECVD	BCl <sub>3</sub> , NH <sub>3</sub> , H <sub>2</sub> , Ar	Deposition temperature of about 550-900°C.	76,77
PECVD	BH <sub>3</sub> N(C <sub>2</sub> H <sub>5</sub> ) <sub>3</sub> , NH <sub>3</sub>	Deposition temperature of about 200-350°C. Amorphous structure.	78-80
LPCVD	B <sub>2</sub> H <sub>6</sub> , NH <sub>3</sub>	Deposition temperature of about 300-400°C.	81-83
MFCVD	B <sub>10</sub> H <sub>14</sub> , NH <sub>3</sub>	Deposition temperature of about 300°C	84
Sputtering	B, BN, N <sub>2</sub>	Films deposited without heating the substrate.	85-88
Ion beam	B, N <sub>2</sub> , NH <sub>3</sub>	Ion beam plating of electron-beam evaporated B	89-94
Pulse Plasma	B <sub>2</sub> H <sub>6</sub> , N <sub>2</sub> , H <sub>2</sub>	Plasma decomposition, Cubic structure method.	95-97

Various chemical materials have been used to deposit BN. The major ones are:

- a) thermal decomposition of trichloroborazole ( $B_3Cl_3N_3H_3$ ) and hexachloroborazole ( $B_3N_3Cl_6$ ) [70],
- b) reactions of  $NH_3$  with boron trifluoride ( $BF_3$ ), diborane ( $B_2H_6$ ), boron trichloride ( $BCl_3$ ), trimethyl borate ( $B(OCH_3)_3$ ), boric acid ( $H_3BO_3$ ), and decaborane ( $B_{10}H_{14}$ ) [68,71]

Rand and Roberts [51], Murarka et al. [52] and Hirayama and Shohno [53] prepared BN thin films from diborane ( $B_2H_6$ ) and ammonia ( $NH_3$ ) by using inert carrier gas according to the reaction,



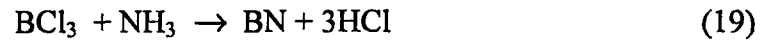
Rand and Roberts [51] used different substrates such as silicon, tantalum, molybdenum, germanium, and fused silica and kept the substrates at various temperatures ranging from 600 to 1080°C. They achieved deposition rates of 12.5-60 nm/min in hydrogen or helium, and 100 nm/min in nitrogen. The dependence of the deposition rate on temperature, and on  $NH_3/B_2H_6$  ratio was found to be quite complicated. The deposition rate exhibited a maximum at 800°C and decreased as the  $NH_3/B_2H_6$  ratio was increased from 0 to 20.

Murarka et al. [52] studied the growth process on silicon substrates. The deposition rate was proportional to the flow rate of  $B_2H_6$  and to the inverse fifth power of the flow rate of  $NH_3$ . For a fixed  $NH_3/B_2H_6$  ratio, the deposition increased linearly with the flow rate. The deposition rate increased with temperature in the range 400-700°C and it became almost independent on further increase of the temperature.

Hirayama and Shohno [53] used silicon substrate, keeping the substrates at temperatures between 700 to 1250°C. The growth rate of the film was about 50 nm/min at 700°C.



Steele and coworkers [54,55], Baronian [56], Sano and Aoki [57], Motojima et al. [58] and Takahashi et al. [59,60] have used  $\text{BCl}_3$  and  $\text{NH}_3$  with the following reaction;



Steele and coworkers [54,55] used a large variety of substrate at temperatures ranging from 800 to 1600°C. They found that the nature of the substrate could greatly influence the degree of preferred orientation of the crystallites.

Baronian [56] deposited BN thin films on quartz substrates successfully at temperatures ranging from 600 to 900°C. Sano and Aoki [57] used silica and shapphire substrates at temperatures varying from 600 to 1100°C. Motojima et al. [58] used copper substrates at temperatures in the range 250-700°C. The films deposited at temperatures below 450°C were unstable in a moist atmosphere.

Takahashi et al. [59,60] studied in detail the effect of the substrate material on the growth process. According to their results, iron and nickel were the favorite elements for forming BN crystalline deposits. The formation of the first layer of BN was initiated by a catalytic action of the iron atoms. BN thin films have also been prepared by the action of  $\text{NH}_3$  with  $\text{BF}_3$  [68] and by the decomposition of  $\text{B}_3\text{N}_3\text{Cl}_6$  [70].

Recently, Nakamura [85] proposed a new CVD method for depositing BN films using  $\text{NH}_3$  and  $\text{B}_2\text{H}_6$  between 300 and 1200°C. He has reported that the composition of the films could be closely controlled by regulating the pressure of source gases and stoichiometric BN films could be deposited at  $\text{NH}_3$  to  $\text{B}_2\text{H}_6$  ratios of 20 or more at a substrate temperature of 850°C.

A few other less popular chemical systems have been reported for BN production. Options are the use of organic compounds, such as the complexes  $\text{BH}_3\text{HN}(\text{CH}_3)_2$ ,  $\text{BHN}(\text{C}_2\text{H}_5)_3$ , or  $\text{B}_3\text{N}_3\text{H}_3(\text{CH}_3)_3$  with a ring structure and many others, which become usually liquids at slightly elevated temperatures ranging from 20 to

100°C[101,102]. Maya and Richards [103] used polymeric cyanoborane  $(CNBH_2)_n$ , as a single source for chemical vapor deposition of BN films. Paine and Narula [50] used poly borazinyamine precursors as starting materials in high temperature pyrolyses or in CVD to prepare hexagonal boron nitride. The system  $B_{10}H_{14}/NH_3$  has been reported to form both boron rich and stoichiometric BN films at a substrate temperature of 850°C.

Most of the research in the past was concentrated on the synthesis by using  $BCl_3$  or  $B_2H_6$  since they have sufficiently high vapor pressure at room temperature. In this study reactions of boron trichloride ( $BCl_3$ ) and ammonia ( $NH_3$ ) have been used to deposit boron nitride.  $BCl_3$  has been chosen for several reasons [67]:

- a)  $BCl_3$  is easier to handle than  $B_2H_6$ ,
- b)  $B_2H_6$  is explosive,
- c)  $BCl_3$  is less costly than  $B_2H_6$ , its price is about 10% that of  $B_2H_6$

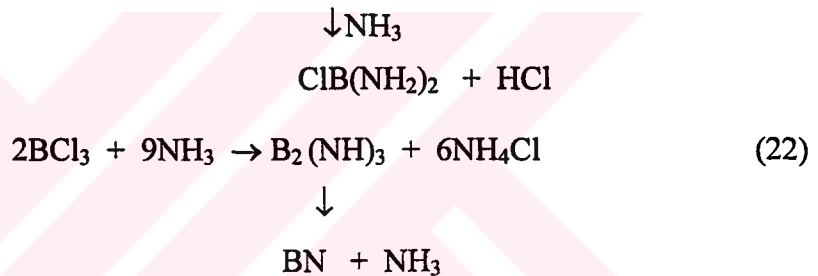
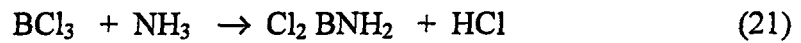
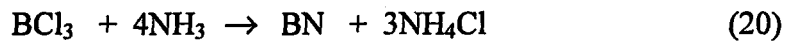
## 5.2 Properties of Boron Nitride

Some important properties of BN are its very high melting point, low specific gravity, low thermal expansion, high thermal conductivity, very high hardness, and chemical inertness. Structurally, BN exhibits two distinct crystal forms; namely, hexagonal and cubic. Hexagonal BN, which is the most common crystallographic form, has layers of alternating boron and nitrogen atoms arranged in a hexagonal network similar to that of graphite. It has been referred to as white graphite. There is also a cubic form of BN whose atomic structure and physical properties are similar to those of diamond. The theoretical density of BN is  $2.25 \text{ g/cm}^3$  [68]. It has been reported that the density of BN prepared by CVD varied strongly with deposition temperature and pressure and ranged from 1.35 to  $2.20 \text{ g/cm}^3$ . Trimethylborate-ammonia reaction produces a low density deposit in the range of 1.2 to  $1.5 \text{ g/cm}^3$  even at 1700°C[68].  $BCl_3-NH_3$  reaction produces deposits with densities of  $1.5 \text{ g/cm}^3$  at 1300°C but when the deposition

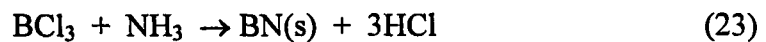
temperature is increased to 1600°C they obtained 2.0 g/cm<sup>3</sup> deposition. BN synthesized at 600°C is white powder [58]. It can be easily scratched and rubbed off, but it is sticky. Its porosity determined by BET nitrogen adsorption resulted in a surface area of 2.38 m<sup>2</sup>/g. However when sintered at 1600 K it turned into a transparent hard glassy material with negligible porosity. Thermal stability of BN films depends on the deposition conditions. Boron nitride does not display a normal melting behavior; however, it is reported to sublime under an atmosphere of nitrogen at 2300°C.

### 5.3 Chemical Reactions of BN Film Deposition

The reaction between BCl<sub>3</sub> and NH<sub>3</sub> is quite complicated, and the following reactions are believed to take place [105];



The overall reaction is,



During CVD reactions at 875 K, besides BN, other undesired chlorine and amine compounds of boron (given in eq.20-22) are also formed and they or their derivatives may deposit on the surface of substrate. The substrate should be sintered at high temperatures (1575 -1875 K) to evaporate these undesired compounds. At this stage a considerable weight decrease is expected. The sintering of the substrate will also help to form hexagonal or other crystal structures of BN. Sintering increases the mechanical properties of BN.

## CHAPTER 6

### FISSION REACTION AND NEUTRON TRANSPORT

#### 6.1 Comparison of Nuclear and Chemical Reactions

In chemical reactions the energy is released from the rearrangement of electrons after burning the fuel. The electrons of products have lower energy levels than those of reactant substances. The difference in energy levels comes out as heat of reaction.

In a nuclear reaction protons and neutrons (i.e., nucleons) are rearranged in the nucleus. The actual mass of a nucleus (also of the atom) is always less than the sum of the masses of the constituent nucleons. The energy equivalent difference of this mass is called binding energy. It gives a very strong force which keeps protons and neutrons together in the nucleus. In large nuclei such as uranium the electrostatic repulsion between protons become very important. Since the strong force has a very small range (i.e., in the order of  $10^{-13}$  cm which is about the size of nucleus), the nucleus becomes unstable and emit alpha and beta radiations. The nuclei such as U-235, U-233, and Pu-239 can be splitted into two even with a zero kinetic energy neutrons, i.e., they undergo fission. The energy introduced in the form of neutron mass is sufficient to cause fission. The probability of fission (e.g., fission cross section) decreases with increasing neutron energy as shown in Fig. 3 of Section 2.3. This is in contrast with the case in chemical reactions where the reaction rate increases with the speed (or temperature) of the reactants. The binding energy per nucleon in U-235 is about 7.6 MeV which is less than the mass energy of a neutron [110].

Since nuclei are small, most of the neutrons striking the target pass through the target without interacting with any of the nuclei. The number of collisions is proportional to the beam intensity. If there are  $n$  neutrons per volume (neutrons/cm<sup>3</sup>) in the beam and  $v$  (cm/s) is the speed of the neutrons, then “ $n \cdot v$ ” is called the flux of the beam. In chemical reactions the rate constant “ $k$ ” denotes the fraction of successful collisions giving chemical reaction per unit volume while the cross section “ $\sigma$ ” for nuclear reactions denote the number of successful collision on the surface of a target material. Its unit is “barn, (b)” and one barn is equal to  $10^{-24}$  cm<sup>2</sup>. There are a number of different reactions of neutrons with the target nuclei, each has a different cross section. These reactions are summarized in Table 6 [13,110].

**Table 6. Reactions of Neutron with Matter**

Type of interaction	Reaction	$\sigma$
Elastic	$n + X \rightarrow n + X$	$\sigma_s$
Inelastic	$n + X \rightarrow n + X^*$ $\downarrow$ $X + \gamma$	$\sigma_i$
Capture	$n + \frac{A}{Z}X \rightarrow \frac{A+1}{Z}X$	$\sigma_c$
Fission	$n + \frac{235}{92}U \rightarrow X + Y + 2.43n + \gamma$	$\sigma_f$

The sum of the microscopic cross sections for all possible interactions is known as the total microscopic cross section and is shown by the symbol  $\sigma_t$ , that is,

$$\sigma_t = \sigma_s + \sigma_i + \sigma_c + \sigma_f \quad (24)$$

The total microscopic cross section measures the probability that an interaction of any type will occur when neutron strikes a target. The sum of the microscopic cross sections of all absorption reaction is known as the absorption cross section

and is denoted by  $\sigma_a$ . Since capture and fission are absorption reactions we can express  $\sigma_a$  as;

$$\sigma_a = \sigma_c + \sigma_f \quad (25)$$

Note that  $\sigma_f$  is zero for non fissile materials. In Table 7,  $\sigma_f$  and  $\sigma_c$  values for some nuclei are given [13,110-113].

**Table 7. Microscopic Cross Section Data**

	Thermal Region (b)		Intermediate region (b)		Fast region 1.4-2.5 MeV (b)	
	$\sigma_f$	$\sigma_c$	$\sigma_f$	$\sigma_c$	$\sigma_f$	$\sigma_c$
U-233	529	46	760	140	1.93	0.04
U-235	583	98	275	140	1.28	0.06
U-238	4*	2.68	1.3*	277	0.49	0.06
Pu-239	742	269	300	200	1.93	0.04

\*  $\mu\text{b}$

The product of the atomic number density  $N$  (number density of nuclei in the target) and the microscopic cross section  $\sigma$  is called “macroscopic cross section,  $\Sigma$ ” and characterizes the probability of neutron interaction in a macroscopic piece of material (the target), whereas the microscopic cross section characterizes the probability of interaction with a single nucleus.

$$\Sigma \equiv N\sigma \equiv \text{cm}^{-1} \quad (26)$$

Similar to  $\sigma$  we can define macroscopic elastic scattering, inelastic scattering, capture and fission cross sections as  $\Sigma_s$ ,  $\Sigma_i$ ,  $\Sigma_c$ , and  $\Sigma_f$ , respectively. The total macroscopic cross section  $\Sigma_t$  is then equal to the sum of all these quantities. In Table 8 thermal region macroscopic cross sections of some materials have been presented.

**Table 8. Macroscopic Cross Section (2200 m/s)**

Element	$\Sigma_a$ (cm <sup>-1</sup> )	$\Sigma_s$ (cm <sup>-1</sup> )	$\Sigma_t$ (cm <sup>-1</sup> )
H <sub>2</sub> O	0.002	0.002	0.002
B	103.	0.346	104.
Gd	1403.	--	1403.
U	0.367	0.397	0.765
UO <sub>2</sub>	0.169	0.372	0.542
Pu	51.1	0.478	51.6

The product of the neutron speed  $v$  and  $\Sigma_t$  gives the frequency with which reactions occur and is shown as,

$$\text{Collision frequency} \equiv v\Sigma_t = \left[\frac{\text{cm}}{\text{s}}\right][\text{cm}^{-1}] \quad (27)$$

In chemical reactions the rate constant  $k_T$  depends on the temperature according to the Arrhenius relation,

$$k_T = k_0 e^{(-E_a/RT)} \quad (28)$$

where  $E_a$  is the activation energy. If the temperature of the medium increases the energy of the molecules or atoms becomes more energetic and their probability of collision is increased. When the collisions caused the necessary deformation (e.g., excitation of electrons) in orbits, a new product formation takes place. The high temperature (or high speed of molecules) helps to overcome the coulombic repulsion of electrons in the orbits. Therefore, the higher the temperature, the higher the penetration of molecules to each other, so the higher the deformation of molecules, and the higher the probability of new product formation.

In fission reaction, zero energy neutron has sufficient energy (i.e., mass energy) to cause fission as mentioned above. A neutron must spend sufficient time around nucleus so that it is captured. Therefore, fast neutrons are absorbed with difficulty by nucleus. As a result of this fission cross section decreases with neutron energy

as seen from Fig. 3 of Chapter 2.3. The intermediate zone involves too much fluctuations and is called resonance region. It has a quantum mechanical explanation. When the wavelength of neutron is exactly equal to the energy gap of shells in the nucleus we observe a resonance peak.

The fact that  $\sigma_f$  increases with decrease in neutron energy necessitates to slow down fast neutrons created in fission. Fast neutrons have an average energy of about 2 MeV and their spectrum is given in Appendix C. The conservation of momentum principle tells that the maximum speed loss occurs when equivalent mass objects collide with each other. Therefore, the neutrons must be collided with low mass atoms such as hydrogen, deuterium, beryllium and carbon for maximum momentum loss. These materials are called moderator. They slow the neutrons down to energies comparable to thermal energies of the nuclei in the reactor core. Reactors which are designed to work with low energetic neutrons are called thermal reactors. Such reactors require the minimum amount of fissile material for fueling and are the simplest reactor types to build and operate.

## 6.2 Equation of Continuity

In treating nuclear reactions, the equation of continuity is used. If the density of neutrons (or molecules) is higher in one part of the reactor than in another part, there will be a net flow of neutrons into the region of lower neutron density. The equation of continuity similarly gives the rate of change in number of neutrons in an arbitrary volume  $V$  within a medium containing neutrons. Neutron density in a system can be found by simply balancing the various mechanisms by which neutrons can be gained or lost from an arbitrary volume  $V$  within the system. In particular it follows that [111],

$$\left[ \begin{array}{l} \text{time rate of change} \\ \text{in number of} \\ \text{neutrons in } V \end{array} \right] = \left[ \begin{array}{l} \text{rate of gain} \\ \text{of neutrons} \\ \text{in } V \end{array} \right] - \left[ \begin{array}{l} \text{rate of} \\ \text{loss of} \\ \text{neutrons in } V \end{array} \right].$$



### 6.2.1 Rate of Change in Number of Neutrons in the Volume

The number of neutrons in  $V$  with energy  $E$  in  $dE$  and traveling in a direction  $\hat{\Omega}$  in  $d\hat{\Omega}$  within this volume is given as,

$$\# \text{ of neutrons in } V = \left[ \int_V n(\mathbf{r}, E, \hat{\Omega}, t) d^3r \right] dE d\hat{\Omega} \quad (29)$$

$\mathbf{r}$  denotes the space dependency of neutrons and  $d^3r$  the unit volume. In a nuclear reactor the target elements are stationary while neutrons are bouncing around due to collisions. The number density of neutrons is not homogenous because the reactor is a heterogeneous medium mainly made of fuel, structural materials and moderator. The interactions given in Table 6 are different in different media so this results in a nonuniform number density and nonuniform neutron flux distributions in a reactor.

In velocity coordinate system,  $\theta$  is the angle between the velocity vector  $\mathbf{v}$  and  $v_z$  coordinate while  $\phi$  is the angle between the projection of  $\mathbf{v}$  on  $v_x$ - $v_z$  plane and  $v_x$  coordinate.

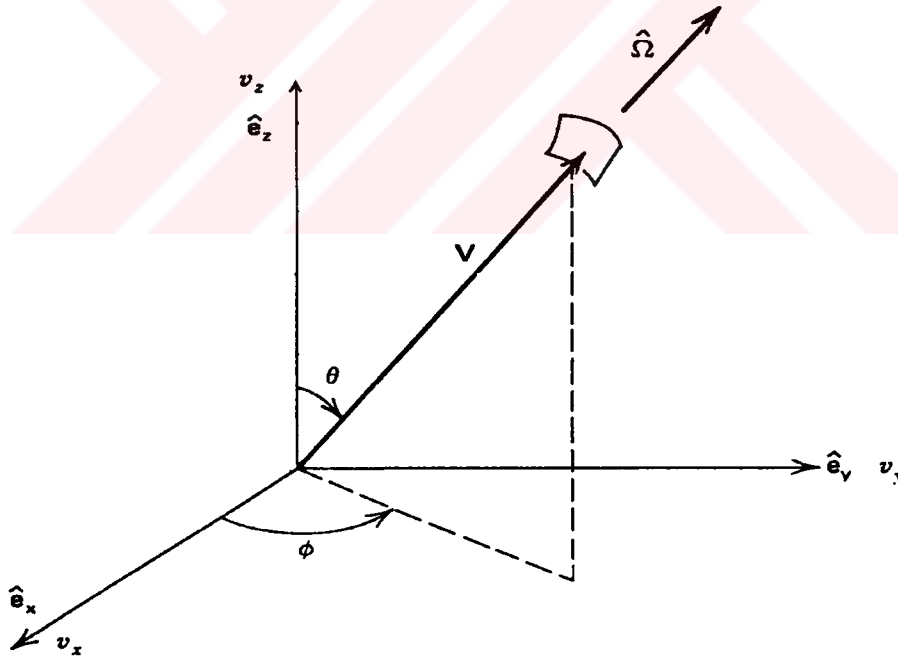


Figure 5. The neutron direction vector  $\hat{\Omega}$  in spherical coordinates.

In reactor analysis it will be more convenient to describe the neutron motion with slightly different variables. Neutron velocity vector will be decomposed into two components, one variable characterizing the neutron speed and a second variable for the neutron direction of motion. The kinetic energy of neutron  $E=1/2mv^2$  is used instead of the neutron speed. To specify the direction of neutrons the unit vector  $\hat{\Omega}$  is introduced such that,

$$\hat{\Omega} = \frac{\mathbf{v}}{|\mathbf{v}|} = \hat{e}_x \sin\theta\cos\phi + \hat{e}_y \sin\theta\sin\phi + \hat{e}_z \cos\theta. \quad (30)$$

Since  $n(\mathbf{r}, E, \hat{\Omega}, t)$  is “density” in  $E$  and  $\hat{\Omega}$  space, we must multiply it by  $dE$  and  $d\hat{\Omega}$  to get a number. The time rate of change of this number, then is given by,

$$\frac{\partial}{\partial t} \left[ \int_V n(\mathbf{r}, E, \hat{\Omega}, t) d^3r \right] dE d\hat{\Omega} = \text{gain in } V - \text{loss from } V \quad (31)$$

$$\frac{\partial}{\partial t} \left[ \int_V n(\mathbf{r}, E, \hat{\Omega}, t) d^3r \right] dE d\hat{\Omega} = \left[ \int_V \frac{\partial n}{\partial t} d^3r \right] dE d\hat{\Omega} \quad (32)$$

## 6.2.2 Gain Mechanism

### 6.2.2.1 Neutron Source in the Volume (e.g., fission)

The neutron source term, can be given by,

$$\left[ \int_V s(\mathbf{r}, E, \hat{\Omega}, t) d^3r \right] dE d\hat{\Omega} \quad (33)$$

where,

$$s(\mathbf{r}, E, \hat{\Omega}, t) d^3r dE d\hat{\Omega} \equiv \left[ \begin{array}{l} \text{rate of source neutrons} \\ \text{appearing in } d^3r \text{ about } \mathbf{r}, dE \text{ about } E, \\ \text{and, } d\hat{\Omega} \text{ about } \hat{\Omega} \end{array} \right]$$

### 6.2.2.2 Scattering of Neutrons from other Energies and Directions

Another gain mechanism of neutrons may come from scattering collision of neutrons from other energies  $E'$  and directions  $\hat{\Omega}'$ . If a neutron of energy  $E$  will suffer scattering collision, then scattering probability (i.e., microscopic cross section) is found by integrating differential cross section  $\sigma_s(E \rightarrow E')$  over all final energies  $E'$  from zero to infinity. It is,

$$\sigma_s(E) = \int_0^{\infty} \sigma_s(E \rightarrow E') dE' \quad (34)$$

Once again if the differential scattering cross section which describes the probability that  $n$  number of neutrons scatters from incident direction  $\hat{\Omega}$  to a final direction  $\hat{\Omega}'$  is  $\sigma_s(\hat{\Omega} \rightarrow \hat{\Omega}')$  then the scattering probability to all directions of neutrons is,

$$\sigma_s(\hat{\Omega}) = \int_{4\pi} \sigma_s(\hat{\Omega} \rightarrow \hat{\Omega}') d\Omega' \quad (35)$$

note that,

$$\Sigma_s(E \rightarrow E') \equiv N\sigma_s(E \rightarrow E') \quad (36)$$

$$\Sigma_s(\hat{\Omega} \rightarrow \hat{\Omega}') \equiv N\sigma_s(\hat{\Omega} \rightarrow \hat{\Omega}') \quad (37)$$

where,

$N$  = atomic number density

$\Sigma_s$  = macroscopic scattering cross section

Finally the probability of scattering of neutrons from  $dE$  about  $E$ ,  $d\hat{\Omega}$  about  $\hat{\Omega}$  from other energies  $E'$  and directions  $\hat{\Omega}'$  is found in terms of double differential scattering cross sections,

$$\left[ \int_{4\pi} d\hat{\Omega}' \int_0^{\infty} v \Sigma_s(E' \rightarrow E, \hat{\Omega}' \rightarrow \hat{\Omega},) n(\mathbf{r}, E', \hat{\Omega}', t) dE' \right] dE d\hat{\Omega} \quad (38)$$

If Eq.38 is integrated over the volume V then neutrons suffering a scattering in V is found from,

$$\left[ \int_V d\mathbf{r}^3 \int_{4\pi} d\hat{\Omega}' \int_0^{\infty} v \Sigma_s(E' \rightarrow E, \hat{\Omega}' \rightarrow \hat{\Omega},) n(\mathbf{r}, E', \hat{\Omega}', t) dE' \right] dE d\hat{\Omega} \quad (39)$$

### 6.2.3 Loss Mechanism

#### 6.2.3.1 Neutrons in the Volume Suffering Collision

Neutrons may be lost due to elastic and inelastic collisions, and capture and fission reactions. The probability of a neutron which may be lost in a collision is found by multiplying the number of neutrons with general collision frequency which is given by  $v\Sigma_t$  term. The rate at which neutrons suffer collision at a point  $\mathbf{r}$  is then expressed as,

$$v\Sigma_t(\mathbf{r}, E) n(\mathbf{r}, E, \hat{\Omega}, t) \quad (40)$$

and if this term (collision rate) is integrated over the volume V, then the loss term due to all collisions is found from,

$$\text{loss} = \left[ \int_V v\Sigma_t(\mathbf{r}, E) n(\mathbf{r}, E, \hat{\Omega}, t) d^3\mathbf{r} \right] dE d\hat{\Omega} \quad (41)$$

#### 6.2.3.2 Leakage into or Diffusion from the Volume

Neutrons may also be lost by diffusion from the volume V or some neutrons may leak into the volume V. The concept of angular current density  $\mathbf{j}(\mathbf{r}, E, \hat{\Omega}, t)$  is used to calculate the net leakage of neutrons through the total surface S. The leakage rate of neutrons at energy E and direction  $\hat{\Omega}$  from the surface  $dS$  is written as,

$$\mathbf{j}(\mathbf{r}, E, \hat{\Omega}, t) \cdot d\mathbf{S} = v\hat{\Omega}n(\mathbf{r}, E, \hat{\Omega}, t) \cdot d\mathbf{S} \quad (42)$$

Thus, the total leakage contribution over the entire surface area  $S$  is

$$\int_S v\hat{\Omega}n(\mathbf{r}, E, \hat{\Omega}, t) dS \quad (43)$$

Making the use of the Gauss's theorem,

$$\int_S (\mathbf{A}(\mathbf{r})) dS = \int_V (\nabla \cdot \mathbf{A}(\mathbf{r})) d^3r, \quad (44)$$

to find

$$\left[ \int_S v\hat{\Omega}n(\mathbf{r}, E, \hat{\Omega}, t) dS \right] dEd\hat{\Omega} = \left[ \int_V \nabla \cdot v\hat{\Omega}n(\mathbf{r}, E, \hat{\Omega}, t) d^3r \right] dEd\hat{\Omega} \quad (45)$$

Since  $v$  and  $\hat{\Omega}$  do not depend on  $\mathbf{r}$ , one can write

$$\nabla \cdot v\hat{\Omega} = v\hat{\Omega} \cdot \nabla$$

Hence, using this relation, Eq. 45 becomes,

$$\left[ \int_V v\hat{\Omega} \cdot \nabla n(\mathbf{r}, E, \hat{\Omega}, t) d^3r \right] dEd\hat{\Omega} \quad (46)$$

#### 6.2.4 Combination of all the Terms

We can now summarize the above arguments as:

1. rate of change of neutron source is,

$$\left[ \int_V n(\mathbf{r}, E, \hat{\Omega}, t) d^3r \right] dEd\hat{\Omega} \quad (47)$$

2. gain of neutrons from neutron source is,

$$\left[ \int_V s(\mathbf{r}, E, \hat{\Omega}, t) d^3r \right] dEd\hat{\Omega} \quad (48)$$

3. gain of neutrons from different energies  $E'$  and directions  $\hat{\Omega}'$  into  $E$ , and  $\hat{\Omega}$  due to scattering collisions,

$$\left[ \int_V d\mathbf{r}^3 \int_{4\pi} d\hat{\Omega}' \int_0^\infty v \Sigma_s(E' \rightarrow E, \hat{\Omega}' \rightarrow \hat{\Omega}) n(\mathbf{r}, E', \hat{\Omega}', t) dE' \right] dE d\hat{\Omega} \quad (49)$$

4. loss of neutrons due to elastic and inelastic collisions, and capture and fission reactions is,

$$\left[ \int_V v \Sigma_t(\mathbf{r}, E) n(\mathbf{r}, E, \hat{\Omega}, t) d^3\mathbf{r} \right] dE d\hat{\Omega} \quad (50)$$

5. neutrons leaking into or diffusing from the  $V$  is

$$\left[ \int_V v \hat{\Omega} \cdot \nabla n(\mathbf{r}, E, \hat{\Omega}, t) d^3\mathbf{r} \right] dE d\hat{\Omega} \quad (51)$$

Finally, the rate of change of neutrons is found by adding the gain terms (Eq.48 and 49) and subtracting the loss terms (Eq.50 and 51), such that,

$$\int_V d^3\mathbf{r} \left[ \frac{\partial n}{\partial t} + v \hat{\Omega} \cdot \nabla n + v \Sigma_t n(\mathbf{r}, E, \hat{\Omega}, t) \right] dE d\hat{\Omega} - \int_0^\infty dE' \int_{4\pi} d\hat{\Omega}' v \Sigma_s(E' \rightarrow E, \hat{\Omega}' \rightarrow \hat{\Omega}) n(\mathbf{r}, E', \hat{\Omega}', t) - s(\mathbf{r}, E, \hat{\Omega}, t) \Big] dE d\hat{\Omega} = 0 \quad (52)$$

and since mathematically,

$$\int_V f(\mathbf{r}) d^3\mathbf{r} = 0 \Rightarrow f(\mathbf{r}) \equiv 0. \quad (53)$$

then we arrive at a balance equation,

$$\begin{aligned} & \frac{\partial n}{\partial t} + v \hat{\Omega} \cdot \nabla n + v \Sigma_t n(\mathbf{r}, E, \hat{\Omega}, t) \\ & = \int_{4\pi} d\hat{\Omega}' \int_0^\infty dE' v \Sigma_s(E' \rightarrow E, \hat{\Omega}' \rightarrow \hat{\Omega}) n(\mathbf{r}, E', \hat{\Omega}', t) + s(\mathbf{r}, E, \hat{\Omega}, t). \end{aligned} \quad (54)$$

In chemical reactions the temperature dependence of the constant  $k_T$  can be formulated with Arrhenius law so the solution of this equation is quite simple. However neutron transport equation is very difficult to solve because the cross

section dependence on energy is extremely complicated including resonance structure, threshold effect, and so on. Figure 3 of Section 2.3 gives cross section dependence on energy for U-235 isotope. These considerations would immediately suggest that any attempt to solve the transport equation for a realistic system involves heavy use of computers. Some approximations need to be made to solve Eq.54.

### **6.3 One Group Model**

The simplest model of neutron transport equation is the application of one group theory. It assumes that all of the neutrons can be characterized by only a single speed or energy. One group method assumes all neutrons to be thermal.

The one group treatment is highly approximate, but it is very simple and leads to conclusions which are qualitatively correct.

### **6.4 Two Group Model**

Although one group method works at all, the practical reactor calculations will require a more realistic treatment of the neutron energy dependence. A second approximation to that is to assume that all the neutrons can be divided into two groups, namely fast and thermal neutrons. The cut of energy of 0.625 eV is set arbitrarily and below this energy level neutrons are considered as thermal and above are considered as fast neutrons.

### **6.5 Multigroup Model**

Two group method has been still further advanced by introducing additional neutron energy groups. This is achieved by assuming neutron energy variable  $E$  as a continuous variable ranging from  $10^{-3}$  eV up to  $10^7$  eV and discretizing it into energy intervals. The neutron transport equation is then integrated over each energy group to define appropriate average values of the various cross sections

characterizing each group. For example one would define the absorption cross section characterizing a group  $g$  as

$$\Sigma_{a_g} \equiv \frac{\int_{E_g}^{E_{g-1}} \Sigma_a(E) \phi(E) dE}{\int_{E_g}^{E_{g-1}} \phi(E) dE} \quad (55)$$

where  $\phi$  is neutron flux [111].

Within each group, the neutrons are assumed to diffuse, without energy loss, until the average number of collisions would be required to decrease their energy to that of the lower group. At this point it is supposed that the neutrons are suddenly transferred to the latter group. This process is supposed to continue while neutron energy is degraded from the group of highest (fast group) energy to the lowest (thermal groups) energy.

In multigroup model, the solution of the differential equations obtained is a major problem, and such set of equations can be solved using numerical methods by using computers. Sometimes one or more independent variables may be eliminated. The most useful approximation to the transport equation is to eliminate angular variable .



## CHAPTER 7

### EXPERIMENTS

#### 7.1 Objective

As mentioned in Section 1.5 the aim of this study is first to obtain  $\text{UO}_2$  and  $\text{UO}_2$ - $\text{Gd}_2\text{O}_3$  nuclear fuels by sol-gel technique, and then to coat the fuel pellets with boron nitride thin layers by chemical vapor deposition process. The final stage is to show the fuel utilization behavior enhanced, and plutonium yield by using WIMS-D/4 code.

Most fuels are usually made with powder technique which results in lower physical properties than sol-gel technique. So sol-gel fuel production has been one of the objectives of this work.

All fuels developed so far in the world contains either gadolinia or  $\text{ZrB}_2$  as burnable absorber. In this research a new boron layer, BN has been studied, and the effects of two burnable absorbers on the neutronics has been investigated.

In summary the followings have been done in this research work:

- a) sol-gel technique has been very roughly studied in the past by others for nuclear fuel coating, and it has investigated here in full detail,
- b) neither BN nor CVD technique has been used before by others, and investigated first time in this work,

- c) a fuel with two burnable absorbers has been produced, and its physical properties have been studied,
- d) neutronic calculations of the fuel produced have been carried out.

## 7.2 Experimental Methods

The experimental procedure was shown diagrammatically in the following figure:

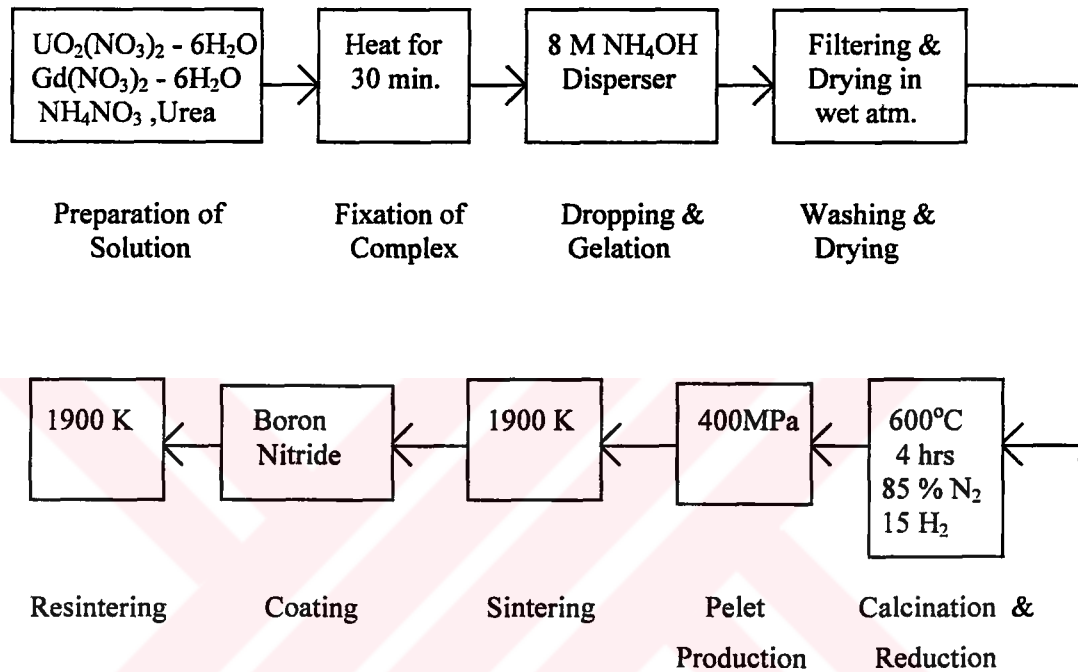


**Figure 6. Schematic summary of the experimental steps**

The raw materials used are;

Uranyl nitrate hexahydrate	: UO <sub>2</sub> (NO <sub>3</sub> ) <sub>2</sub> ·6H <sub>2</sub> O
Gadolinium nitrate, hexahydrate	: Gd(NO <sub>3</sub> ) <sub>3</sub> · 6H <sub>2</sub> O
Ammonium solution, 8-12 M	: NH <sub>4</sub> OH
Urea	: H <sub>2</sub> N-CO-NH <sub>2</sub>
Ammonium nitrate	: NH <sub>4</sub> NO <sub>3</sub>
Boron trichloride	: BCl <sub>3</sub>
Ammonia gas	: NH <sub>3</sub>
Gases (nitrogen, hydrogen, argon)	: N <sub>2</sub> , H <sub>2</sub> , A

Equipments used : Stirrer, drier, press, furnace (medium and high temperature).

### 7.2.1. Sol-Gel Fuel Preparation

Small spherical particles of  $\text{UO}_2$  or  $\text{UO}_2\text{-Gd}_2\text{O}_3$  were produced from their nitrate solutions by this process which mainly consisted of ten operations:(a) sol preparation, (b) sol drop dispersion, (c) gelation, (d) washing of gelled microspheres, (e) aging, (f) drying, (g) calcination, (h) reduction, (i) pellet making, and (j) sintering.

In this work three types of solutions were prepared to obtain fuels with the following compositions:

- a)  $\text{UO}_2$ -only,
- b)  $\text{UO}_2\text{-Gd}_2\text{O}_3$  (5%),
- c)  $\text{UO}_2\text{-Gd}_2\text{O}_3$  (10%).

#### 7.2.1.1 Sol Preparation

The solution compositions used in the experiments is given in Table 9.

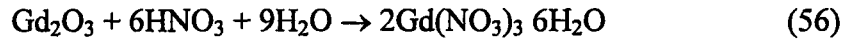
**Table 9. Compositions of Solutions**

Chemicals	Solution I	Solution II	Solution III
Uranyl nitrate hexahydrate	27.00*	25.95	25.95
Gadolinium nitrate hexahydrate	---	1.83	3.86
Ammonium nitrate	22.54	21.67	21.67
Urea	14.44	13.88	13.88
Water	36.02	36.67	34.64

\*numbers are weight percentages

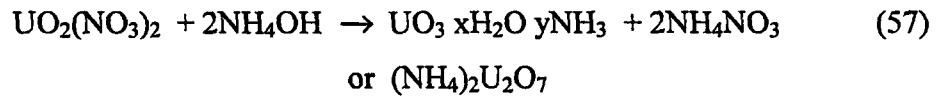
The weight percentages of uranyl nitrate, ammonia solution, and urea have been taken to be in accordance with literature values [38-39]. This composition is known to have good gelation property.

Gadolinium nitrate was prepared from its oxide according to the following chemical reaction;

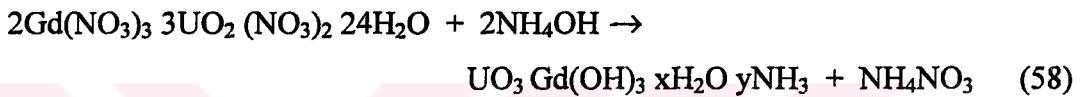


The product was heated above 91°C which is the melting point of the crystal, and recrystallized in cold water.

In general, the gelation of the droplets is accomplished by neutralizing uranyl nitrate or uranyl nitrate-gadolinium nitrate solution with ammonia in a precipitation reaction,



or



The solution was boiled for half an hour to prevent the precipitation of urea. The complexing of  $\text{UO}_2^{+2}$  with urea is completed and stabilized by boiling. A clear and stable solution was obtained. The pH of the solution was measured at 20°C and was found to be 3.5.

The ammonia concentration must be at least 8 M. At lower concentrations the precipitation is slowed down, and the spheres can be deformed by mechanical stress during collection and subsequent transport [106].

### 7.2.1.2 Dropping and Gelation

Sol drops can be formed from a larger mass of sol by applying forces, such as gravity, centrifugal field, shear, inertia, interfacial tension, and electrostatic repulsion. Some dispersers and the forces of importance are as follow:

a) two fluid nozzles: interfacial tension,

- b) rotary feeder: shear and centrifugal,
- c) shear nozzle: shear and inertia,
- d) electrostatic nozzle: electrical potential,
- e) falling drop dispersers: gravity,
- f) vibrating capillary: interfacial tension, inertia, and shear.

Falling drop disperser has been the most useful sol dispersion device and used in this study. Gelation was carried out in the sol-gel apparatus shown in Fig.7. The solution is sent through the inner capillary and nitrogen gas is sent from the outside zone. The solution is atomized under the effect of pressurized nitrogen gas. The sol-gel apparatus contains two phases. The upper phase is water immiscible and is composed of 50% toluene and 50% isoamyl alcohol. The lower phase is 8M ammonium hydroxide. The fine droplets formed in the nozzle hit the surface of the organic phase. Isoamyl alcohol partly dissolves ammonium hydroxide in the upper phase and thus provides prehardening. Gelation is completed in the lower phase. The gelled particles were then collected at the bottom of the apparatus.

#### **7.2.1.3 Washing, Aging and Drying**

The gelled spherical particles were washed and filtered with concentrated ammonium hydroxide solution to remove ammonium nitrate. The microspheres were then aged in 8M ammonia solution. During aging 70-80% shrinkage was observed. In the experiment, the time of aging was 30 minutes and the temperature was 40-50°C. The aged particles were then dried in an oven under wet atmosphere which minimizes cracking of particles. Then the particles were dried in a wet atmosphere for 1-2 hours [106-107]. The temperature should not exceed 400 K. Figure 8 shows the photographs of dried microspheres.

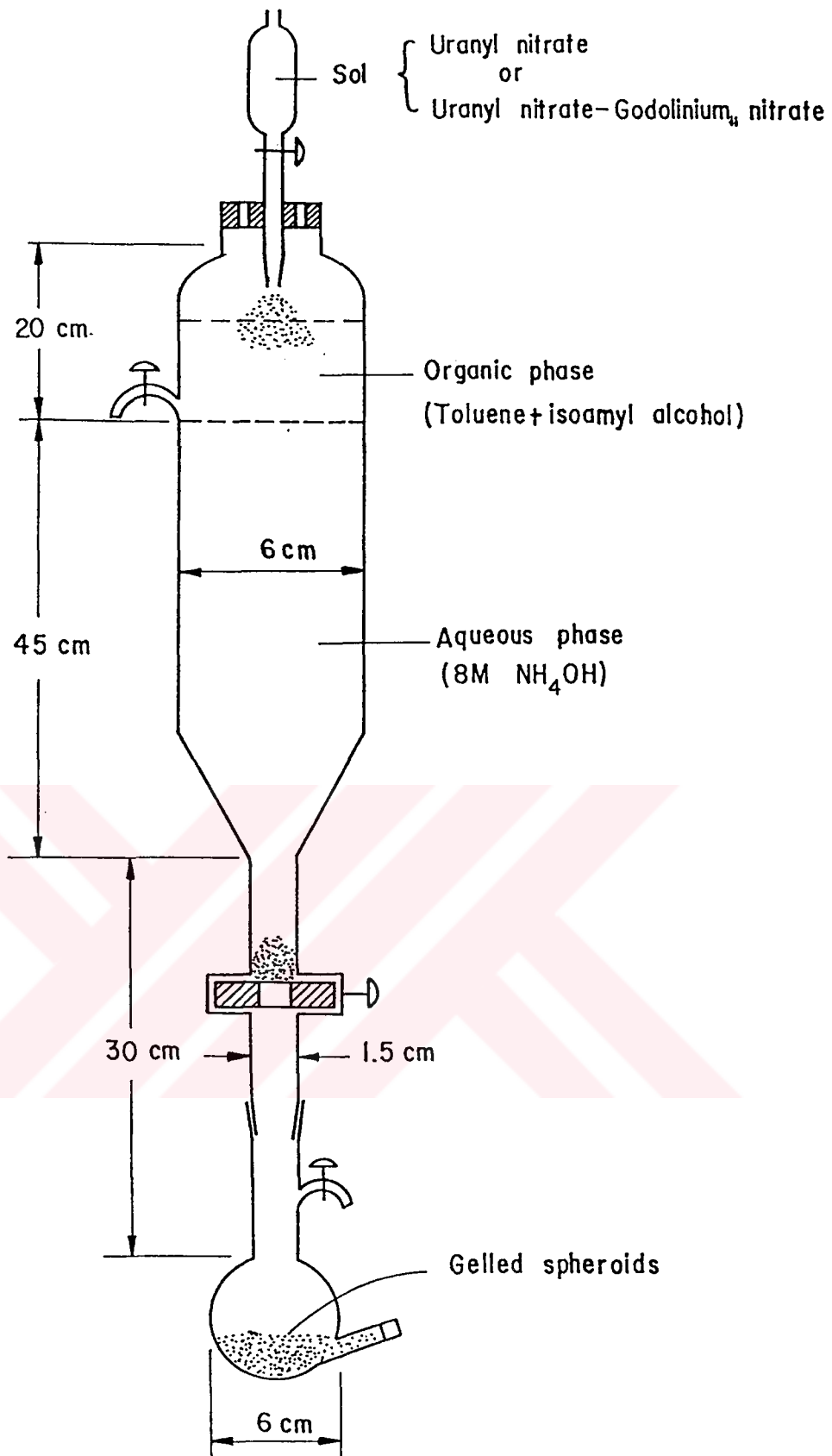


**Figure 7. Sol-gel apparatus**

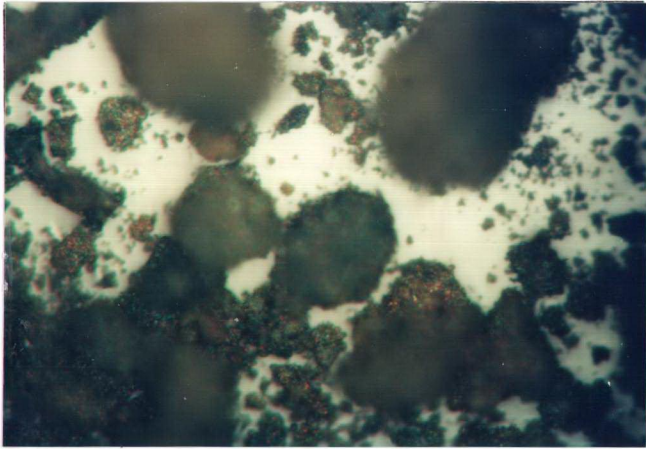


Figure 8 a. Pure  $\text{UO}_2$  microspheres (yellow cake)

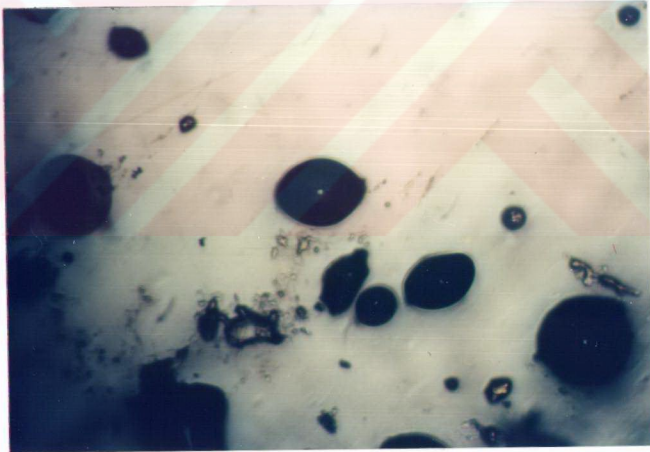


Figure 8 b.  $\text{UO}_2$ -5%  $\text{Gd}_2\text{O}_3$  mixture

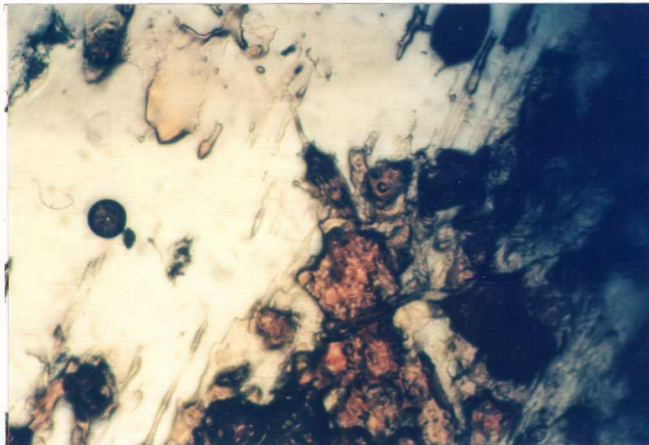


Figure 8 c.  $\text{UO}_2$ -10%  $\text{Gd}_2\text{O}_3$  mixture

#### 7.2.1.4 Calcination and Reduction

For calcination, dried and gelled microspheres were introduced into a tube furnace (Heraeus type : ROM 5170) in an alumina boat. It was then heated to 673 K under nitrogen atmosphere. The temperature was kept constant for four hours. Denitration takes place and triuranium octoxide ( $\text{U}_3\text{O}_8$ ) forms. Then 15%  $\text{H}_2$  + 85%  $\text{N}_2$  gas mixture was introduced into the furnace to reduce  $\text{U}_3\text{O}_8$  to uranium dioxide ( $\text{UO}_2$ ). Reduction lasted about 3-4 hrs and then the furnace was cooled down to room temperature under the same gas mixture. Finally, the reduced samples were passivated with air in a very short time period to reduce the rate of reoxidation at room temperature and to permit longer storage time before sintering the pellets. The reduction experiment was repeated at 1000 K to investigate the effect of reduction temperature on the fuel properties.

The reduction and sintering were carried at the same tube furnace which is heated by molybdenum silicide heating wire and is kept under pure hydrogen atmosphere to prevent oxidation. The furnace is shown in Fig 9. The powder or pellet samples were put into alumina boats and then introduced into the central zone of the furnace.[108-109]



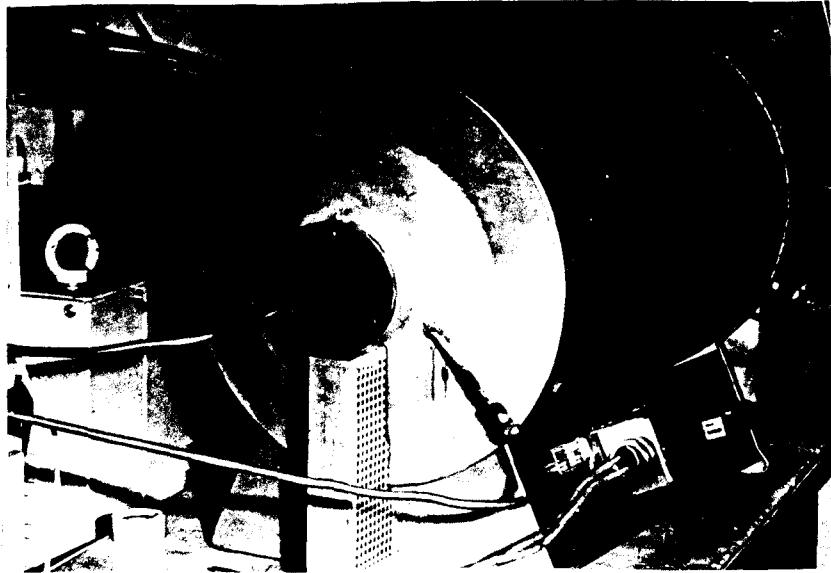


**Figure 9. Reduction and sintering furnace**

The porosity and total surface area of powder was measured by a surface analyzer (Micromeritics, Model:220 GB). Pore size distribution of powder was determined by using a nitrogen adsorption surface area and pore size analyzer, by BET method (Micromeritics 5, Model: 200-34002-01), and the pore size distribution of pellets was determined by a mercury porosimeter (Micromeritics 5, Model: 9310). The powder flowability was measured by using a device built up according to Turkish Standards (TS 4483, April 1985). The crystal structure was examined by using an X-ray diffractometer, XRD (Philips, Model:PW-1840). The oxygen to uranium ratio (O/U) of specimens was studied by using a thermal gravimetric analyzer (Schimadzu, Model TM30). The powder flowability and thermal gravimetric analyses were carried in ÇNAEM

#### **7.2.1.5 Pellet Production**

Pellets were compacted at three different pressures which were 200 MPa, 400 MPa, and 600 MPa. A green pellet (i.e., unsintered pellet) had a diameter of 6 mm and an height of about 5-7 mm. The binder was added to the reduced powder to eliminate the cracking of the pellets during compaction. Stearic acid, polyvinyl alcohol (PVA), polyethylene glycol, and paraffin were the main binders used in

ceramic technology. In this study the effect of binders on porosity distribution was investigated by using stearic acid and PVA. The binders were added at about 3 wt%. Stearic acid was directly mixed with powder, on the other hand, PVA was introduced by mixing 10 % solution in alcohol with powder. It was dried at around 50°C before making pellets.

The effect of grinding of  $\text{UO}_2$  powder on the porosity distribution was investigated by preparing two different powder samples. One sample was sufficiently ground but not sieved, the other one was passes through a 400 mesh sieve which had a screen size of 37  $\mu\text{m}$ .

#### 7.2.1.6 Sintering

Sintering was carried under 15%  $\text{H}_2$  + 85%  $\text{N}_2$  gas mixture at 1900 K, for three hours, then the furnace was cooled to room temperature under the same gas atmosphere. Figure 10 shows the calcined (green pellet) and sintered pellet.

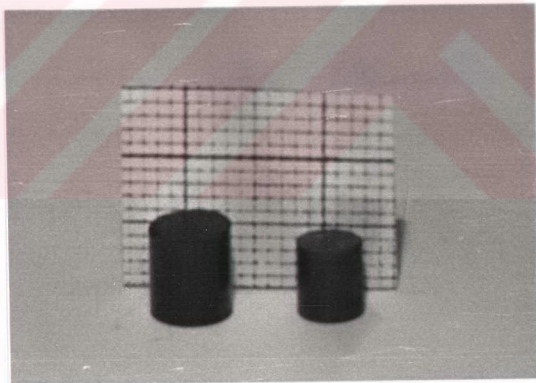


**Figure10. The calcined (green pellet, on the left) and the sintered fuel pellet (on the right)**

The porosity of the sintered specimens were measured by using a mercury porosimeter (Micromeritics, Model:200-34002-01) and grain sizes were analyzed by a scanning electron microscope (JSM, model:6400).

### 7.3 Boron Nitride Film Deposition and Sintering Experiments

The BN films used in these experiments were formed by reacting  $\text{NH}_3$  and  $\text{BCl}_3$  at temperatures ranging from  $400^\circ\text{C}$  to  $600^\circ\text{C}$  in a CVD tube furnace heated by silicon carbide heating element at 1 atm. pressure using the reactant system,  $\text{BCl}_3$ ,  $\text{NH}_3$ ,  $\text{H}_2$  and argon (Ar). Since  $\text{BCl}_3$  readily reacts with  $\text{NH}_3$  at room temperature and forms a white powder, these gases were introduced separately into the furnace in order to mix them in the vicinity of the substrate and to avoid premature reaction. Figure 11 shows the CVD tube furnace used and Fig. 12 shows the white BN powder produced at the outlet of the furnace.

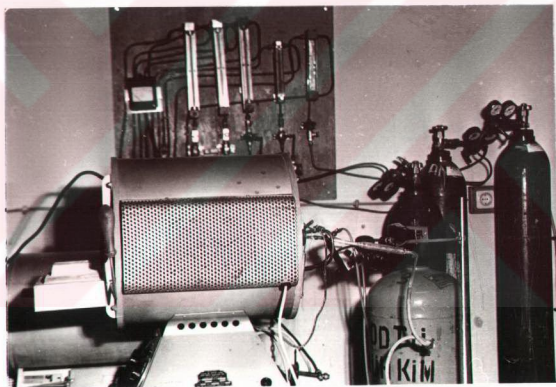
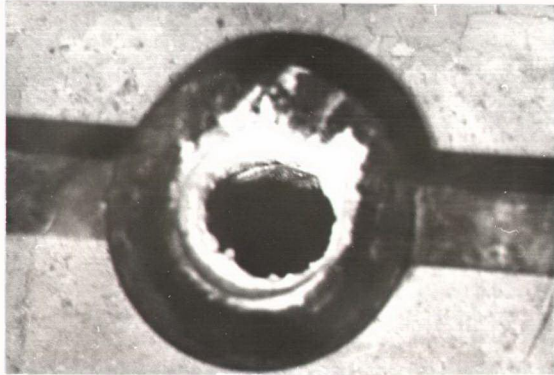


Figure 11. Tube furnace for CVD



**Figure 12. White powder at the outlet of the furnace**

A mixed gas of  $\text{NH}_3$  and  $\text{H}_2$  was introduced directly into the center of the reaction tube through a thin alumina tube, while another mixed gas of  $\text{BCl}_3$  and Ar was introduced at a location 20 mm ahead of the first stream. The mixing zone of  $\text{BCl}_3$  and  $\text{NH}_3$  gases are one of the important factors for the synthesis of BN film using  $\text{BCl}_3+\text{NH}_3$  system. Various methods of introducing reactant gases separately into the reactor were developed [59,60,62]. Clerc and Gerlach [62] mixed  $\text{BCl}_3$  and  $\text{NH}_3$  at a distance of 90 mm from the substrate. Takahashi et al. [59,60] mixed the gases at 50 and 20 mm from the inlet.

In this study, some preliminary experiments were carried out to determine the optimum distance between the substrate and the mixing zone of  $\text{BCl}_3\text{-NH}_3$  system. The deposition of BN was done on quartz plates as shown in Fig. 13. Then fuel pellets were kept at the appropriate position. The minimum distance was about 30 mm.

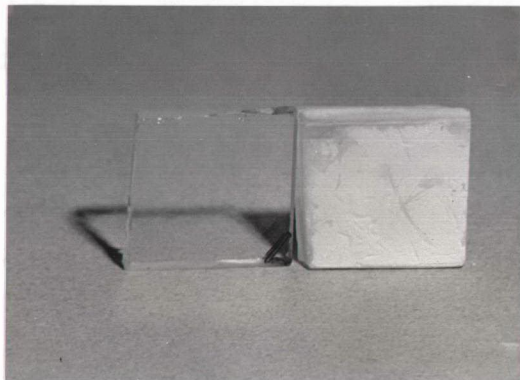


**Figure 13. Plain quartz plate (on the left) and BN deposited quartz plate (on the right)**

Although  $\text{BCl}_3$  and  $\text{NH}_3$  readily react, the outlet gases were bubbled through a basic water solution to decompose the possible unreacted  $\text{BCl}_3$ , according to reaction,

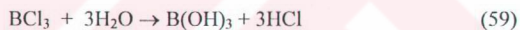
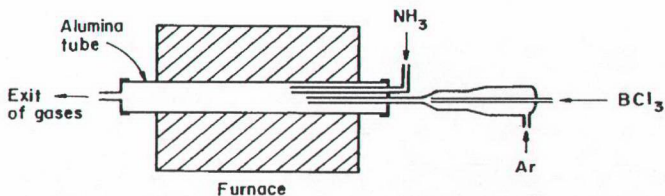
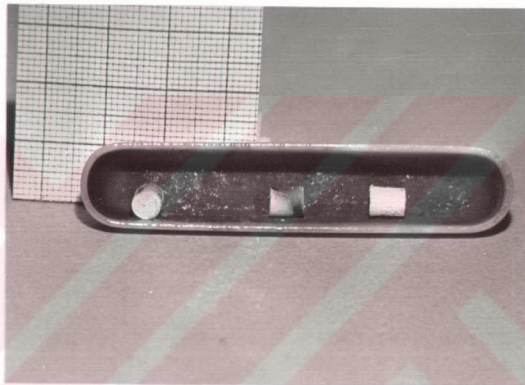


Figure 14 shows the schematic representation of the furnace used in CVD of BN.



**Figure 14. CVD furnace**

The general deposition procedure was as follows: After the substrates were placed inside the reactor, it was heated to the desired temperature under Ar atmosphere. The deposition started when the reactants were simultaneously fed into the furnace. The deposition was terminated by stopping  $\text{BCl}_3$  and  $\text{NH}_3$  flows and subsequently cooling the furnace again under Ar atmosphere. After the deposition the substrate was heated to sintering temperatures (1575, 1875 K) then, the furnace was cooled down to room temperature in a stream of Ar. Figure 15 shows fuel pellets after the deposition experiments.



**Figure 15. BN deposited fuel pellets.**

The porosity and IR spectra of white powder obtained at the outlet of the furnace was measured by a surface area analyzer (Micromeritics, Model: 220 GB), and IR spectrophotometer (Schimadzu, Model: IR 470) respectively. The crystal structure of powder and sintered BN was examined by using XRD (Philips, Model: PW-1840) and by using SEM (JSM, Model: 6400).

## CHAPTER 8

### FRACTAL ANALYSIS OF FUEL GRAINS

The notion of fractals has been introduced about two decades ago and revolutionized our understanding of nonlinear phenomena. The concept has found very wide application in basic sciences from atoms to galaxies, in all engineering fields, and also in medicine, biology, music, and sociology. Examples range from definition of the convoluted structure of proteins, molecule/surface interactions, description of porous surfaces (such as coals, catalysts etc.), characterization of aggregates, for example concrete and other engineering materials, investigation of adsorption, desorption, and diffusion characteristics of molecules, and other fields of sciences such as crystal growth, oil sciences, chromatography, electrochemistry, hydrology, oil technology, ceramics, animal and plant population dynamics, nerve conduction, and heart beats in animals, stock market exchanges, business administration, etc.

#### 8.1 Models of Surfaces

##### 8.1.1 Euclidean Geometry : Man Made Surfaces

The majority of man made surfaces and natural surfaces are mimic simple Euclidean geometric forms such as spheres, cylinders, planes, or their derivatives. In an Euclidean model the surface is thought of as the sum of two parts: first, a simple, analytic, Euclidean shape that describes the overall form of the object and, second, a random departure from the Euclidean ideal which is often called

“roughness”. The roughness of man made surfaces can be described with a stationary model, which means that the average or mean value of the topography does not vary strongly with position.

### 8.1.2 Fractal Geometry

Most natural surfaces are nonstationary which means that the roughness features change as a function of positions. Because fractal geometry does not rely on Euclidean shapes, fractal models provide more realistic framework for the descriptions of many natural surfaces.

## 8.2 Principles of Fractal Geometry

In order to characterize so-called irregular geometric structures Mandelbroth [121] has developed a new non-Euclidean geometry. He showed that many naturally occurring irregular or random structures can be measured and categorized successfully in terms of well-defined basic concepts. The fractal dimension,  $d_F$  is a measure of self-similarity which implies that a structure is invariant to changes of scale. An example to self similarity is given in Fig.16 [122].

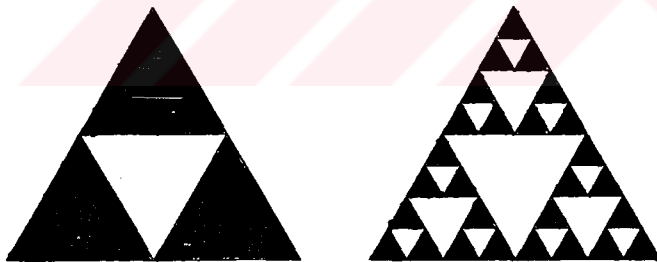


**Figure 16. Example of a fractal object: the Sierpinski gasket**



The concept of self similarity is central to fractal geometry: the fractal object contains features of different sizes that are invariant under ordinary geometric scaling, i.e., they look similar at different magnifications. If a surface, for example, is self similar, a small portion of the surface, when magnified isotropically, will appear statistically identical to the entire surface. The fractal dimension is equal to the exponent that relates the number of self-similar subunits of an object to the size of the subunit. If  $N(S)$  is the number of subreplicas of dimension  $S$ , then it is found that  $N(S)$  can be related to the size of its subsequent subunits as,

$$N(S) = AS^{-d_F} \quad (60)$$

where  $d_F$ , the fractal dimension, depends on the particular problem being solved. For example the famous Sierpinski gasket consists of triangles embedded within triangle. Successively smaller triangles have edges of size  $L/2^n$ , where  $n$  is the number of subreplications. Likewise there are  $3^n$  triangles at every level of subdivision hence for arbitrary  $n$ ;

$$N(S)=3^n \quad (61)$$

and,

$$S=L/2^n \quad (62)$$

Eliminating  $n$  between Eq.61 and 62 one obtains:

$$N(S) = (L/S)^{-d_F} \quad (63)$$

where in this case  $d_F$  turns out to be  $\ln(3)/\ln(2)=1.585$ .

There are information and correlation fractal dimensions also. However,  $d_F$  given in Eq.60 is the most common fractal dimension. It is also called capacity or Hausdorf dimension.

### 8.3 Fractal Exponent

For any scale, the dependence of the measured function  $y$  on the size of the measure  $x$  can be described by a power function,

$$y = ax^{[D_E - d_F]} \quad (64)$$

where  $D_E$  denotes Euclidean dimension. It is an integer value and changes as 1, 2, and 3. For rod shaped (i.e., one dimensional) objects it is 1, for plate shaped (i.e., two dimensional) objects it is 2, and for spheroids it is 3. Fractal dimension,  $d_F$  is not an integer value. The value of the fractal exponent  $D_E - d_F$ , the dimensional excess, may change according to the degree of irregularity observed. Thus the fractal exponent defines a measure of the degree of structured organization, given by a certain geometrical or statistical rule of substructure formation. In ranges where there is no dependence on the measure of scale,  $d_F$  is equal to  $D_E$ . If, however, the extent of gradation remains identical over a wide range of scales (i.e., a smooth object), and therefore the fractal exponent remains constant, i.e.,  $D_E - d_F = \text{constant} = b$ , then the fractal system becomes self-similar [116,122]. In this case, the fractal dependence becomes a simple power function with a constant exponent  $b$ , such that,

$$y = ax^b \quad (65)$$

In a log-log plot it gives a straight line with slope  $b = D_E - d_F$ .

In this research work the grains and the boundaries of grains of fuels produced have been analyzed for their fractal dimensions.

#### 8.3.1 Structured Walk Method

The fractal dimension of the  $UO_2$  grains are obtained by structured walk method. In structured walk procedure for characterizing the fractal dimension of a rugged boundary, a series of polygons of side  $\lambda$  were constructed on the perimeter using a compass. As the step length decreases and the segments closely follow the profile,

the estimate of the polygon length increases and approaches the true value. The perimeter estimate  $P$  is related to distance  $\lambda$  according to the scaling power law [117].

$$P \propto \lambda^m \quad (66)$$

where,

$P$  = polygon perimeter of side  $\lambda$  normalized with respect to maximum projected length ( $L$ ) of the profile (i.e., Feret diameter)

$\lambda$  = side of polygon normalized with respect to maximum projected length of the profile

$m$  = slope of the dataline of a log-log plot of  $P$  against  $\lambda$

The structured perimeter,  $P$ , is plotted against the variable size length,  $\lambda$ , and the slope of such a graphical representation was computed according to Eq. 66. Both perimeter and length  $\lambda$  were normalized with respect to the maximum diameter of the profile (i.e., Feret diameter). Finally, the values of the profile fractal dimension,  $d_F$ , were obtained using the relationship,

$$d_F = 1 + |m| \quad (67)$$

The figure given below shows that for Britain Island  $d_F$  was calculated as 1.24. For a straight line the fractal dimension is equal to one. If the ruggedness is increased then the fractal dimension also increases. Thus a sponge of 2.4 fractal dimension (two dimensional space and Euclidean dimension is equal to 2) would occupy space more efficiently and have more surface area than a 2.3 fractal dimension sponge.

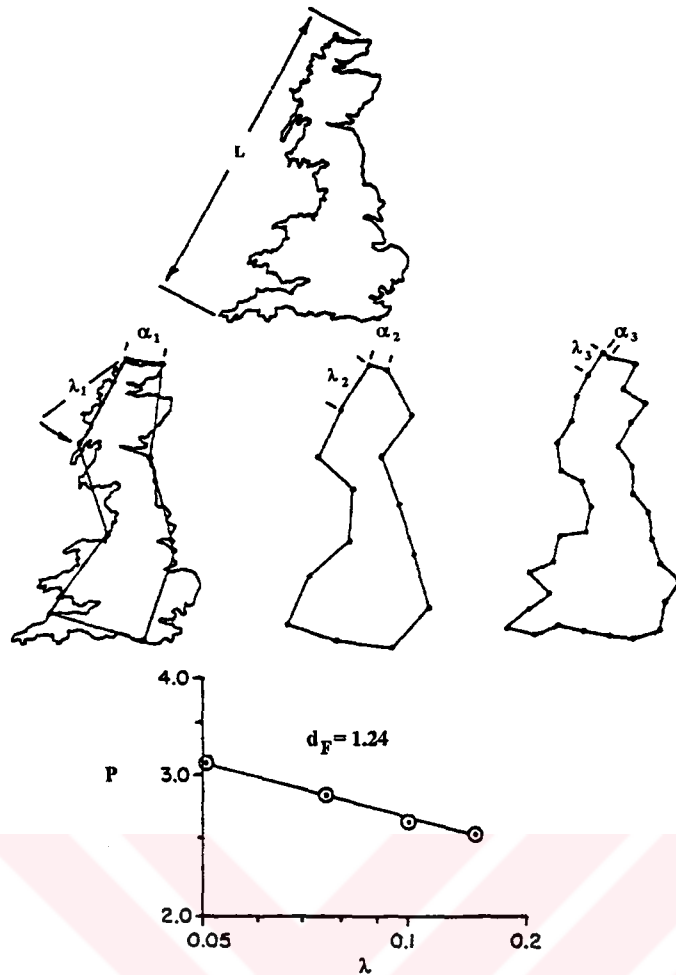


**Figure 17. Application of the structured walk method to Britain Island.**

This procedure was applied to calculate the fractal dimensions of the grain boundaries of urania-only and  $\text{UO}_2\text{-Gd}_2\text{O}_3$  (5%) and  $\text{UO}_2\text{-Gd}_2\text{O}_3$ (10%) fuel pellets by using their magnified SEM pictures.

#### 8.4 Limited Self Similarity

Self similarity may also exist between the number of grains and their sizes. This similarity was first discovered by Korchak [118] for Aegean islands. In 1938, Korchak claimed that all the island of the world could be discovered by one numerical relationship. He discovered that if one plotted the logarithm of the number of island greater than or equal to a stated size, "A", against the logarithm

of “A”, one obtains a linear relationship. The relationship for the Aegean islands is shown in Fig. 18. This fact inspired Mandelbroth [121] to introduce his fractal dimension concept.

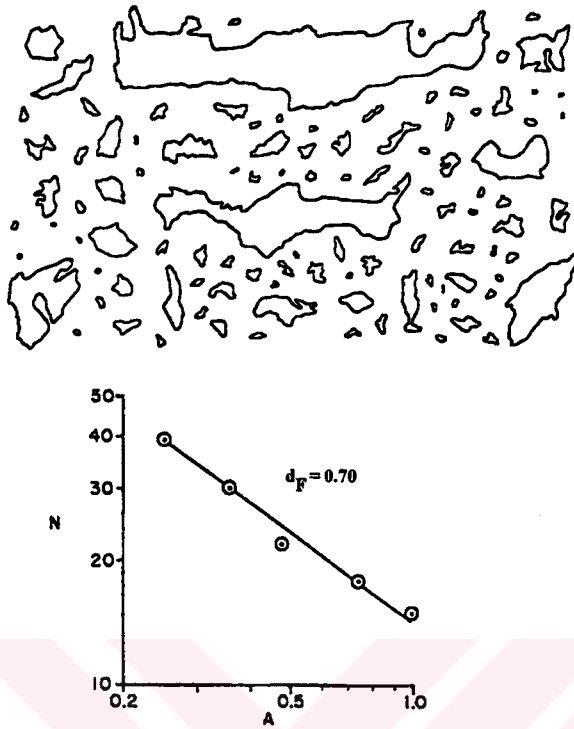


**Figure 18. The size distribution of the Aegean islands and log-log plots of the size distribution of the islands**

In contrast to the unlimited mathematical case, natural systems are self similar only within certain limits and are bounded by upper and lower limits namely physical constraints of the structural elements.

This consideration was formulated by B. Gelleri and M. Sernetz [119] as,

$$f_{\text{logit}} = \frac{f_i - f_U}{f_L - f_i} \quad (68)$$

where,

$f_{\text{logit}}$  is log-logistic fraction

$f_L$  and  $f_U$  are lower and upper limits

$f_i$  is any experimental value

In this study the grain boundaries of SEM photographs of the urania only and, 5% and 10% Gd<sub>2</sub>O<sub>3</sub> fuels have been digitized and converted to geometrical entities to be used in AutoCAD software using a personal computer and a digitizer attached. Then all the areas were found by using the entities representing the grain boundaries and necessary software commands including calibration. Before digitizing, it was necessary to enlarge the original SEM photographs nearly four times in order to increase the digitizing precision.

Using dBASE software, the fraction of the area distribution was calculated and sorted, then by using the limited self similarity formula given by Eq.68, log-logistic fractions of the areas of the grains were calculated.

## CHAPTER 9

### PERFORMANCE CALCULATIONS OF THE FUEL USING WIMS-D/4 COMPUTER CODE

There are many software programs available in the market to solve multigroup transport equations. For example WIMS-D/4, LASER, LEOPARD, CPM2, XSDRN, DORT, ANISN are several of them. In this study WIMS-D/4 is used.

The computer code WIMS (Winfrith Improved Multi-group Scheme) is a general lattice cell program which uses transport theory to calculate flux as a function of energy and the position in the cell [133]. The code will accept rod or plate fuel geometries in either regular or in clusters and the energy group structure has been chosen for both thermal and fast reactor calculations. In addition to the basic calculations the program may be used to carry out point burn-up calculations and to solve multi-cell problems. The basic library has been compiled with 14 fast groups, 13 resonance groups, and 42 thermal groups, but the user is offered the choice of accurate solutions in many groups or rapid calculations in few groups. WIMS-D/4 was developed as FORTRAN language code which runs on IBM compatible computers.

The main advantages of this software are:

1. WIMS-D/4 has a capability of fuel bundle calculations in addition to one fuel rod calculation,
2. It has a capability of burnup calculation.

The fuel utilization behavior, plutonium yield, uranium-235, boron and gadolinium depletion behavior of the boron nitride coated and gadolinium oxide mixed fuel have been calculated using WIMS-D/4 computer code. Table 10 gives a sample input data used in WIMS-D/4 [125]. The data of pitch distance, fuel pellet radius and cladding thickness are German KWU data [125].

**Table 10. Sample Data Input**

Fuel	UO <sub>2</sub> , UO <sub>2</sub> -Gd <sub>2</sub> O <sub>3</sub>
Moderator	H <sub>2</sub> O
Cladding material	Zirconium
Fuel element pitch	1.27 cm
Fuel pellet radius	0.4025 cm
Cladding thickness	0.064 cm
Density of UO <sub>2</sub>	10.4 g/cm <sup>3</sup>
Density of UO <sub>2</sub> /Gd <sub>2</sub> O <sub>3</sub> in term of Gd <sub>2</sub> O <sub>3</sub> amount	10.4-(0.04xG)* g/cm <sup>3</sup>
Density of BN	1.5 g/cm <sup>3</sup>
Density of Zr	6.4 g/cm <sup>3</sup> [122]

\* G represents the weight percentage of Gd<sub>2</sub>O<sub>3</sub> [126]

The number of energy groups in the calculation was taken as 18 groups (7 fast groups, 6 intermediate groups, 5 thermal groups). The isotopic abundance data of U, Gd and B used in the calculations are given in Table 3 in Chapter 2 and Table 4 in Chapter 4.

The performance of the fuels in a PWR core was studied by using cluster option of the WIMS-D/4 code. The fuel performance calculations were based on the data of typical 1000 MWe PWR data. The reactor core contains 177 square cross section fuel assemblies (see Fig. 19).



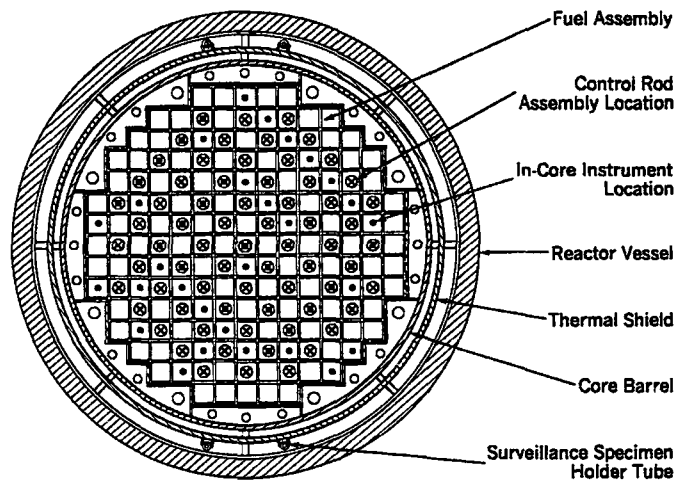


**Figure 19. 1000 MWe PWR Core Cross Section**

Figure 20 shows a cross section through a 18 x 18 PWR reactor core. The calculations in this work were based on about 1/16 th of a PWR fuel assembly where the pitch distance was 1.27 cm. The small matrix used in the calculations makes a 5 x 5 assembly. There is only one fuel rod at the center, the second shell contains 8 fuel rods, and the third one 16 fuel rods. Guide thimbles, instrumentation tubes, grids etc. were not considered, and there was no boron in water. The enrichment of fuel was 5%, and gadolinia was changed as 0, 5, and 10 %.

The fuel element which contains gadolinia was located at the center, and all fuel elements had their fuel pellets coated with BN. However, some calculations were also done without BN and/or without gadolinia.

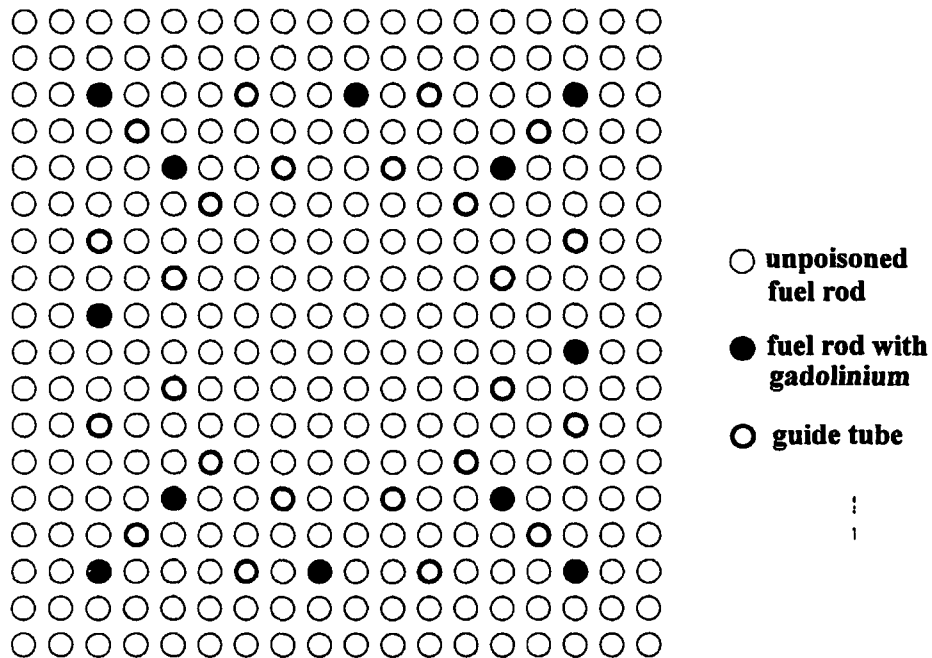


**Figure 20. 1000 MWe PWR Fuel Assembly Cross Section**

Two different BN coating thicknesses were considered as  $30\mu\text{m}$  and  $70\mu\text{m}$ . In the calculations two different cases were considered. In the first case the fuel diameter was kept constant and the pitch distance was changed by changing the number of fuel elements (25, 22, 16, 10 fuel rods) in an assembly. Hence the ratio of cross sectional area of the total number of rods to the cross sectional area of the moderator changed. Pitch distances were calculated to be 1.2700, 1.3538, 1.5875, and 2.0080 cm for 25, 22, 16, and 10 fuel rods respectively.

In the second case the radius of fuel elements were increased, but the total area of the moderator and the number of fuel rods in an assembly (25 fuel rods) were kept constant so the ratio of the total cross sectional area of the fuel elements to the cross sectional area of the moderator changed.

## CHAPTER 10

### RESULTS AND DISCUSSIONS

#### 10.1. Properties of Uranium Dioxide

During the fission reaction, certain gases (iodine, bromine, krypton, xenon etc.) are produced in the fuel pellets and they can diffuse out from micropores and deposit in the zone between the fuel pellets and the clad. If the density of the fuel approaches to the theoretical density, the fission gases may crack the fuel pellet and deform it. It may then cause some material failure problems. On the contrary highly porous fuel is not desired either due to neutron economy or heat transfer problems. The best fuel is the one which provides structural stability throughout residence in core. However the densities close to the theoretical density usually give satisfactory results.

Figure 6 in Section 7.2 gives a summary of the experimental steps in sol-gel technique. Each step has certain effect on the properties of the final product.

##### 10.1.1 Properties of Yellow Cake

Yellow cake pictures of different samples ( $\text{UO}_2$  and  $\text{UO}_2\text{-Gd}_2\text{O}_3(5\%)$  and,  $\text{UO}_2\text{-Gd}_2\text{O}_3(10\%)$  have been presented in Section 7.2.1.3. A close inspection shows that gadolinium containing samples are more spherical than pure urania. The BET surface area of pure urania yellow cake is  $0.0072 \text{ m}^2/\text{g}$  while the surface area of gadolinia containing samples could not be measured, that is expected to be lower.

## 10.1.2 Properties of Calcined and Reduced Powder

### 10.1.2.1 Color

The color of  $\text{UO}_2$  powders varies from brown to black. In general,  $\text{UO}_2$  powders prepared by hydrogen reduction procedures are brown. Oxidation converts brown  $\text{UO}_2$  into a black product. The color of  $\text{UO}_2$  also varies with its particle size. Since small particles reoxidize to larger extents, they become darker than large particles[126]. Gadolinia makes the reduced powder blackish. The color of all powders and the sintered pellets produced in this research work were dark brown.

### 10.1.2.2 Stoichiometry

Uranium, due to the complicated electronic configuration with  $5f^36d7s^2$ , where the outer shells have very close energy levels, is a very strongly electropositive element and a powerful reducing agent. Uranium has 4+ oxidation state but because of the electropositive nature of uranium, higher oxidation states ( $\text{U}^{5+}$  or  $\text{U}^{6+}$ ) always develop.  $\text{U}^{5+}$  state is highly unstable. The uranium dioxide at room temperature is usually expressed as  $\text{UO}_{2+x}$ .

Thermogravimetric (TGA) and differential thermal analyses (DTA) data were used for the calculation of U/O ratio of samples. The powder samples were heated under atmospheric condition so that  $\text{UO}_2$  interacts with atmospheric oxygen to form  $\text{U}_4\text{O}_9$  which is black in color.  $\text{U}_4\text{O}_9$  is in fact a compound between  $\text{UO}_2$  and  $\text{U}_3\text{O}_7$ . After TGA analyses x values of the fuel have been calculated as 0.10 for pure urania and 0.19 for  $\text{UO}_2\text{-Gd}_2\text{O}_3(5\%)$ , and 0.24 for  $\text{UO}_2\text{-Gd}_2\text{O}_3(10\%)$ . Figs 22-24 shows the results of TGA analysis. In these figures the increasing curve designates the increase in the weight of the sample due to oxygen uptake. While the second curve is the differential increase in weight. The decrease in weight seen shortly after the heating is started must be due to the removal of moisture from powder. In Figure 21 there is a sharp increase in oxygen content showing  $\text{U}_4\text{O}_9$  formation. In Figs 22 and 23 the oxygen uptake is very small. It is seen that the

presence of gadolinia highly decreases the reactivity of  $\text{UO}_2$  for atmospheric oxygen.

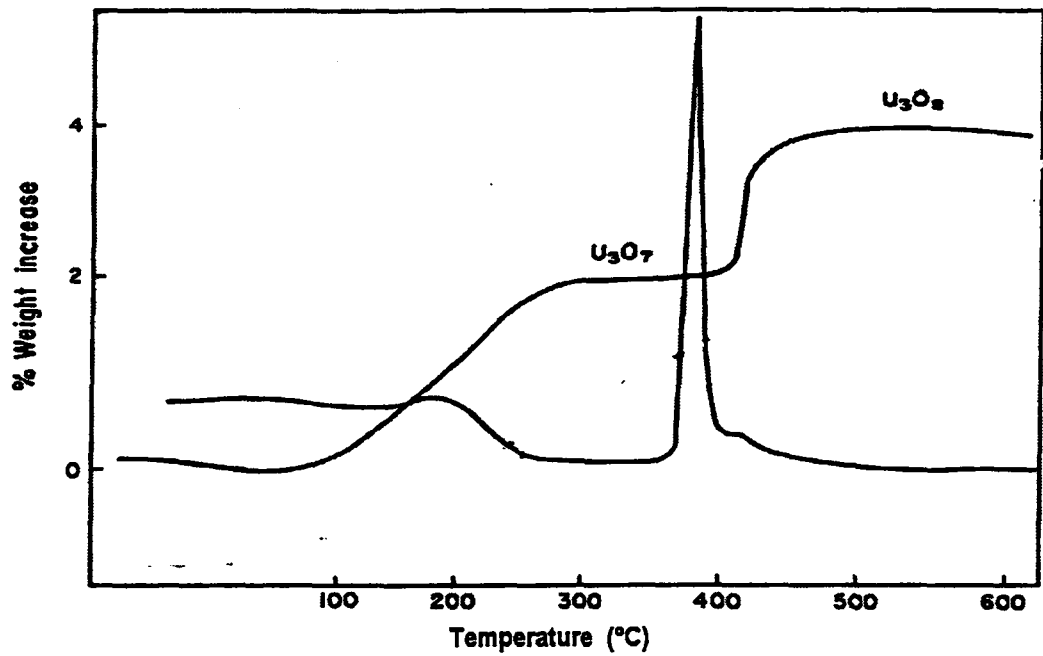


Figure 21 TGA of  $\text{UO}_2$

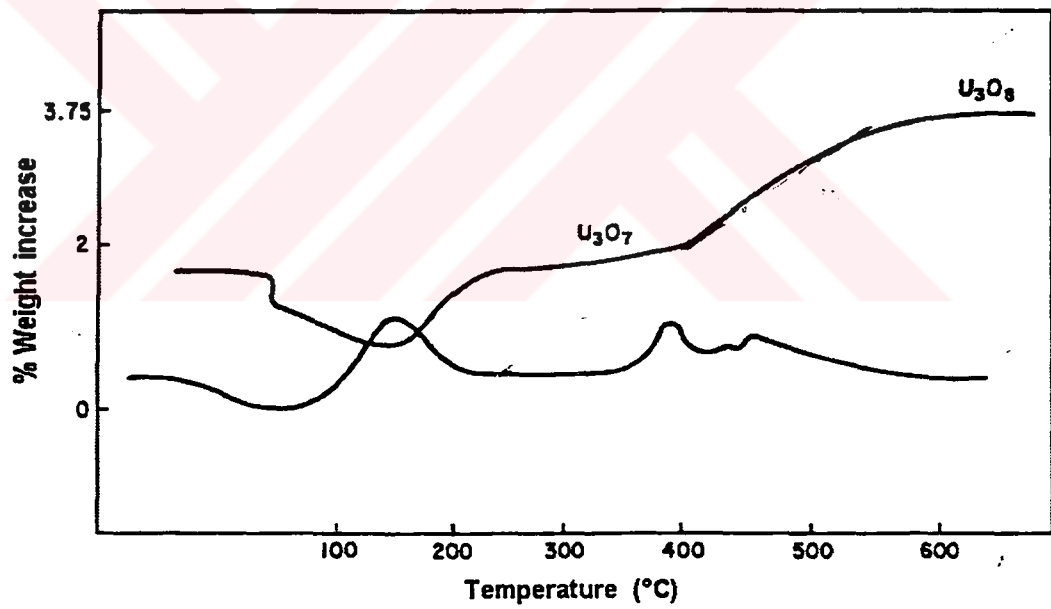


Figure 22 TGA of  $\text{UO}_2$ -5% $\text{Gd}_2\text{O}_3$

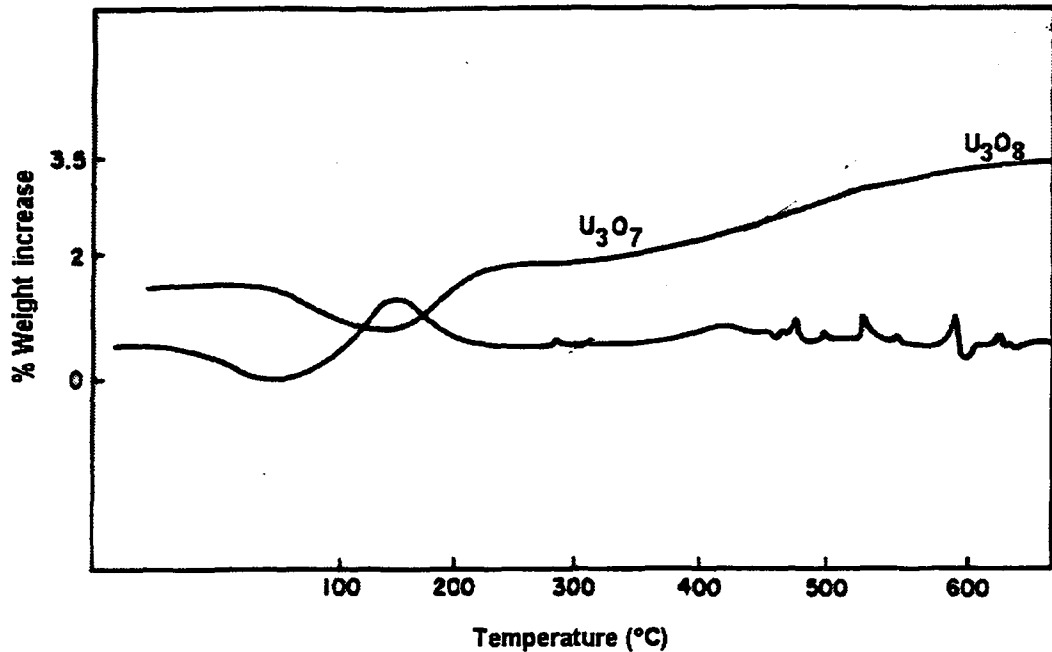


Figure 23. TGA of  $\text{UO}_2\text{-Gd}_2\text{O}_3(10\%)$

#### 10.1.2.3 BET Surface Area of the Powder

The BET surface area of the fuel powders were measured by nitrogen adsorption technique in a pore size analyzer, (Micromeritics 5, Model 9310). The BET surface area, the average pore diameter, and the cumulative pore volume of the powders were given in Table 11. The pore size distributions of the powders were given in Fig. 24. In the figure, “U”, “5 % Gd”, and “10 % Gd” denote pure urania, 5 %, and 10% gadolinia containing fuels, respectively. BET surface area is the lowest in pure urania case, while the average pore diameter and the cumulative pore volume achieved the highest values in  $\text{UO}_2\text{-Gd}_2\text{O}_3(5\%)$  case. This result will be discussed later in Section 10.1.4.2.

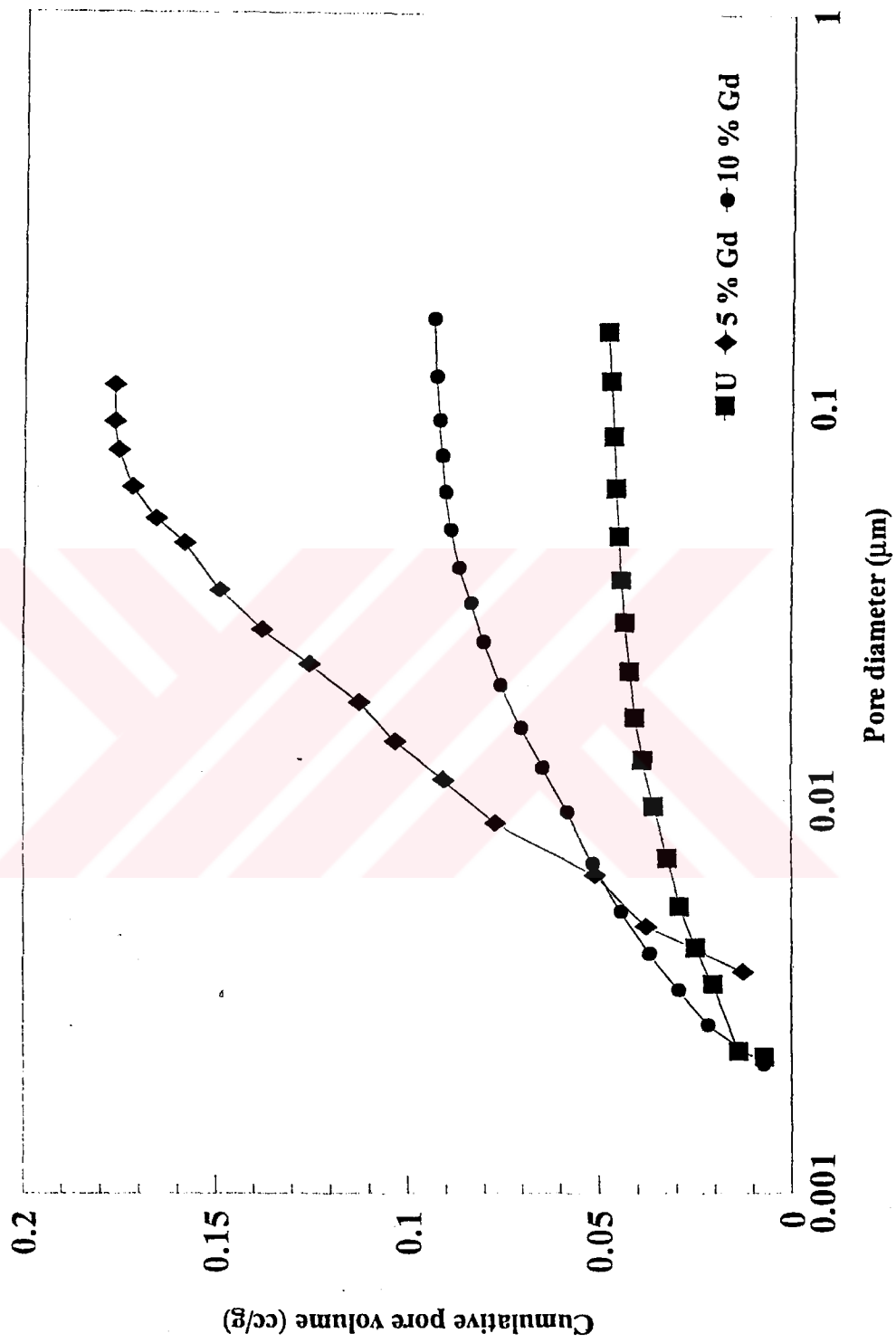


Figure 24. Pore size distributions of calcined and reduced powders

**Table 11. BET Results of the Powder**

Fuel Type	BET surface area (m <sup>2</sup> /g)	Average pore diameter (°A)	Cumulative pore volume (cm <sup>3</sup> /g)
UO <sub>2</sub>	10.37	159.1	0.05
5% UO <sub>2</sub> -Gd <sub>2</sub> O <sub>3</sub>	14.55	396.4	0.175
10% UO <sub>2</sub> -Gd <sub>2</sub> O <sub>3</sub>	15.16	204.5	0.15

**10.1.2.4 Powder Flowability.**

The powder flowabilities came out as 1.90, 2.88 and, 4.7 g/s for UO<sub>2</sub>, UO<sub>2</sub>-Gd<sub>2</sub>O<sub>3</sub>(5%), UO<sub>2</sub>-Gd<sub>2</sub>O<sub>3</sub>(10%), respectively.

**10.1.3 Green Pellet Density and Porosity**

The densities of green pellets were given in Table 12. Green pellet densities are reported to change between 45 to 55 % in conventional powder technology. Sol-gel technique also gives similar results as seen from the last column of Table 12.

**Table 12. Green Pellet Densities.**

Fuel type	Green density (g/cm <sup>3</sup> )	Theoretical percentage
UO <sub>2</sub>	5.0-5.5	46-50
UO <sub>2</sub> -Gd <sub>2</sub> O <sub>3</sub> (5%)	4.7-4.8	44-48
UO <sub>2</sub> -Gd <sub>2</sub> O <sub>3</sub> (10%)	5.1-5.3	48-50

Figure 25 gives the pore size distributions of the green pellets. Gadolinia increases the porosity of green pellets.



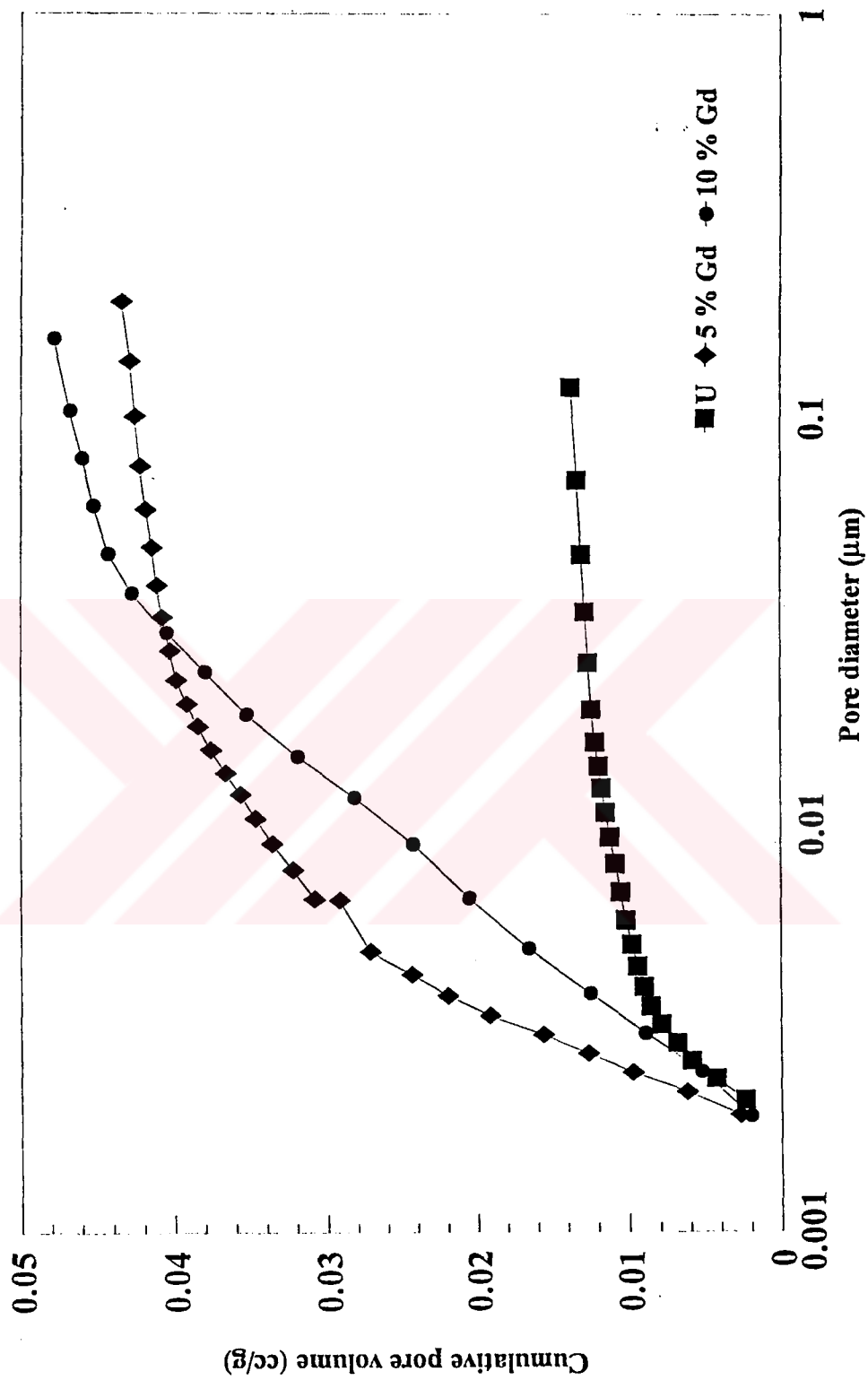


Figure 25 . Pore size distributions of green pellets

The comparison of Tables 11 and 13 shows that the cumulative pore volume decreases 3.33 times in  $\text{UO}_2$ , 3.97 times in  $\text{UO}_2\text{-Gd}_2\text{O}_3(5\%)$ , and 3.12 times in  $\text{UO}_2\text{-Gd}_2\text{O}_3(10\%)$  due to compaction at 200 MPa.

**Table 13. BET Results of the Green Pellets**

Fuel Type	BET surface area ( $\text{m}^2/\text{g}$ )	Average pore diameter ( $^{\circ}\text{A}$ )	Cumulative pore volume ( $\text{cm}^3/\text{g}$ )
$\text{UO}_2$	5.3	101.6	0.015
$\text{UO}_2\text{-Gd}_2\text{O}_3(5\%)$	10.4	155.4	0.044
$\text{UO}_2\text{-Gd}_2\text{O}_3(10\%)$	12.4	146.7	0.048

#### 10.1.4 Properties of the Sintered Pellet

##### 10.1.4.1 Density

Theoretical density of  $\text{UO}_2$  is known to be  $10.95 - 10.97 \text{ g/cm}^3$ . The recommended value for the theoretical density of  $\text{UO}_2$  is  $10.96 \text{ g/cm}^3$ . The published data on densities vary depending on the experimental technique (dry or sol-gel) and the method of preparation (compaction pressure, grinding the powder, use of binder material, reduction and sintering temperature and atmosphere) of uranium dioxide. The density is a significant characteristics of both as-pressed (green) and sintered  $\text{UO}_2$  and  $\text{UO}_2\text{-Gd}_2\text{O}_3$  pellets. The following three equations were taken from literature to calculate the theoretical density of  $\text{UO}_2\text{-Gd}_2\text{O}_3$  [127]

$$\rho = 10.96 - 0.03485 G \quad (69)$$

$$\rho = 10.96 - 0.033 G \quad (70)$$

$$\rho = 10.96 - 0.020413 G - 0.0027075 G^2 + 0.0001535 G^3 \quad (71)$$

where  $\rho$  is the theoretical density in  $\text{g/cm}^3$  and  $G$  is the weight fraction of gadolinia added ( $0 \leq G \leq 12$ ).

According to Yuda and Une [31] there is a distinct difference between the densification rates of  $\text{UO}_2$  and  $\text{UO}_2\text{-Gd}_2\text{O}_3$  particles. Due to particulate behavior local and nonuniform volumetric changes take place in sintering in the conventional powder mixing method. The stress thus generated causes microcracks resulting in open pores. Such problems originating from heterogeneous distribution of oxides are minimized in the case of sol-gel fuel due to mixing of urania and gadolinia oxides at molecular level.

In this research work the density of  $\text{UO}_2$  was found to be 98.01% of theoretical density, which is a very high achievement. The reported values for the conventional techniques is 94-96%. The densities of  $\text{UO}_2\text{-Gd}_2\text{O}_3(5\%)$  and  $\text{UO}_2\text{-Gd}_2\text{O}_3(10\%)$  fuels were determined to be 95.3 and 95.9 % of theoretical density respectively. These are also well above the reported values [27,131].

#### 10.1.4.2 Microstructure of Sintered Pellets

There has been a number of publications on the sintering of  $\text{UO}_2\text{-Gd}_2\text{O}_3$  pellets. Eventhough most of the investigations have recently been made [1-4] the relationship between the percent theoretical density, lattice parameter, oxygen to uranium ratio and possible structures of the solid solutions are still not fully understood.

Uranium dioxide has a cubic fluorite-type structure and  $\text{Gd}_2\text{O}_3$  can be considered to have a cubic fluorite structure. Therefore, solid solutions of cubic fluorite types structures are easily formed due to mixing of  $\text{UO}_2$  with  $\text{Gd}_2\text{O}_3$ . Gadolinia can be used as a stabilizing agent for  $\text{UO}_2$ . The o- and p- shells of gadolinium are filled as follows

	o			p	
5s	5p	5d	6s	6p	6d
2	6	1	2		

The  $Gd^{3+}$  occurs due to removal of electrons from 6s and 5d. The remaining orbitals (e.g. 5s and 5p) contain 8 electrons therefore  $Gd^{3+}$  is a very stable ion and is usually insensitive to the changes in the crystalline field [130].

When gadolinia is homogeneously mixed with  $UO_2$ , the Gd atoms replace the position of U atoms in the fluorite crystal structure of  $UO_2$ . That is solid solution is formed by interdiffusion of  $Gd^{3+}$  ions into  $UO_2$  lattice, and  $U^{4+}$  ions into  $Gd_2O_3$  lattice. The results of this study and some literature results [127,131] show that the addition of  $Gd_2O_3$  to  $UO_2$  first decreases the density, but after 4-6 wt %  $Gd_2O_3$  it increases it slightly again up to 10 wt %  $Gd_2O_3$  (maximum at 8 wt %  $Gd_2O_3$  ). After this level the density decreases very sharply.

Figure 26 shows the pore size distribution of the sintered pellets. It is seen that the cumulative pore volume of sintered pellets decreased almost one order of magnitude (e.g. 10 times) compared to green pellets (see Fig.24).  $UO_2$  fuel has the lowest porosity while  $UO_2-Gd_2O_3(5\%)$  has larger porosity than  $UO_2-Gd_2O_3(10\%)$ . It is well known that gadolinia retards sintering and thus leads to larger pores in sintered pellets [28].

The addition of gadolinia to urania does not only affect the density but also changes lattice parameter, thermal conductivity, fission gas release, grain growth rate and other properties. Some models are available in the literature which explain the change of the crystal structure due to addition of gadolinia. The production of vacancies in the crystal structure and the production of oxygen interstitial are the most important phenomena that take place due to gadolinia addition.

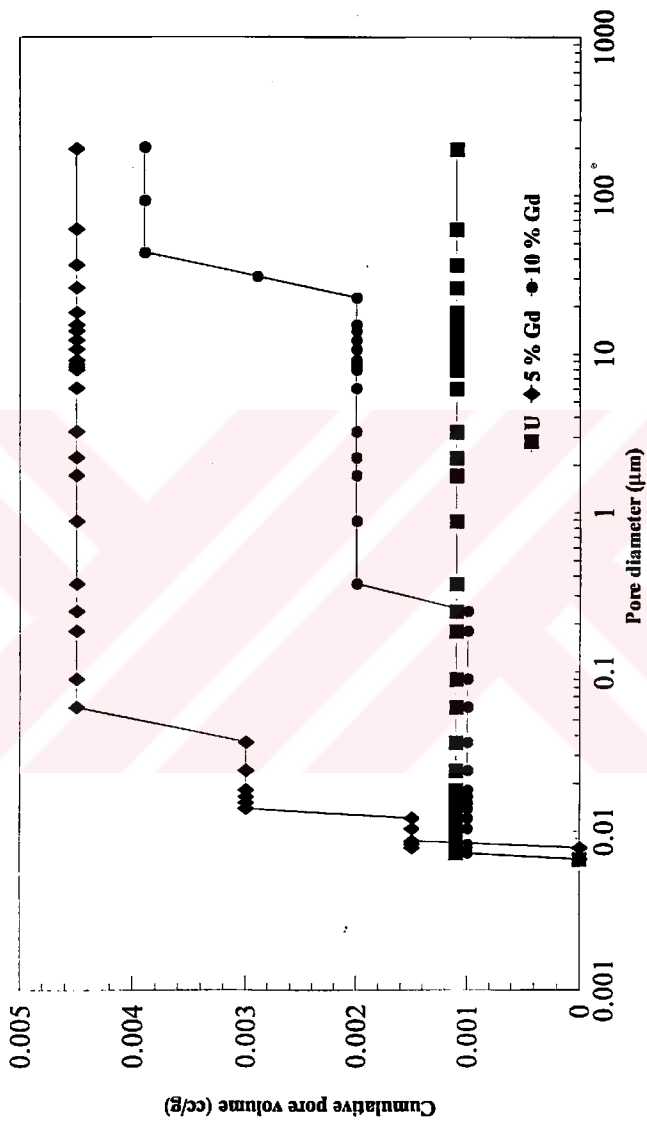
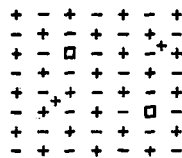


Figure 26. Pore size distributions of sintered pellets (samples reduced at 875 K, and sintered at 1900 K)

### 10.1.4.3 Production of Vacancies in the Crystal Structure

If the uranium ions in the  $\text{UO}_2\text{-Gd}_2\text{O}_3$  solid solutions will remain in the  $\text{U}^{4+}$  state when addition of Gd keeps its +3 charge then to ensure the electrical neutrality (e.g. balance of charges) in the lattice, an oxygen ion may be removed from the lattice, thereby producing a negative ion (anion) vacancy.

These vacancies are called defects from ideal crystal structure and there are various types of defects. Anion Frenkel defects are the predominant intrinsic point defects in  $\text{UO}_2$ . The Frenkel defect is shown in Fig.27.



**Figure 27. Frenkel defect**

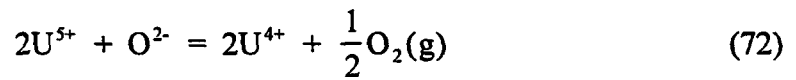
The Frenkel defect consists of the vacancy plus the interstitial. Vacancies are important because they control the rate of matrix or substitutional atom diffusion; that is, atoms are able to move around in a crystalline solid because of the movement of vacancies. Frenkel defect is an intrinsic defect. They do not alter the exact stoichiometry of the crystal. But they provide a mechanism by which atoms move relatively easily within the crystal. It is much easier for an atom to move from an occupied site into a vacancy than for two atoms in occupied sites to change places directly.

Fukushima et al. [127] found that at constant concentration of  $\text{Gd}^{3+}$  the lattice parameter of the solid solution is increased with an increase in oxygen vacancies. This is due to the reason that fewer number of small  $\text{U}^{5+}$  ions (radius of  $\text{U}^{4+}$  ions is 0.1 nm and  $\text{U}^{5+}$  ions is 0.088 nm) are produced. The large x values of  $\text{UO}_{2+x}$  accelerates the production of  $\text{U}^{5+}$ . For small x values  $\text{U}^{5+}$  concentration is

naturally kept low. The incorporation of gadolinia into urania generates the vacancies and we may expect a decrease in the theoretical density. However these arguments can be valid when the material has no macro pores or large intergrain voids. The increase in vacancy number and increase in the lattice parameter of the solid solution may cause a slight decrease in density.

#### 10.1.4.4 Production of Oxygen Interstitials

The replacement of U ions in  $\text{UO}_2$  by  $\text{Gd}^{3+}$  necessitates some U ions to have higher charges than  $\text{U}^{4+}$  to maintain charge neutrality, because the additional negative charges from excess interstitial oxygen are compensated by U ions only, due to high stability of  $\text{Gd}^{3+}$ . In this system, the following equilibrium can be considered between cations and anions in the lattice and oxygen gas,



The application of the law of mass action to this equilibrium yields,

$$K = \frac{[\text{U}^{4+}]^2 P_{\text{O}_2}^{1/2}}{[\text{U}^{5+}]^2 [\text{O}^{2-}]} \quad (73)$$

where K is the equilibrium constant,  $P_{\text{O}_2}$  the oxygen equilibrium partial pressure.

The increase in gadolinia shifts the reaction to the left, therefore an increase in gadolinia increases the  $\Delta\bar{G}_{\text{O}_2}$  value which is  $\Delta\bar{G}_{\text{O}_2} = -RT \ln P_{\text{O}_2}^{1/2}$ . By the introduction of  $\text{Gd}^{3+}$  in  $\text{UO}_2$ , the oxygen sublattice around the  $\text{Gd}^{3+}$  tends to form an oxygen interstitial in the neighborhood to keep nearly stoichiometric composition  $\text{U}_{1-y}\text{Gd}_y\text{O}_{2+x}$ . These series of events would result in an increase in the total number of oxygen clusters. Similar phenomenon has been found in  $\text{UO}_{2+x}$  [127,131-134]. This implies that the presence of oxygen interstitial makes the formation of oxygen clusters easier.

Introducing cations such as Ti, may not cause a significant change in the total number of the oxygen clusters [26]. In fact the smaller radius of  $Ti^{+4}$  (0.065 nm) than  $U^{4+}$  causes densification in pellet [135].

At certain concentration level, the oxidation of  $U^{4+}$  to smaller  $U^{5+}$  and  $U^{6+}$  ions allows for more rapid diffusion, probably causing density increase but a critical level is needed above which diffusivities are inhibited.

It has been explained that the increase of  $Gd^{3+}$  ions in the solid solution converts some of the  $U^{4+}$  ions to  $U^{5+}$  and  $U^{6+}$  ions. Since the ionic radii of these last two ions are smaller than  $U^{4+}$ , they diffuse rapidly in the solid solutions hence densification is achieved. But after some critical concentration, the increase in  $U^{5+}$  and  $U^{6+}$  ions increase the oxygen interstitial, and these series of events would result in the increase of the total number of oxygen clusters, which result a sharp decrease in the density of the solid solution.

The reported values in the literature [127-134] shows that some slight increase in theoretical density is achieved between 8 to 10 %  $Gd_2O_3$ . In this research work the density of  $UO_2-Gd_2O_3(10\%)$  is found to be higher than  $UO_2-Gd_2O_3(5\%)$  fuel (see Fig.26).

#### **10.1.4.5 Effect of Grinding on Density**

The effect of grinding of  $UO_2$ -powder was investigated by preparing two different samples. One sample was sufficiently ground but not sieved, the other one was passed through a 400 mesh sieve which corresponds to a screen size of 37  $\mu m$ . It was found that for  $UO_2$ -only specimen reduced at 1000 K and sintered at 1900 K, a density of about 93 % was achieved in either case, and consequently all other experiments were carried out by using unsieved powder. However grinding down to 2-5 $\mu m$  can be expected to increase density as known from powder technology.



#### **10.1.4.6 Effect of Binder on Pore Size Distribution**

Stearic acid and metal stearates are well known binders used in pellet compaction. The use of stearic acid resulted in some troubles in sintering. This is because stearic acid has definite decomposition temperature of 633 K. Therefore, heating rate must be very well regulated to pass this temperature very slowly. Vacuum heat treatment can help to overcome this problem but was not used in the experiments. In order to eliminate the problems inherited with stearic acid a new binder, polyvinyl alcohol (PVA) was tested. Since it is a polymer it does not have a sharp decomposition temperature and does not cause sudden swelling of pellets. The rate of gas formation due to decomposition is low, therefore the shape of the pellet is not deformed. PVA was introduced by mixing 10% solution in alcohol with powder. The powder is mixed with this solution and dried.

In Figures 28 and 29 the dependence of pore size distributions on binder used are shown. The jump after 10 $\mu$ m in without binder case denotes the interparticle voids. It is seen that the pore size distribution does not show any significant alteration whether one uses binder or not. The same result was achieved with UO<sub>2</sub>-Gd<sub>2</sub>O<sub>3</sub> fuel also even when stearic acid was used. Hence, the type of the binder whether it is stearic acid or PVA does not affect the pore distribution. However, the use of binder helps to make pellets with high green strength. Since PVA decomposes on a wide temperature range it is more advantageous to use it rather than stearic acid. PVA was used as binder in all other specimens.

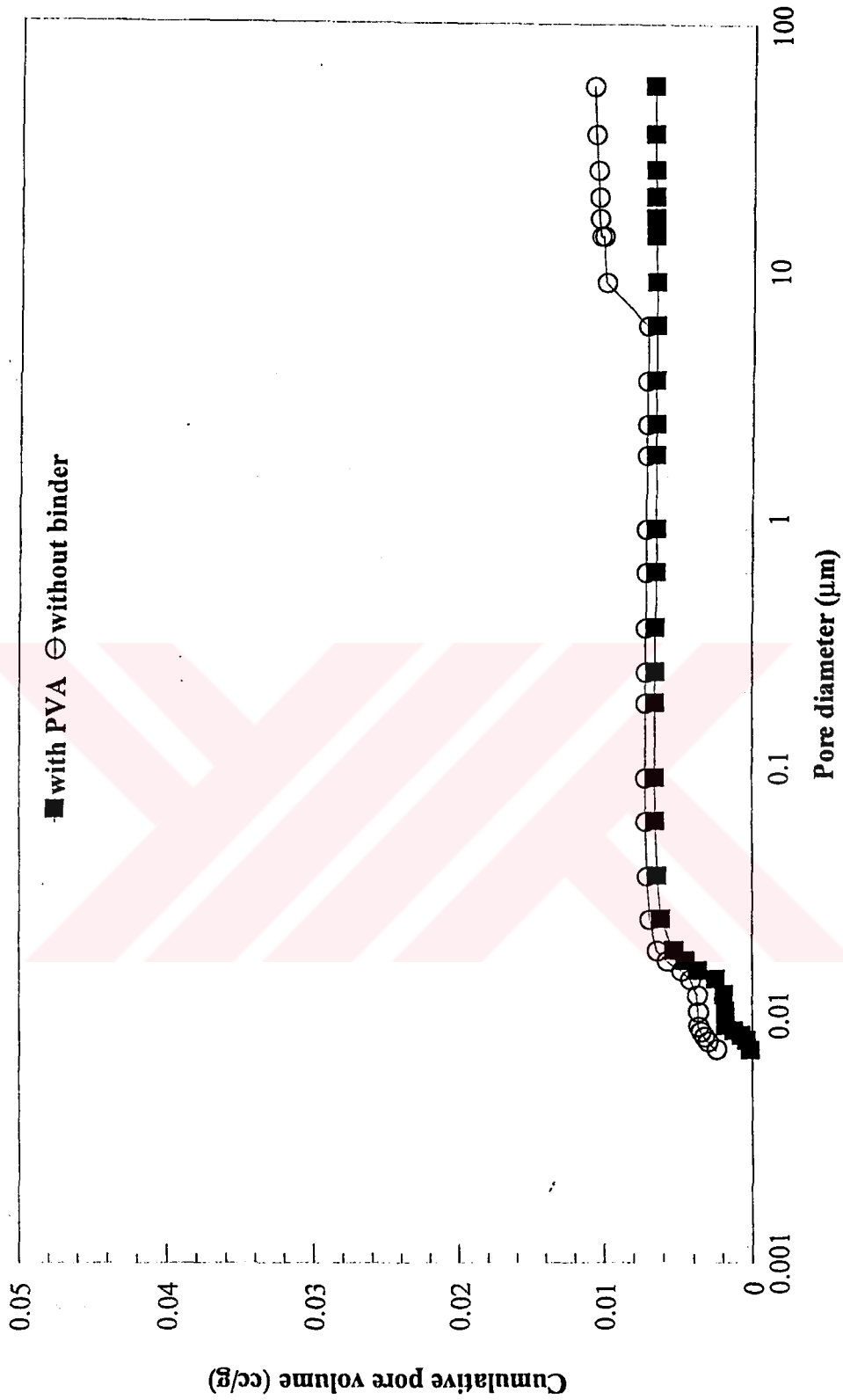


Figure 28. Effect of binder on pore size distribution  
 (sample:  $UO_2$  reduced at 1000 K, sintered at 1900 K)

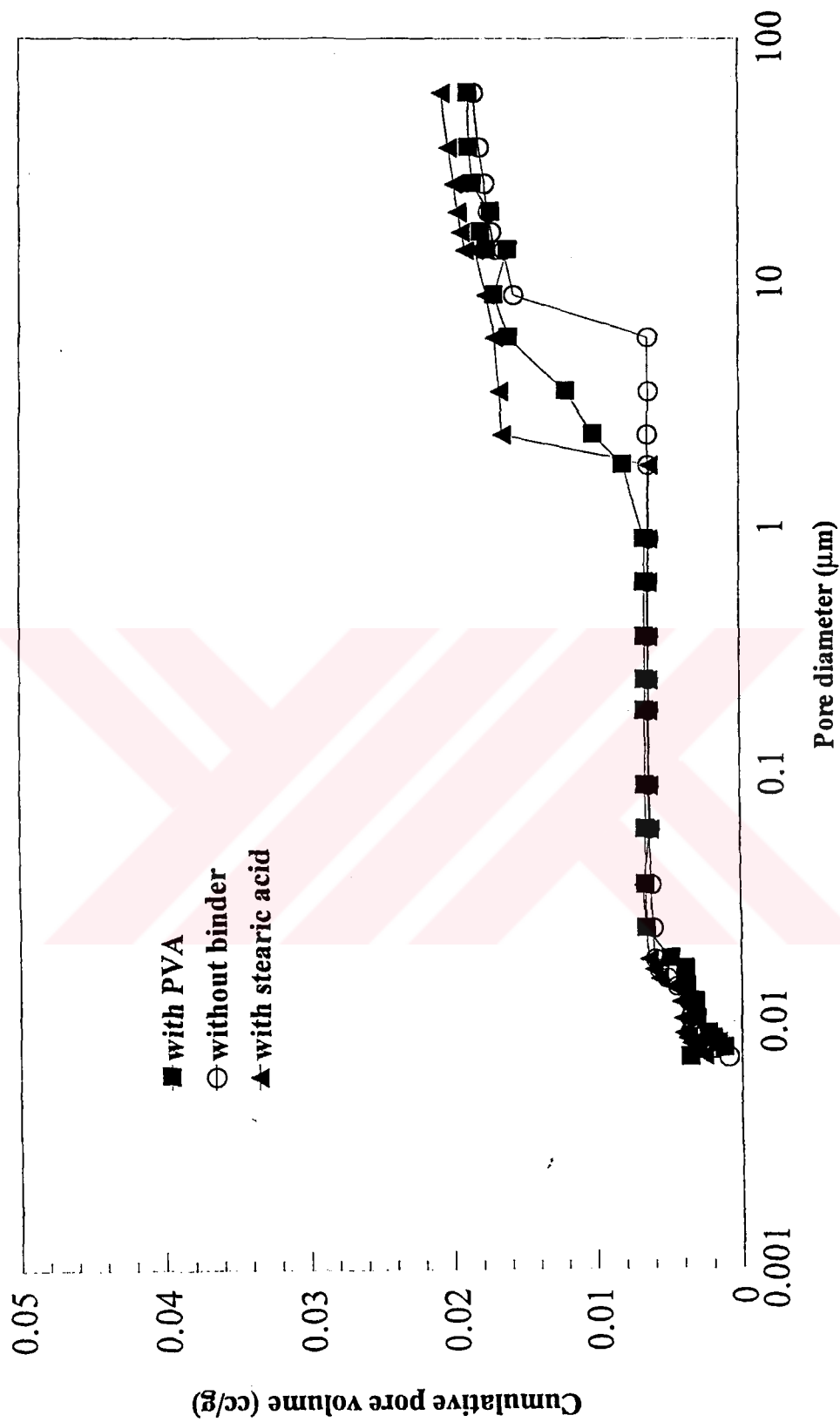


Figure 29. Effect of binder on pore size distribution  
 (sample:  $\text{UO}_2 - \text{Gd}_2\text{O}_3$  reduced at 1000 K, sintered at 1900 K)

#### 10.1.4.7 Effect of Compaction Pressure on Density

The dependence of densities on compaction pressure is very small as seen from Table 14. The simple conclusion is that both urania-only and urania-gadolinia powders obtained by sol-gel technique have such good qualities that a pressure as low as 200 MPa is sufficient to make pellets. As the compaction pressure is increased to 600 MPa the porosity between  $\text{UO}_2$  and  $\text{UO}_2\text{-Gd}_2\text{O}_3$  becomes unnoticeable. At lower compaction pressure gadolinia containing fuel shows larger porosity than  $\text{UO}_2$  only fuel. Gadolinia is known to retard sintering [31]. It therefore yields larger porosity and lower density than  $\text{UO}_2$ -only sample.

**Table 14. The Effect of Compaction Pressure on Density  
(powder reduced at 1000 K, pellets sintered at 1900 K)**

Sample	200 MPa	400 MPa	600 MPa
$\text{UO}_2$	93.19*	93.19	93.40
$\text{UO}_2\text{-Gd}_2\text{O}_3$ (10%)	91.96	91.96	93.21

\*all values are in terms of percent theoretical density

The urania powder obtained by means of sol-gel technique has such a good quality that compaction at low pressures gives pore volume as low as the ones compacted at high pressures. However high pressure compaction must be preferred not only to reduce pores but also to reduce voids which cause severe decrease in density.

#### 10.1.4.8 Effect of Reduction Temperature on Density

The effect of reduction temperature upon density is given in Table 15. A high reduction temperature of powder yields low pellet density. This must be due to the poor characteristics of the powder reduced at 1000 K. In fact very small pores collapse yielding relatively large pores when powder is reduced at a high temperature. Hence the distribution shifts towards large pore sizes [37,38,39]. A kind of premature sintering takes place at 1000 K. This introduces less compaction

while making pellets. Therefore the reduction temperature must be taken as 873 K to obtain pellets with high densities.

**Table 15. The Effect of Powder Reduction Temperature on Pellet Density (pellets sintered at 1900K)**

Sample	1000 K	873 K
UO <sub>2</sub>	93.19	98.01
UO <sub>2</sub> -Gd <sub>2</sub> O <sub>3</sub> (5%)	–	95.30
UO <sub>2</sub> -Gd <sub>2</sub> O <sub>3</sub> (10%)	93.21	95..90

#### 10.1.4.9 Crystalline size

Figure 30, 31, and 32 show XRD pattern of UO<sub>2</sub>, UO<sub>2</sub>-Gd<sub>2</sub>O<sub>3</sub>(5%), and UO<sub>2</sub>-Gd<sub>2</sub>O<sub>3</sub>(10%), respectively. All the reported characteristic peaks of UO<sub>2</sub> are seen in Figure 36. Figure 37 and 38 which are XRD pattern of UO<sub>2</sub>-Gd<sub>2</sub>O<sub>3</sub>(5%) and UO<sub>2</sub>-Gd<sub>2</sub>O<sub>3</sub>(10%), have the same characteristic peaks with UO<sub>2</sub>. This means that gadolinia is mixed with urania homogeneously and single phase solid solution was formed. However when the Gd<sub>2</sub>O<sub>3</sub> content was increased, the peaks broadened especially after  $2\theta > 60$ . It was reported in the literature that [137-139] the lattice parameter decreased with gadolinia content, and it follows the following relation,

$$a = 5.4694 - 0.001956 G \quad (74)$$

where,

“a” is the average lattice parameter (°A) and G is the content of Gd<sub>2</sub>O<sub>3</sub> (wt%).

The gadolinia content above 10%, causes a phase separation [23,42], so 10% Gd<sub>2</sub>O<sub>3</sub> is a limiting value to be used in nuclear fuel production. In fact higher percentage also adversely affects neutron flux distribution in the reactor[137-140].

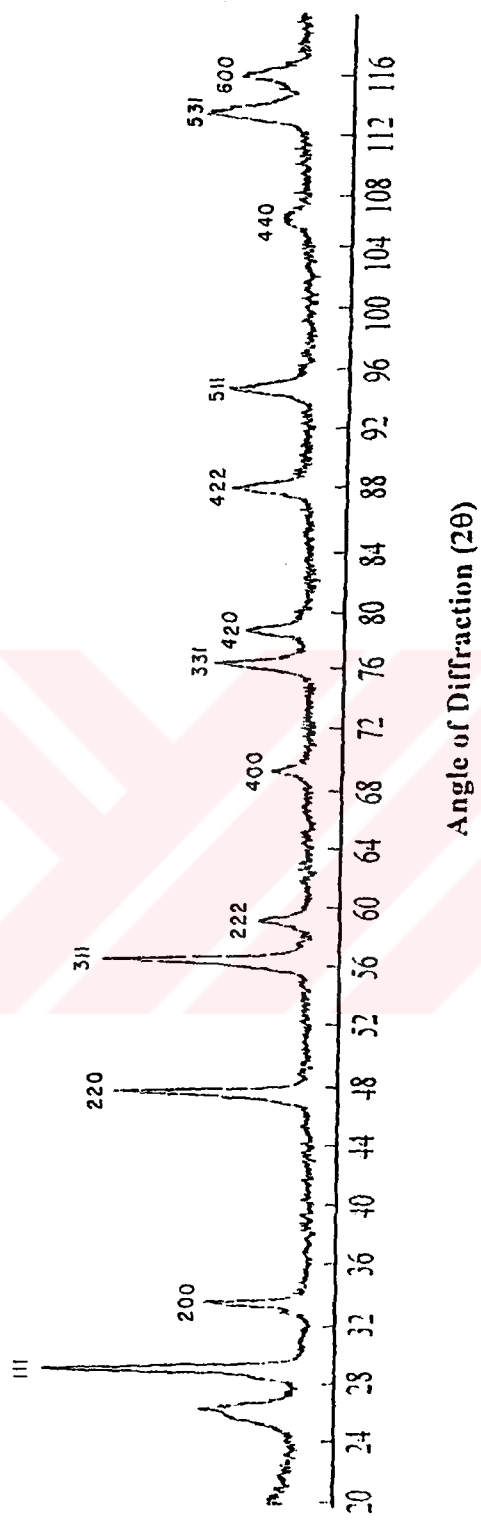


Figure 30. XRD pattern of the uranium dioxide powder

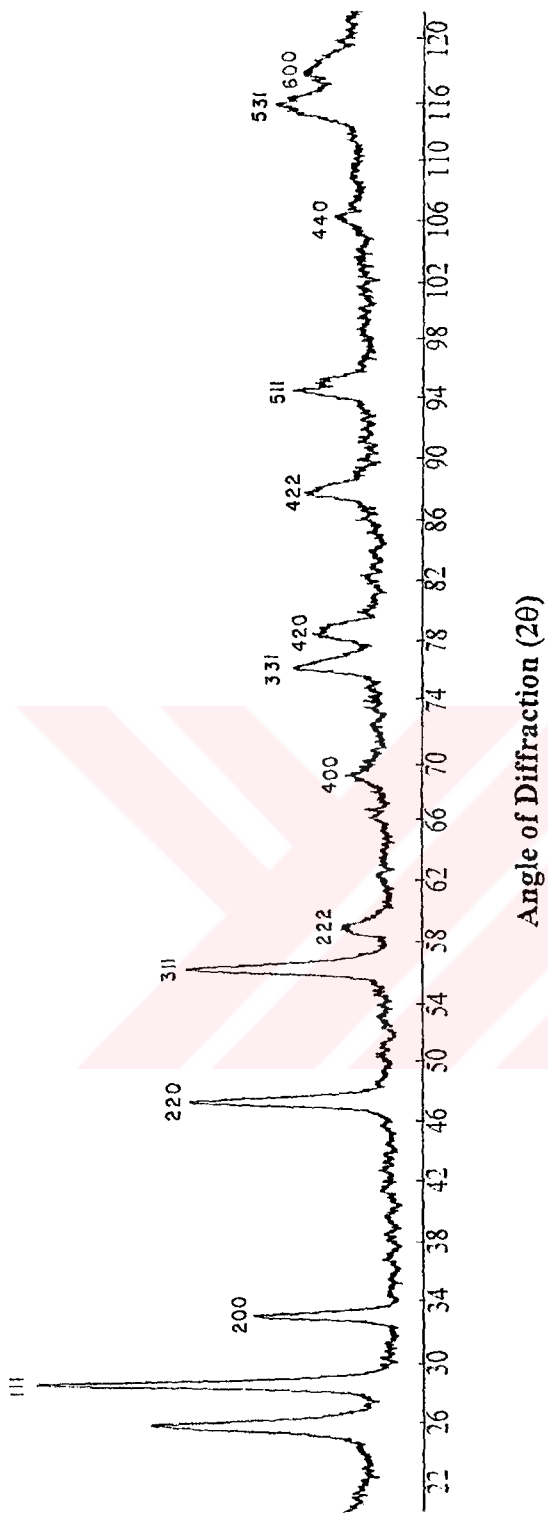


Figure 31. XRD pattern of the uranium dioxide - 5% gadolinium oxide powder

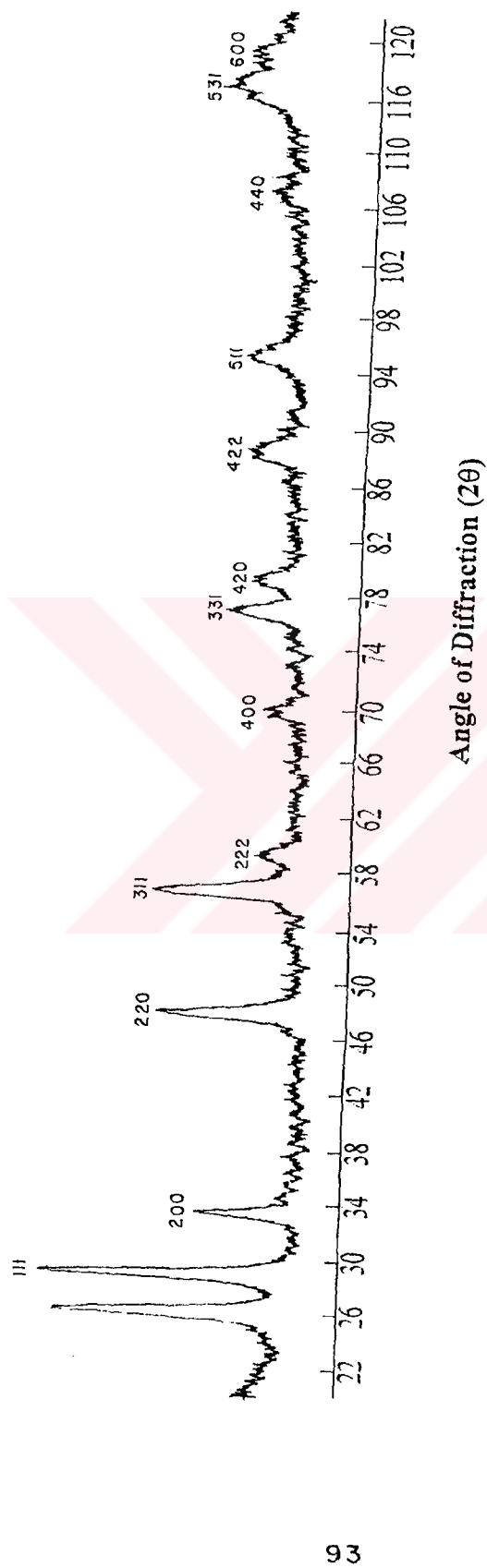


Figure 32. XRD pattern of the uranium dioxide - 10% gadolinium oxide powder



#### 10.1.4.10 Scanning Electron Microscope (SEM)

Surface morphology of the grains of  $\text{UO}_2$  and  $\text{UO}_2\text{-Gd}_2\text{O}_3$  fuel pellets was studied by using scanning electron microscope (SEM) (JSM, Model 6400). Figures 33, 34, and 35 are the SEM pictures of  $\text{UO}_2$ ,  $\text{UO}_2\text{-Gd}_2\text{O}_3(5\%)$ ,  $\text{UO}_2\text{-Gd}_2\text{O}_3(10\%)$ , respectively. The addition of gadolinia does not change the general appearance of grains and their packing mode, but it increases the grain size. Littlechild [140] also observed an increase in grain size in his work. The grain size affects fission product release. Fission product gas retention in the fuel is one of the critical issues of fuel performance[141]. The grain sizes must not be too small or too large, in the former the fission gas retention is low, while in the latter, high amount of fission gas retention can cause cracks in the fuel. In this study the average grain size of  $\text{UO}_2$  was found to be  $4\mu\text{m}$ . The average grain size increased to  $6\mu\text{m}$  for  $\text{UO}_2\text{-Gd}_2\text{O}_3(5\%)$ , and  $12\mu\text{m}$  for  $\text{UO}_2\text{-Gd}_2\text{O}_3(10\%)$ .

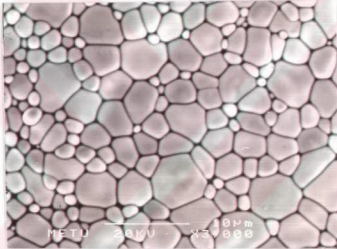


Figure 33 SEM picture of  $\text{UO}_2$

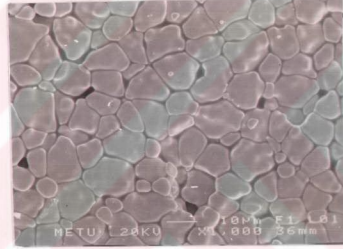


Figure 34 SEM picture of  $\text{UO}_2\text{-Gd}_2\text{O}_3(5\%)$

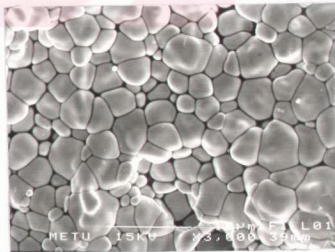


Figure 35. SEM picture of  $\text{UO}_2\text{-Gd}_2\text{O}_3(10\%)$

#### **10.1.4.11 Fractal Analysis of the Grains**

Fractal analysis is an important concept to characterize solid materials. It gives information about the way a material is formed, or the way it has gained its configuration. If we can correlate the fractal dimension with thermal conductivity, fission gas release, swelling, pellet stress or some other phenomena then by only knowing one number (i.e. fractal dimension) we can estimate the other behavior of the fuel under the considered effect.

SEM photographs of the sintered pellets are used for fractal analysis. The grain boundaries of the SEM photographs have been digitized and converted to geometrical entities. These procedures have been presented in Section 7.3.

##### **10.1.4.11.1 Structured Walk Method to Determine the Fractal Dimension of Grain Ruggedness**

Fractal dimension which is found by using structured walk procedure gives information how efficiently the structure fills the space it occupies. The theory and its application to this study have been explained in detail in Section 7.3.1 The analysis was done on an average of three particles. The grains analyzed had a representative average diameter in each case. Some deviations took place in very small size particles. The results are shown in Fig. 36.

The  $d_F$  values found from the slopes are 1.111 for pure urania, 1.044 for  $UO_2-Gd_2O_3(5\%)$ , and 1.042 for  $UO_2-Gd_2O_3(10\%)$ , respectively.

As the fractal dimension increases the efficiency for the grains to fill the space increases. The difference in the ruggedness between  $UO_2-Gd_2O_3(5\%)$  and  $UO_2-Gd_2O_3(10\%)$  is not very significant. The grains of pure urania pellets are more rugged (i.e., has greater  $d_F$ ) than gadolinia containing pellets. Therefore  $UO_2$  fills in the space much more efficiently than gadolinia containing samples.

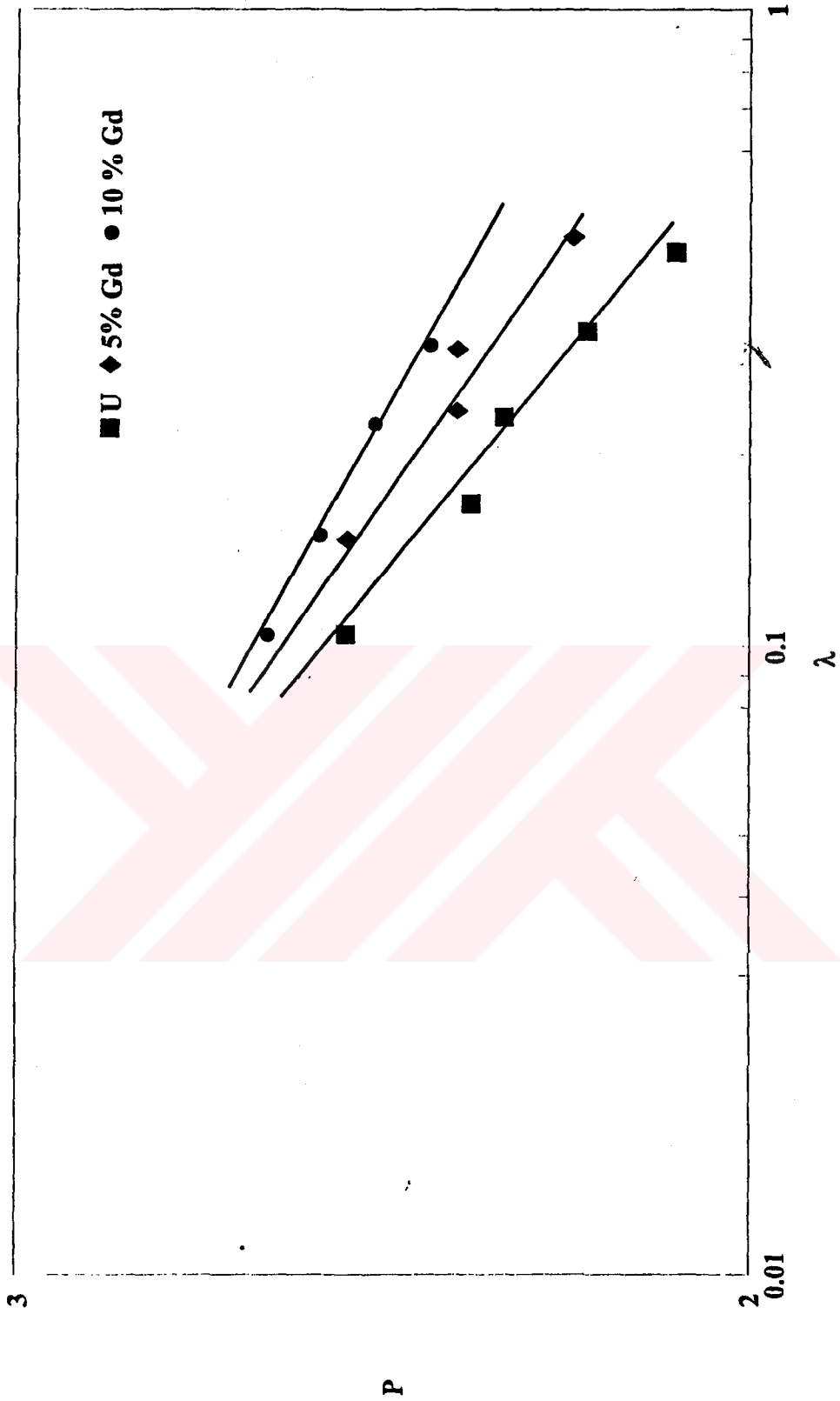


Figure 36. Fractal analysis of grains using structured walk technique

#### 10.1.4.11.2 Limited Self Similarity Method to Determine the Fractal Dimension of Grain Size Distribution

The fractal dimension of the grain pellets was obtained by using limited self similarity method. This theory has also been explained in Section 7.3 in detail. Figure 37 gives plots of the calculated results for all samples. Using this methodology, the fractal dimensions were calculated as 1.44 for  $\text{UO}_2$ , 1.58 for  $\text{UO}_2\text{-Gd}_2\text{O}_3(5\%)$ , and 1.6 for  $\text{UO}_2\text{-Gd}_2\text{O}_3(10\%)$ . The magnitude of fractal dimension gives information about the chaoticity of the parameter considered. We are considering the size of the grains here, and the largest chaoticity takes place in  $\text{UO}_2\text{-Gd}_2\text{O}_3(10\%)$  sample. In fact the generation of oxygen vacancies, interstitials and clusters, due to  $\text{U}^{5+}$  and  $\text{U}^{6+}$  formations and their diffusion in the lattice caused several problems as discussed in Section 10.1.4.4. This in turn affects the grain sizes in an undetermined manner. The large fractal dimensions of gadolinia containing samples show that the grain number dependence on grain sizes is more arbitrary in  $\text{UO}_2\text{-Gd}_2\text{O}_3(5\%)$  and  $\text{UO}_2\text{-Gd}_2\text{O}_3(10\%)$  than in  $\text{UO}_2$ -only sample.

Fractal dimensions can be defined for any parameter which shows a "growing" tendency. Porosity is another example which can be characterized by fractal dimension. When a basic description of the grains of the fuel pellet is calculated, then this relationship can be utilized to describe all the properties of the fuel pellet. For example the strength of the fuel pellet (S) could be related to the pellet porosity (P) and grain size (G) by the equation [125],

$$S = kG^{-a} e^{-bP} \quad (75)$$

where,

S is the strength (MPa)

G is the average grain size ( $\mu\text{m}$ )

P is the porosity (expressed as a fraction)

k, a, and b are constants.

As it is seen from this equation an increase in average grain size or porosity of the fuel pellets decrease the pellet strength. So fractal dimension of the grains can be easily related to the pellet strength. In this study fractal dimension of the pore size distribution of pellets were not studied because the porosities were too small. However in the literature fractal dimension of the pore size distribution of coals or catalysis were studied [157].

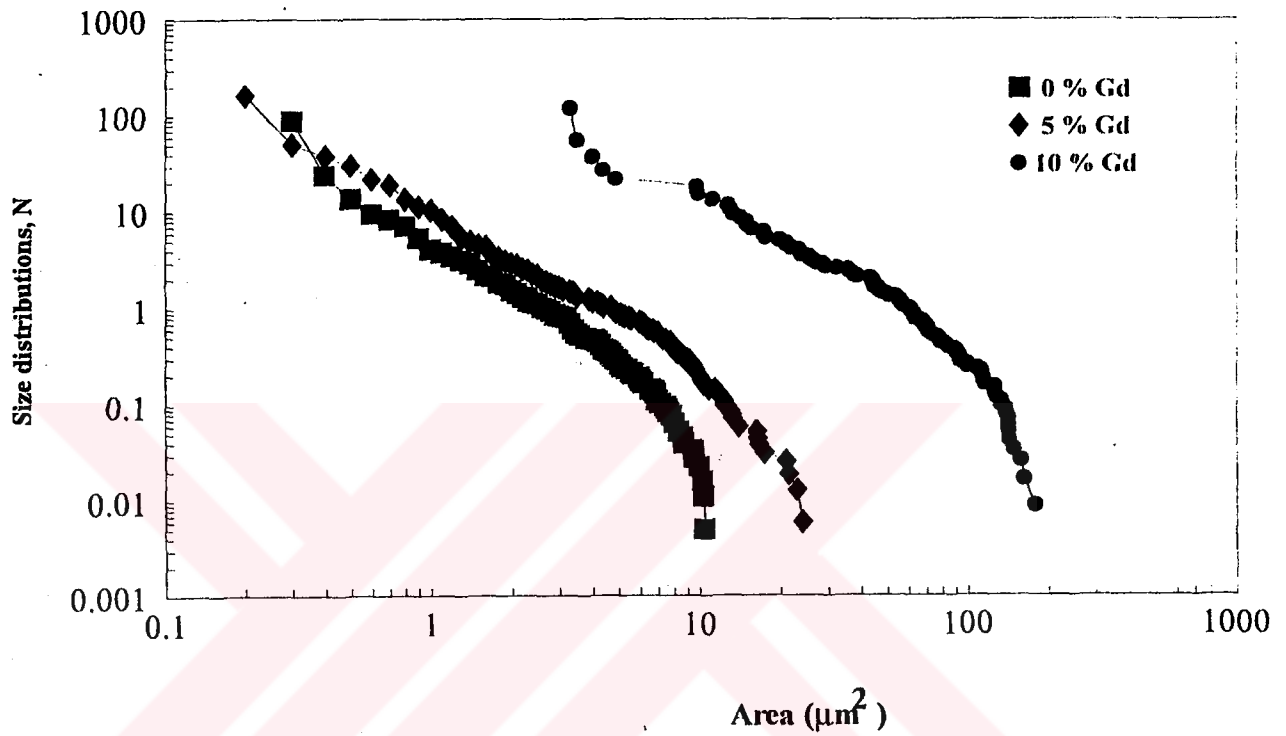


**Figure 37. Log-log plots of the size distributions versus area of the sintered grains using limited self similarity method**

## **10.2 Characterization of Boron Nitride Coating**

The identification of the deposited BN film was primarily based on examination by its color, BET, infrared absorption (IR), XRD, and SEM.

### **10.2.1 Color**

In the literature [68] the color of BN deposits was reported to vary from white to light yellow. These colors were also noted in this study. Some variations of color were observed but could not be correlated with the deposition condition. Boron nitride synthesized at 600 °C is a flaky and sticky white powder, it can easily be rubbed off.

### **10.2.2 Surface Area**

The surface area of BN measured by a surface area analyzer was found to be 2.38 m<sup>2</sup>/g. However, when sintered at 1600 K it turned into a transparent, hard, glassy material with negligible porosity.

### **10.2.3 Infrared Spectrum of BN**

The results of the IR spectrum analyses of BN powder (Fig.38) were found to be in agreement with the ones given in the literature [59,143-151]. The IR transmission spectrum of a pressed powder BN pill was scanned in the spectral range from 400 cm<sup>-1</sup> to 4000 cm<sup>-1</sup>. The strong absorption peak was found at 1400 cm<sup>-1</sup> and a weaker one appeared at about 800 and 880 cm<sup>-1</sup>. The strong peak is of B-N stretching while the weak peak is of B-N-B stretching [144]. It was reported that the IR spectrum of boron nitride is not very sensitive to variations in composition or crystalline form. Amorphous, hexagonal, and cubic polymorphs as well as films with variable B/N ratios have similar spectra.[ 150].

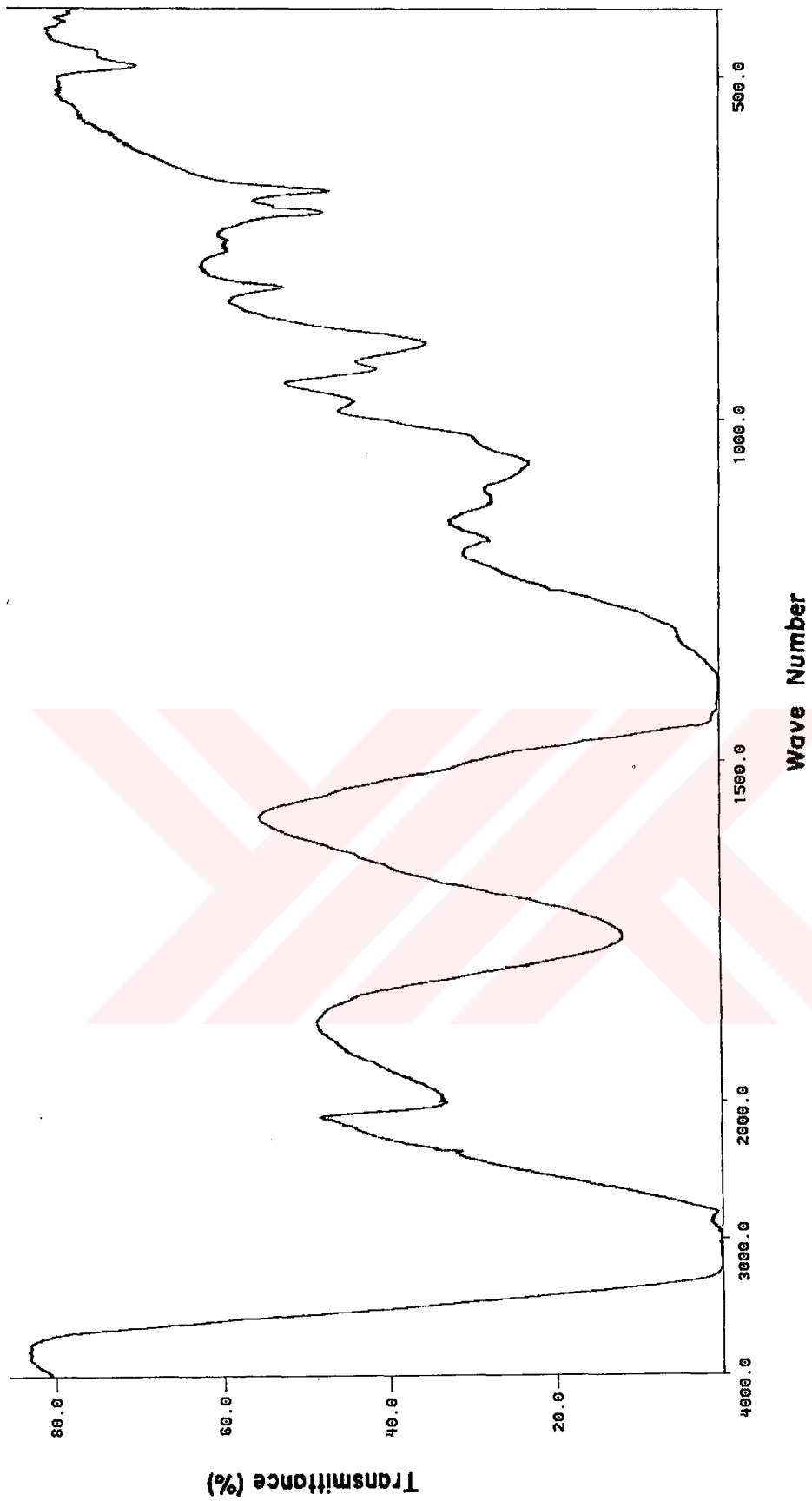


Figure 38. IR spectrum of BN powder

The position of the absorption band for B-N vibration was reported to be independent of the deposition temperature but the magnitude of the absorption changes slightly with the deposition temperature and crystallinity, probably as a result of the change in the number of BN stretching vibrations contributing to the spectrum.

#### 10.2.4 X-ray Diffraction (XRD)

The X-ray diffraction analyses of powder and sintered BN carried between  $2\theta=15-63^\circ$  was found to be in agreement with the ones given in the literature [66,153-156].

X-ray diffraction of BN gives peak at  $2\theta=26$ . It is a peak of hexagonal or turbostratic structure (Fig.39)[65,66,153-156]. The turbostratic BN structure is viewed as a semicrystalline phase with BN layers stacked roughly parallel to each other. The layers show random orientation and translation causing the broadening of the (002) peak. Figure 40 shows that after sintering at  $1300^\circ\text{C}$  the peak become sharp and it shows the polycrystalline formation. The crystal formation takes place above  $900^\circ\text{C}$ . Besides the major (002) peak, some very small peaks of (100), (101), (102), (004), and (103) are also reported [66,35]. These tiny peaks could barely be identified in Fig.s 40 (a) and (b).



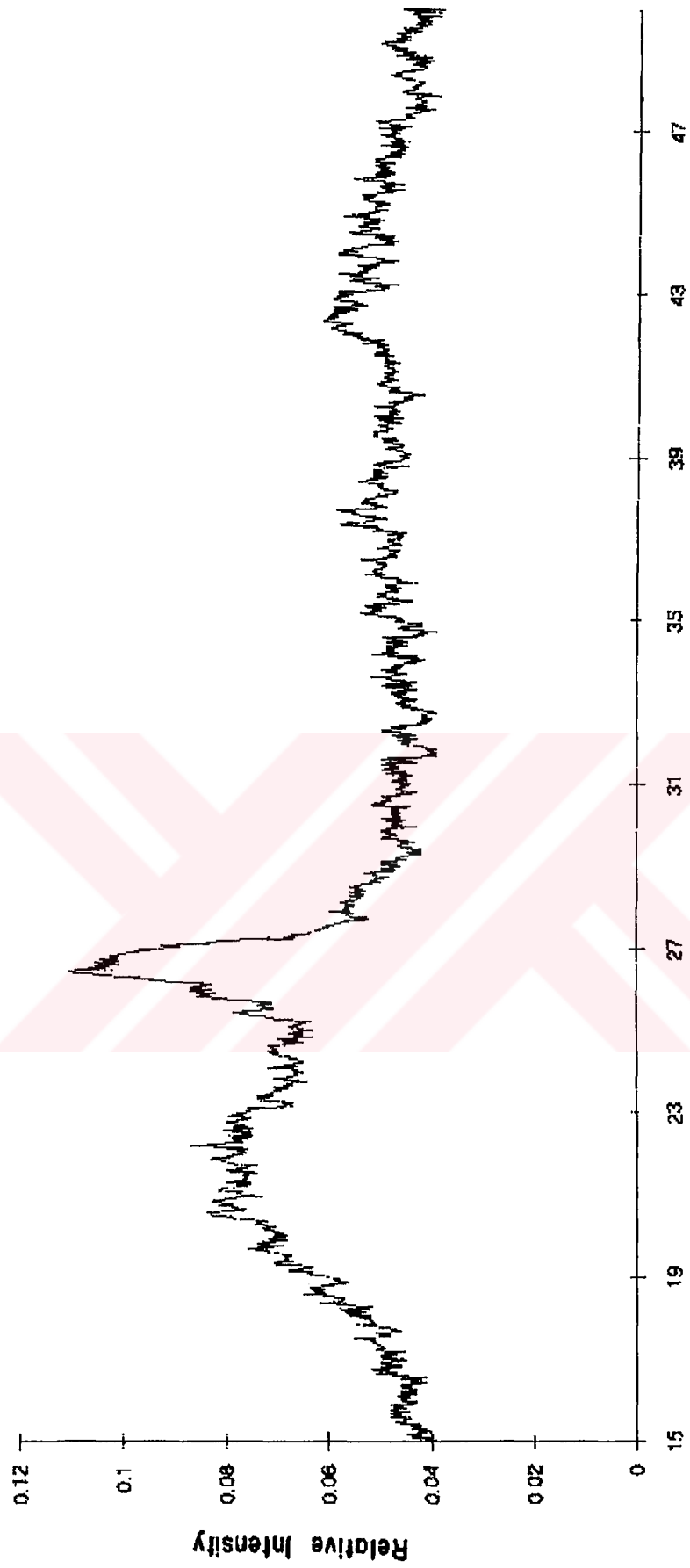


Figure 39. XRD pattern of BN powder

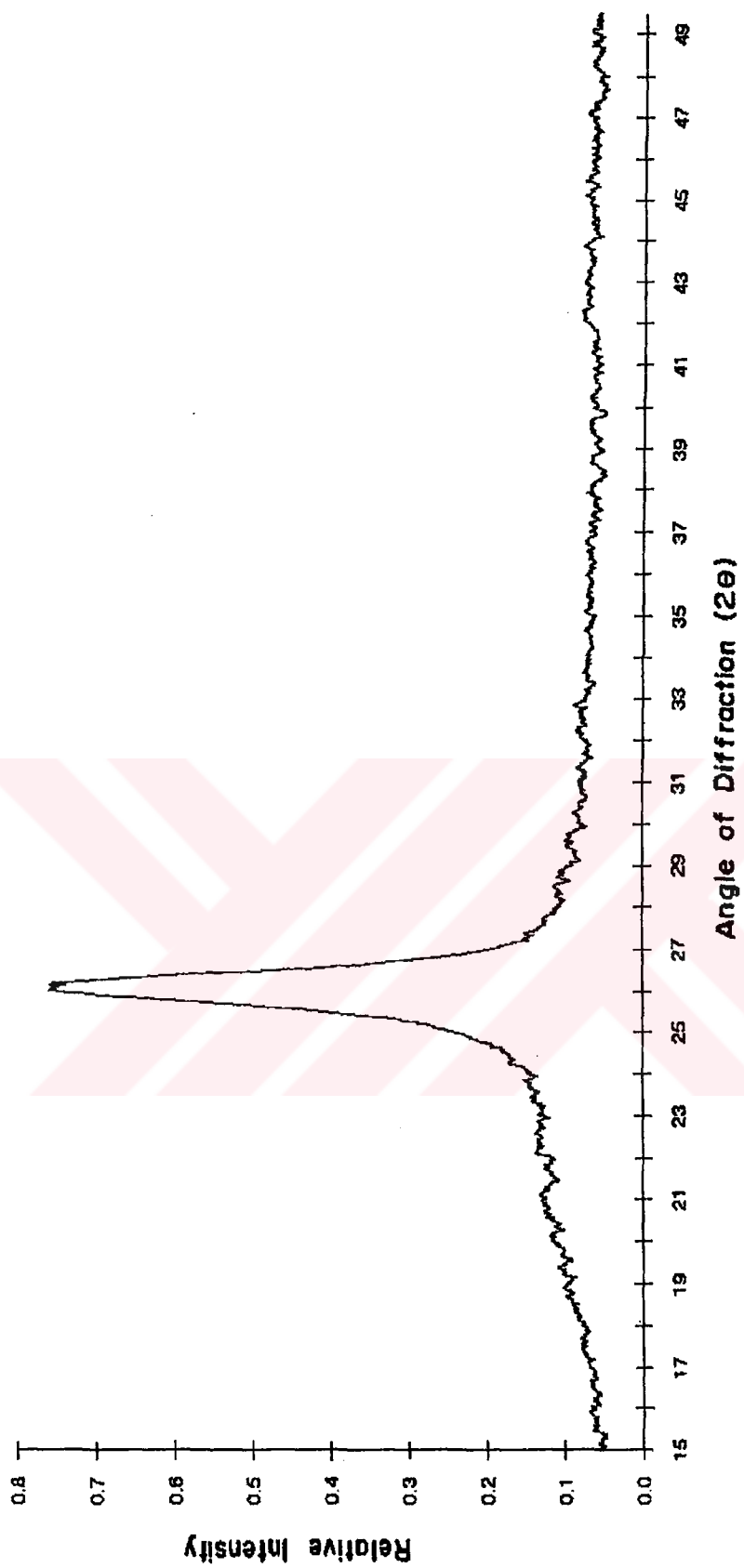


Figure 40 a. XRD pattern of sintered BN ( $2\theta < 50^\circ$ )

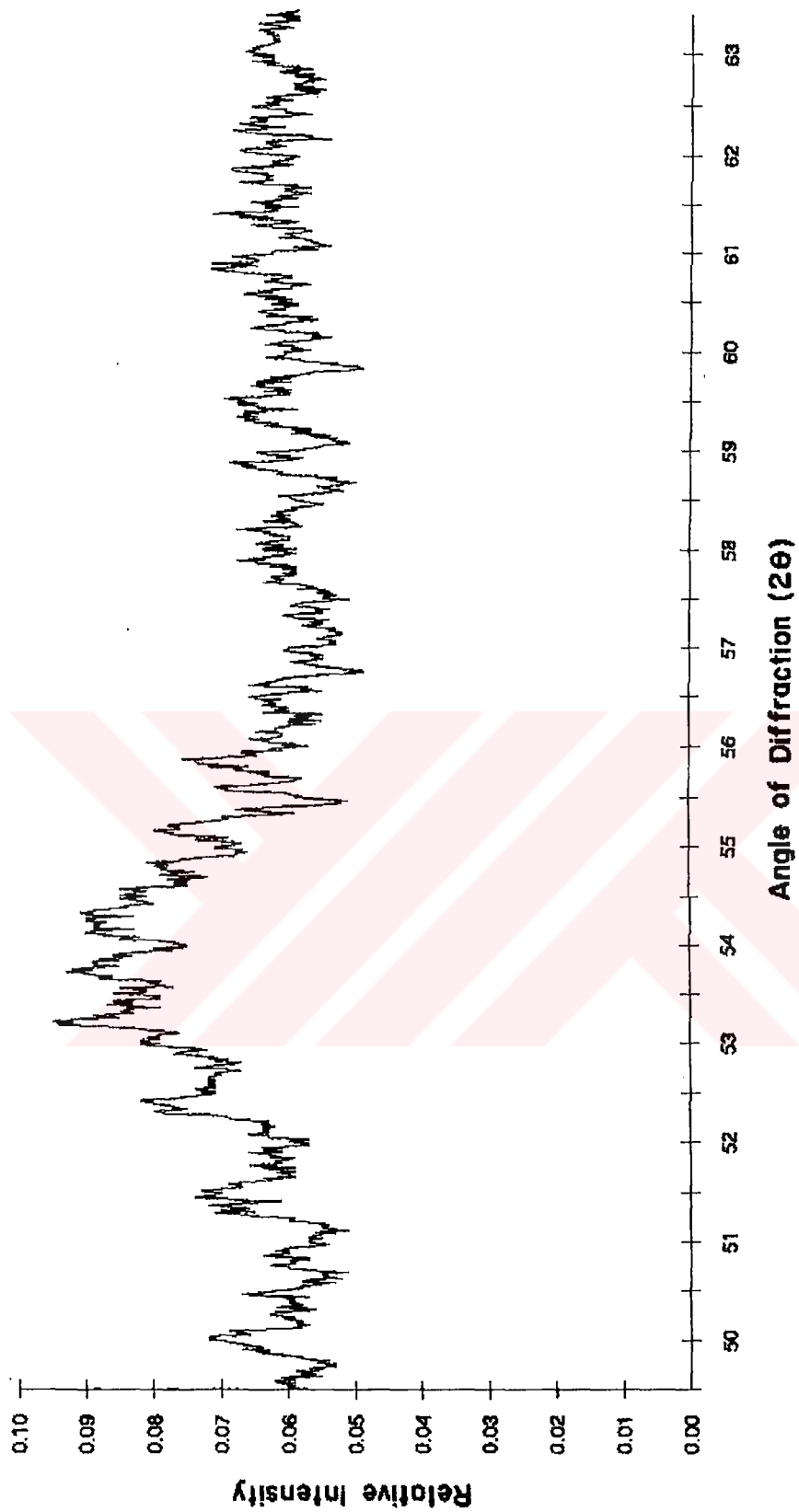


Figure 40 b. XRD pattern of sintered BN ( $2\theta > 50^\circ$ )

### 10.2.5 Scanning Electron Microscope (SEM)

The SEM micrographs are shown in Figs 41-56. The magnifications were shown as x1000, x3000, and x8000 under each photograph.

The BN coating on  $\text{UO}_2$  fuel pellet is shown in Fig.41. A larger magnified view is seen in Fig.42. This is a thin coating. The grains under the coating can be seen. Figure 43 shows even much thinner coating where grains can be seen easily. The uncoated sample is shown in Fig. 33.

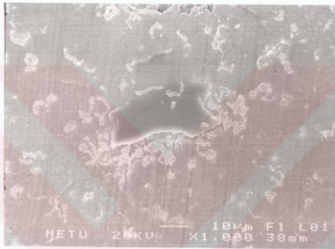


Figure 41. BN coating on  $\text{UO}_2$

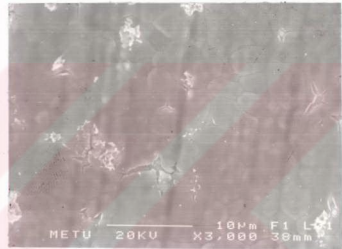


Figure 42. Magnified view of  
Fig.41

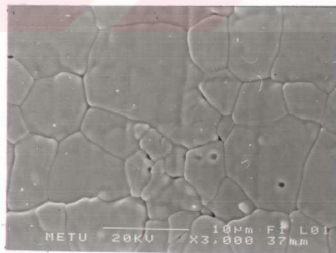
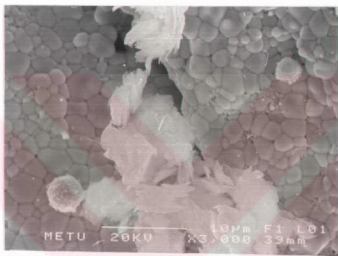
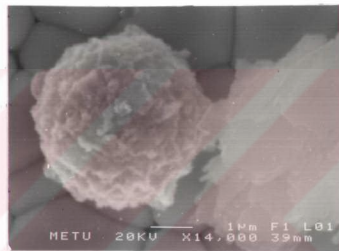


Figure 43. Thin BN coating

When sintering of BN was carried at 1800 K, most of the BN evaporated and the coating was incomplete. The bonds between B and N has to be established between 1400 - 1600 K to form an inorganic polymer. In fact once the BN coating was achieved between these temperatures, further heating to 1900 K did not change the glassy surface appearance. BN coating was persistent as expected. Deformation sites on the pellet creates nucleation sites and some BN forms as seen in Figs.44 and 45.



**Figure 44. BN formation on cracks**



**Figure 45. Magnified view of Fig.44**

Grain boundaries also form nucleation sites as seen in Fig.46.

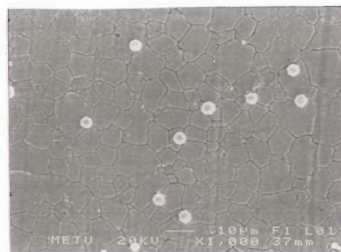
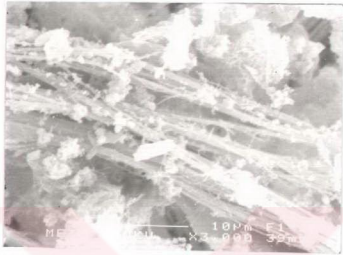
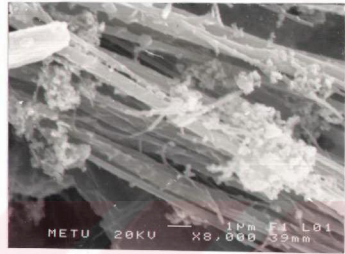


**Figure 46. BN formation on grain boundaries**

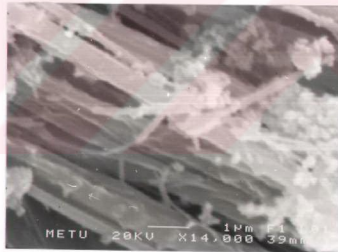
In a few cases fibrous BN formation was observed and it is shown in three different magnifications in Figs.47 a,b,c.



(a)



(b)



(c)

**Figure 47. Fibrous BN formation**

A leaflike BN formation was also rarely observed and it is shown in Fig. 48.

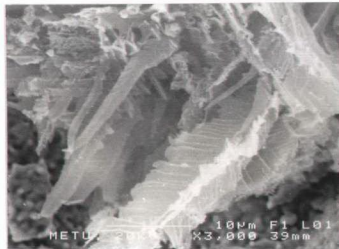
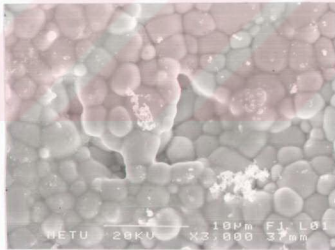


**Figure 48. Leaflike BN formation of  $\text{UO}_2$**

In Figure 49 the coatings on  $\text{UO}_2\text{-Gd}_2\text{O}_3(5\%)$  are shown. The fuel surface is completely covered with thin BN.



(a)



(b)

**Figure 49. BN formation on  $\text{UO}_2\text{-Gd}_2\text{O}_3(5\%)$**

In BN coating of  $\text{UO}_2\text{-Gd}_2\text{O}_3$ (10%), some rodlike formations were observed. They are shown in Fig.50. These formations were not observed in  $\text{UO}_2$  and  $\text{UO}_2\text{-Gd}_2\text{O}_3$ (5%). The surface potential of the substrate affects the geometry of the structure of BN formed. However glassy BN formation could also be easily seen on the surface.

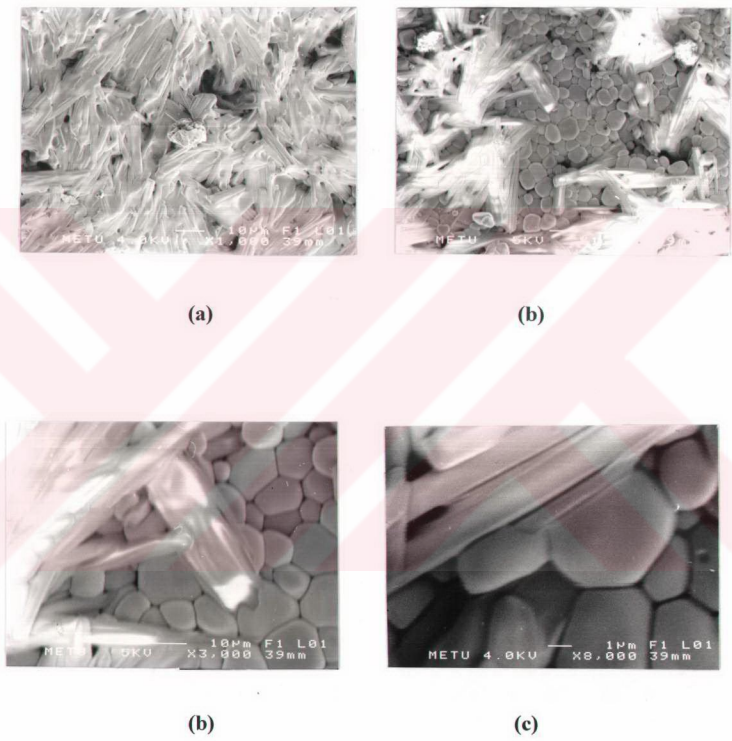
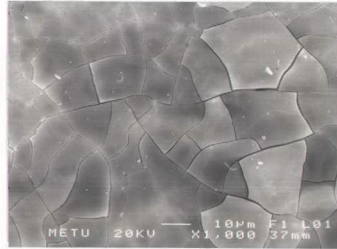


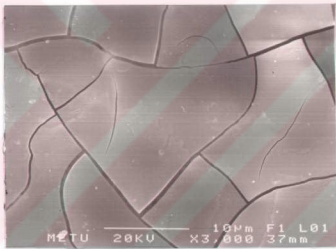
**Figure 50. Rodlike BN formation of  $\text{UO}_2\text{-Gd}_2\text{O}_3$  (10%) with different magnifications**



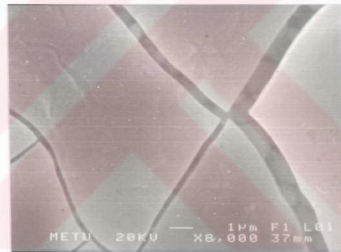
The increased thickness caused cracks on the BN coating as seen from Fig.51. The cracks were observed after sintering at 1650 K. It may result due to thermal stresses during cooling period.



(a)



(b)



(c)

**Figure 51. Cracks on BN coating of  $\text{UO}_2\text{-Gd}_2\text{O}_3$  (10%)**

In Figure 52 a completely formed BN plate is seen on the right upper part while the rest of the surface is coated with granular BN.

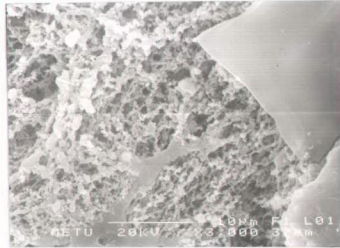
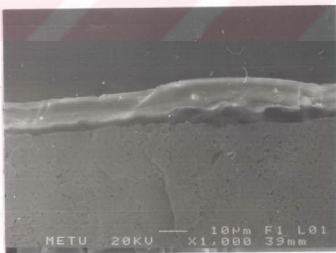
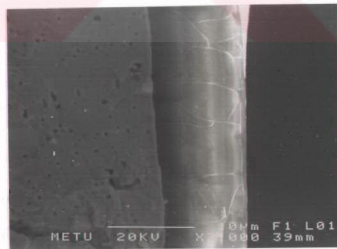


**Figure 52. Partially coated BN formation**

The side views of the coating were also pictured in  $\text{UO}_2$ ,  $\text{UO}_2\text{-Gd}_2\text{O}_3(5\%)$ , and  $\text{UO}_2\text{-Gd}_2\text{O}_3(10\%)$  specimens which are cracked axially. Figure 53 shows the side view of BN coating on urania. The upper layer in the first figure and the layer on the right hand side of the second figure are BN coating which forms only on the surface with no penetration into the fuel in either case. It is seen that there is a very good adherence of BN on substrate. The thickness of the coating is uniform and about  $10\ \mu\text{m}$  in these figures.



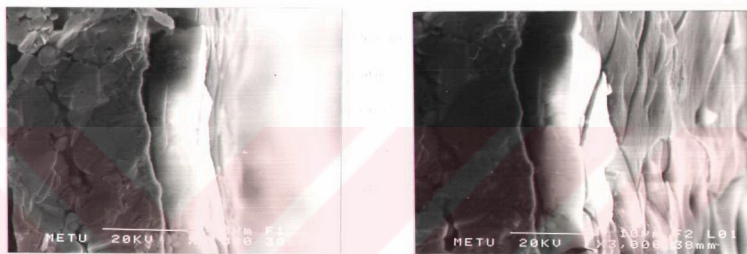
(a)



(b)

**Figure 53. Side views of BN coating on  $\text{UO}_2$   
(x1000 and x3000 magnifications)**

Figure 54(a) shows the side view of BN coating on  $\text{UO}_2\text{-Gd}_2\text{O}_3(5\%)$ . Figure 54(b) is a tilted photograph of the same zone so that we can see both the side and top views. Figure 55 was taken by using backscattering technique. The white area shows the heavy atom zone which is the fuel. BN and fuel atoms are not penetrated into each other. BN stays as an inert unpenetrating smooth coating on the fuel.



(a)

(b)

Figure 54. Side view of BN coating on  $\text{UO}_2\text{-Gd}_2\text{O}_3(5\%)$

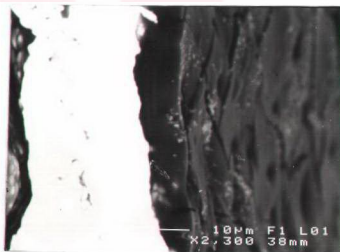
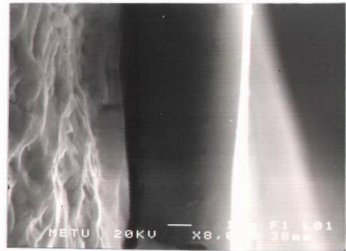


Figure 55. Side view of BN coating with backscattering technique

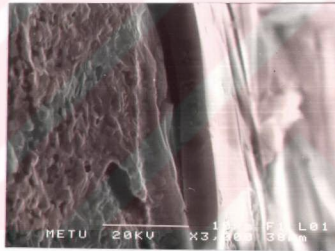
Figure 56(a) shows the side view of BN coating on  $\text{UO}_2\text{-Gd}_2\text{O}_3(10\%)$ , while Figure 56(b,c) are somewhat tilted pictures.



(a)



(b)



(c)

Figure 56. Side view of BN coating of  $\text{UO}_2\text{-Gd}_2\text{O}_3(10\%)$

### 10.3 Neutronic Calculations

The neutronic calculations performed by WIMS-D/4 code have been mainly based on  $k_{\text{eff}}$  and burnup. Although a single fuel rod goes subcritical below  $k_{\text{eff}}=1$ , other rods in the neighborhood may have  $k_{\text{eff}}$  slightly higher than one. Therefore the calculations were extended to  $k_{\text{eff}}$  values lower than one to see all possible changes in the burnup.

Figures 57a,b and 58 show the changes of  $k_{\text{eff}}$  values for 5% and 3.2 % enriched fuels respectively. Figure 57b is identical to Fig. 57a except the burnup axis is extended further. These figures show that the increase of gadolinium content or the increase of BN coating thickness on the fuel have the same type of effect on  $k_{\text{eff}}$  in either case. Although 5% gadolinia fuel has gained high popularity in the last decade, it is seen that “ $\text{UO}_2 + 30 \mu\text{m BN}$ ” fuel is much more effective and efficient than 5% gadolinia fuel. In fact gadolinia was put into the central fuel out of 25 fuels, while BN coating was done in all 25 fuels. Therefore BN coating provides much better neutron flux flattening and much less thermal gradients. Because gadolinia has a very high thermal absorption cross section, it is depleted very fast and “ $\text{UO}_2\text{-Gd}_2\text{O}_3(5\%)$ ” curve joins “ $\text{UO}_2\text{-only}$ ” curve around 10,000 MWd/TU for 5% enriched fuel as seen from Fig.57a. However “ $\text{UO}_2\text{-Gd}_2\text{O}_3(2.5\%)$ ” curve joins “ $\text{UO}_2\text{-only}$ ” curve at lower burnups around 5000 MWd/TU for 3.2% enriched fuel as seen from Fig.58.

The increase of gadolinia from 5% to 10% does not affect the behavior of the curves. Both Fig.57 and 58 show that “ $\text{UO}_2\text{-Gd}_2\text{O}_3(10\%) + 30 \mu\text{m BN}$ ” curve behaves more or less like “ $\text{UO}_2 + 30 \mu\text{m BN}$ ” curve. The former introduces higher negative reactivity which results in lower  $k_{\text{eff}}$ . The same behavior is observed for “ $\text{UO}_2 + 70 \mu\text{m BN}$ ” cases. As BN thickness increases from 30  $\mu\text{m}$  to 70  $\mu\text{m}$ , BN becomes the dominant burnable poison and “ $\text{UO}_2\text{-Gd}_2\text{O}_3(5\%) + 70 \mu\text{m BN}$ ” curve approaches “ $\text{UO}_2 + 70 \mu\text{m BN}$ ” curve.

All poisons seem to have the same effects on  $k_{\text{eff}}$  after 30000 MWd/TU as seen from Fig.57b. However a close inspection shows that highly poisoned fuels yield larger  $k_{\text{eff}}$  values than others at large burnup levels leading higher core cycle life. For instance in 5% enriched fuel, “ $\text{UO}_2\text{-Gd}_2\text{O}_3(5\%) + 30 \mu\text{m BN}$ ” fuel gives 50341 MWd/TU while “ $\text{UO}_2\text{-no BN}$ ” fuel gives 48975 MWd/TU at  $k_{\text{eff}}=1$ . At 3.2 % enrichment (Fig.58), “ $\text{UO}_2\text{-Gd}_2\text{O}_3(5\%) + 30 \mu\text{m BN}$ ” fuel gives 31576 MWd/TU while “ $\text{UO}_2\text{-only}$ ” fuel gives 30343 MWd/TU at  $k_{\text{eff}}=1$ .

The area between the top curve (e.g., pure  $\text{UO}_2$ ) and any of the other curves (which have burnable poisons) corresponds to the net saving. This area is somewhat proportional to the saving in reactor volume. In other words the positive reactivity corresponding to this area had to be controlled by control rods. By using burnable poisons, some of the control rods are eliminated, in addition the available volume can be filled with fuel.

At 5 % enrichment (Fig.57a), “ $\text{UO}_2 + 30 \mu\text{m BN}$ ” fuel provides a criticality at the very beginning since  $k_{\text{eff}}=1$ . This fuel can be used safely without running into reactivity problems. For the fuels giving  $k_{\text{eff}} < 1$  at the beginning, some time must pass to achieve criticality. Therefore, they need less poisoned or highly enriched fuels around.

At 3.2 % enrichment (Fig.58), only 2.5 %  $\text{Gd}_2\text{O}_3$  fuel gives  $k_{\text{eff}} > 1$  value after 3,600 MWd/TU. In 70  $\mu\text{m BN}$  coated fuels criticality is achieved after 10,000 MWd/TU. They somewhat behave as a kind of control rods at the beginning of cycle due to their high negative reactivity. To use 70  $\mu\text{m BN}$  in low enriched fuel is not appropriate.

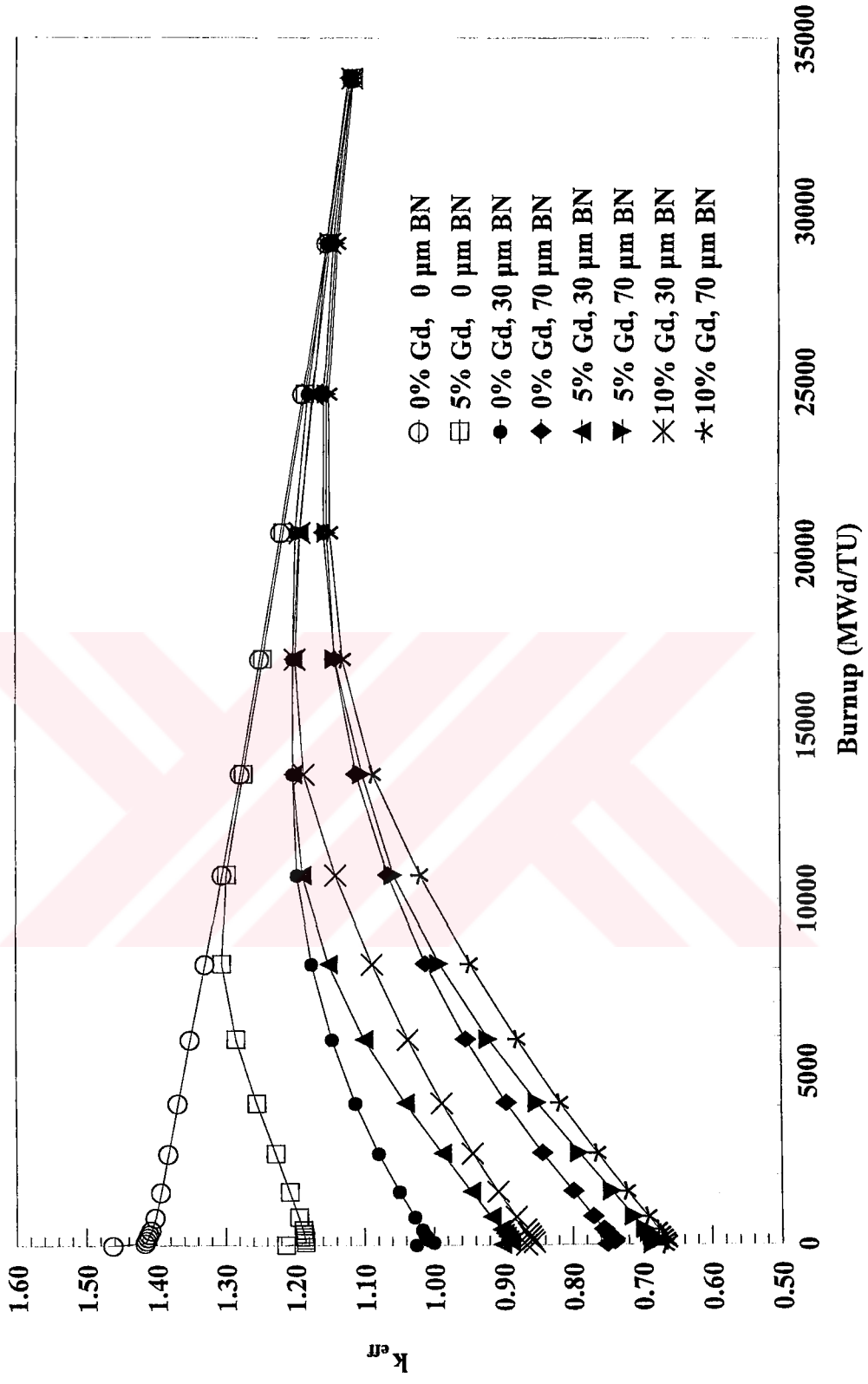


Figure 57 a.  $k_{eff}$  values for uraniumdioxide-gadolinium oxide fuel coated by BN (enrichment: 5%, assembly: 25 rods)

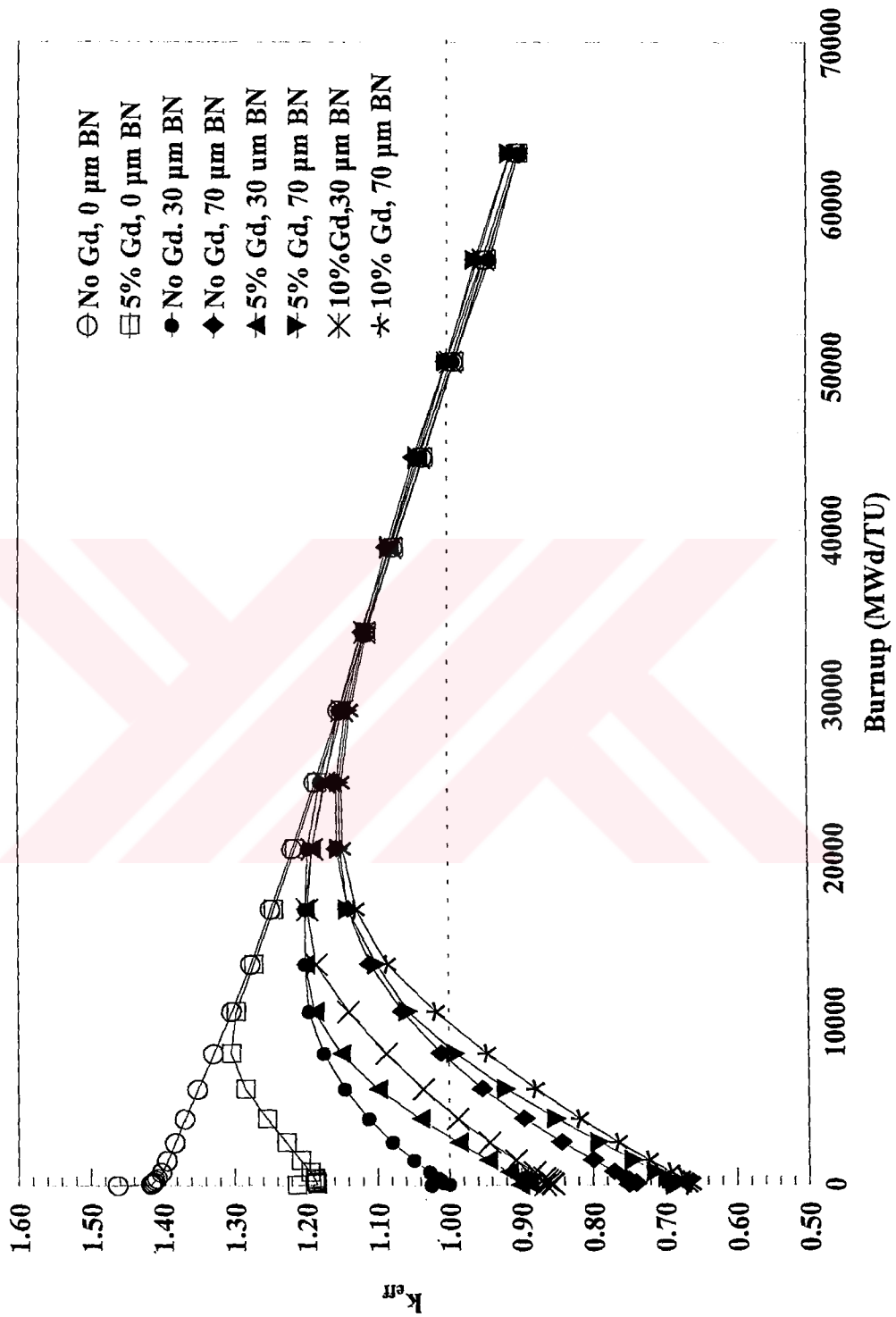


Figure 57 b.  $k_{\text{eff}}$  values for uraniumdioxide-gadolinium oxide fuel coated by BN (enrichment: 5%, assembly: 25 rods)



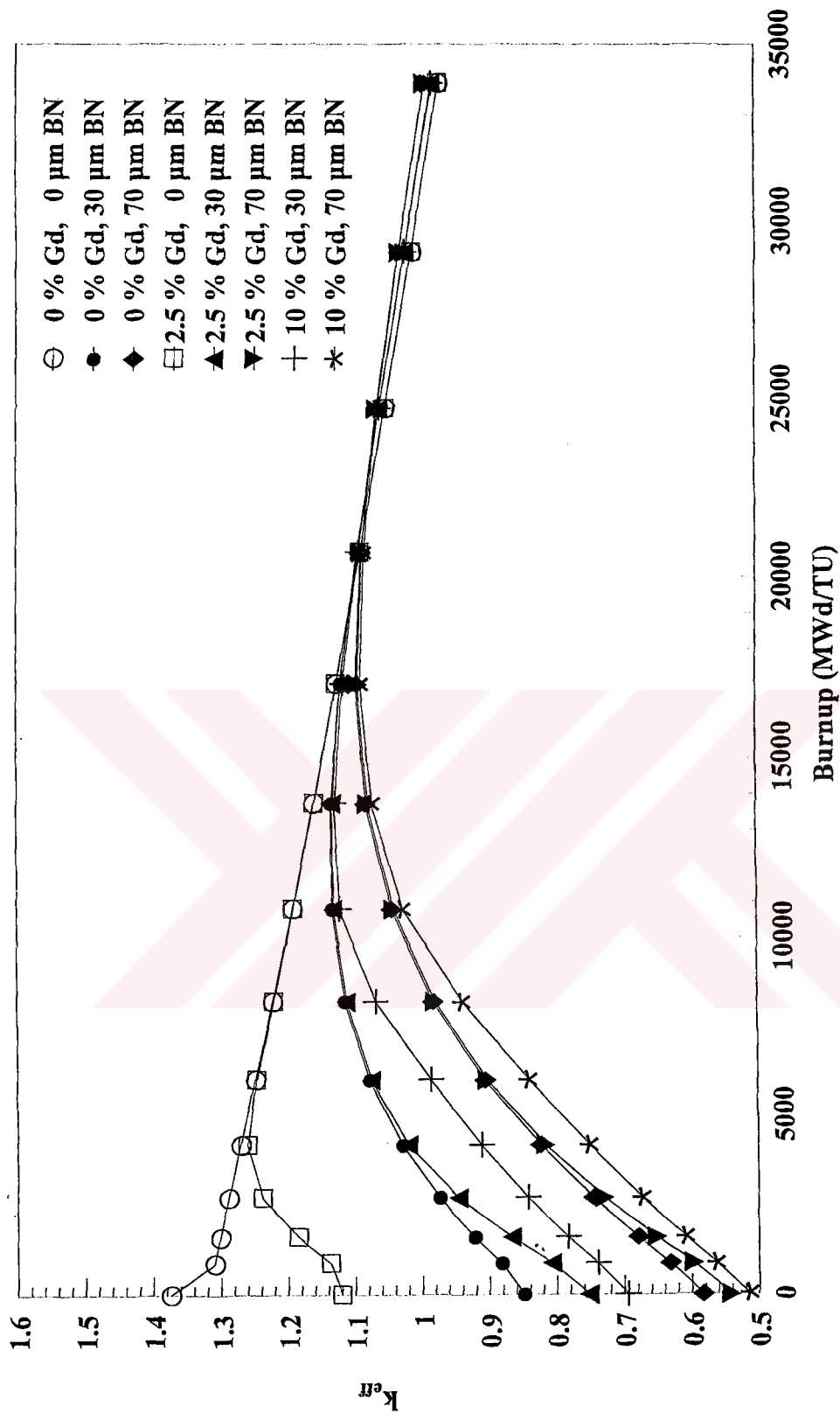


Figure 58.  $k_{eff}$  values for uraniumdioxide-gadolinium oxide fuel coated by BN (enrichment: 3.2 %, assembly: 25 rods)

The geometry used in the calculations can be changed to get the criticality and high burnup by other arrangements of burnable absorbers. The calculations were based on one gadolinia containing fuel at the center and 24 BN coated fuels around it. The BN coating thickness and gadolinia content can be changed to achieve the best burnup.

The BN thickness must be adjusted such that it should completely deplete towards the end of cycle, and thus it should not exert any residual negative reactivity. Figure 59 gives BN depletion concentration in the core for 5% enriched and 30  $\mu\text{m}$  BN coated fuel with different pitch distances. It is estimated that for any type of pitch distance after 40000 MWd/TU burnup, the BN concentration goes to negligible amount. It is lowered to  $4 \times 10^{-5}$  g/cm from the beginning concentration of  $2.2 \times 10^{-2}$  g/cm. In 3.2 % enriched fuel it is lowered to  $6 \times 10^{-6}$  g/cm at 30000 MWd/TU burnup.

Gadolinium depletes at much faster rates due to its high absorption cross section. The rate of depletion for gadolinium isotopes is shown in Fig 60.

The dependence of total energy production on pitch distance was shown in Fig. 61. The pitch distances were changed in the calculations to see the effect of neutron moderation. The larger pitch distance between fuel elements correspond to higher water/fuel volume ratio and thus higher moderation. The linearity is lost below 1.35 cm. The model reactor (i.e., PWR of KWU) has a pitch distance of 1.27 cm. The lower pitch distances result in lower moderation, and thus the lower rate of burning. It may also introduce some thermohydraulic problems. The pitch distance used in KWU, (e.g., 1.27 cm) gives, also the highest burnups for all the fuels studied as seen from Fig. 62. Therefore no core design change is needed for the fuels studied. This is in fact an extremely important point.

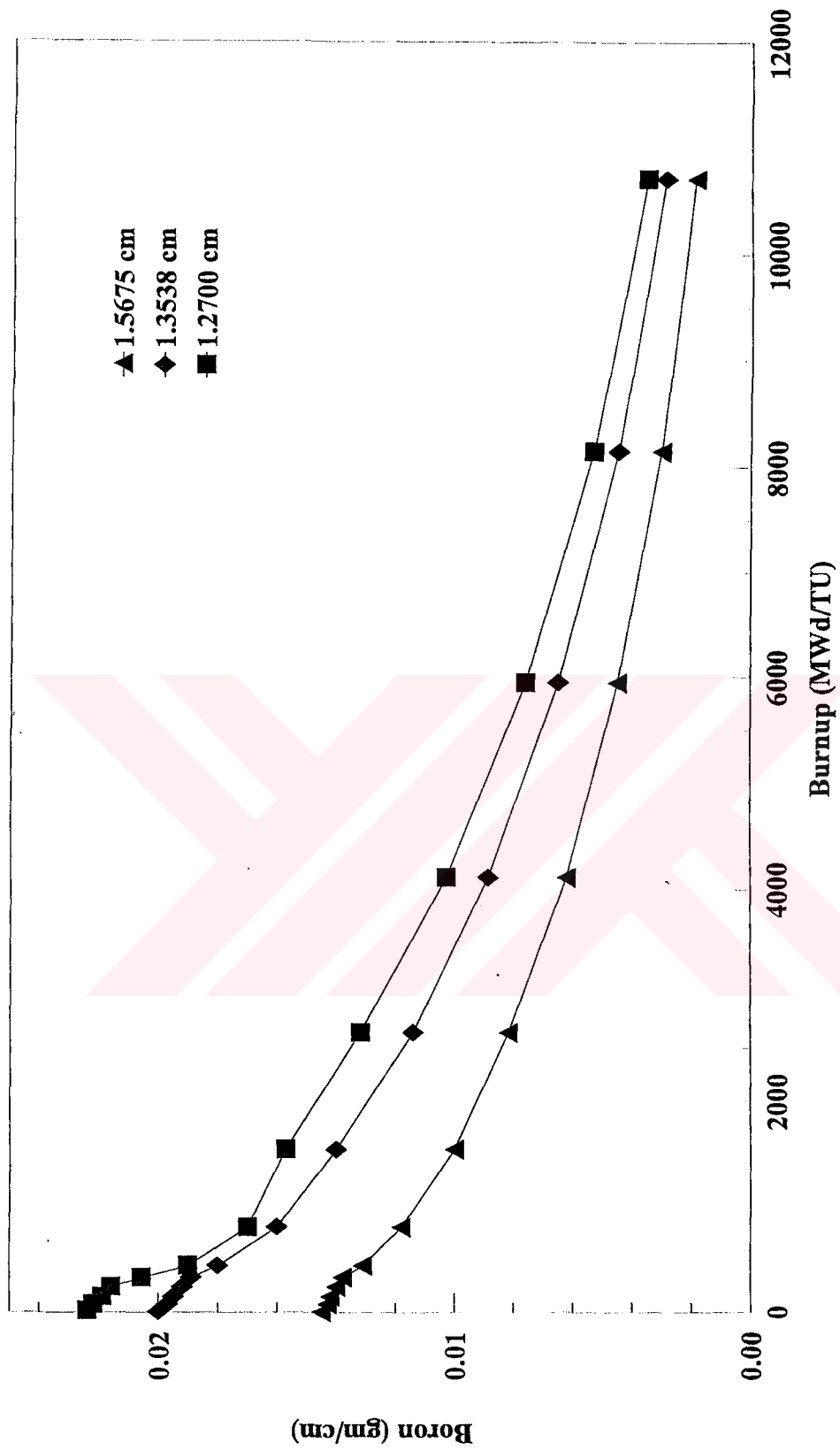


Figure 59. Boron depletion with different pitch distances  
(pure uranium with 30  $\mu$ m BN, 5%enriched fuel)

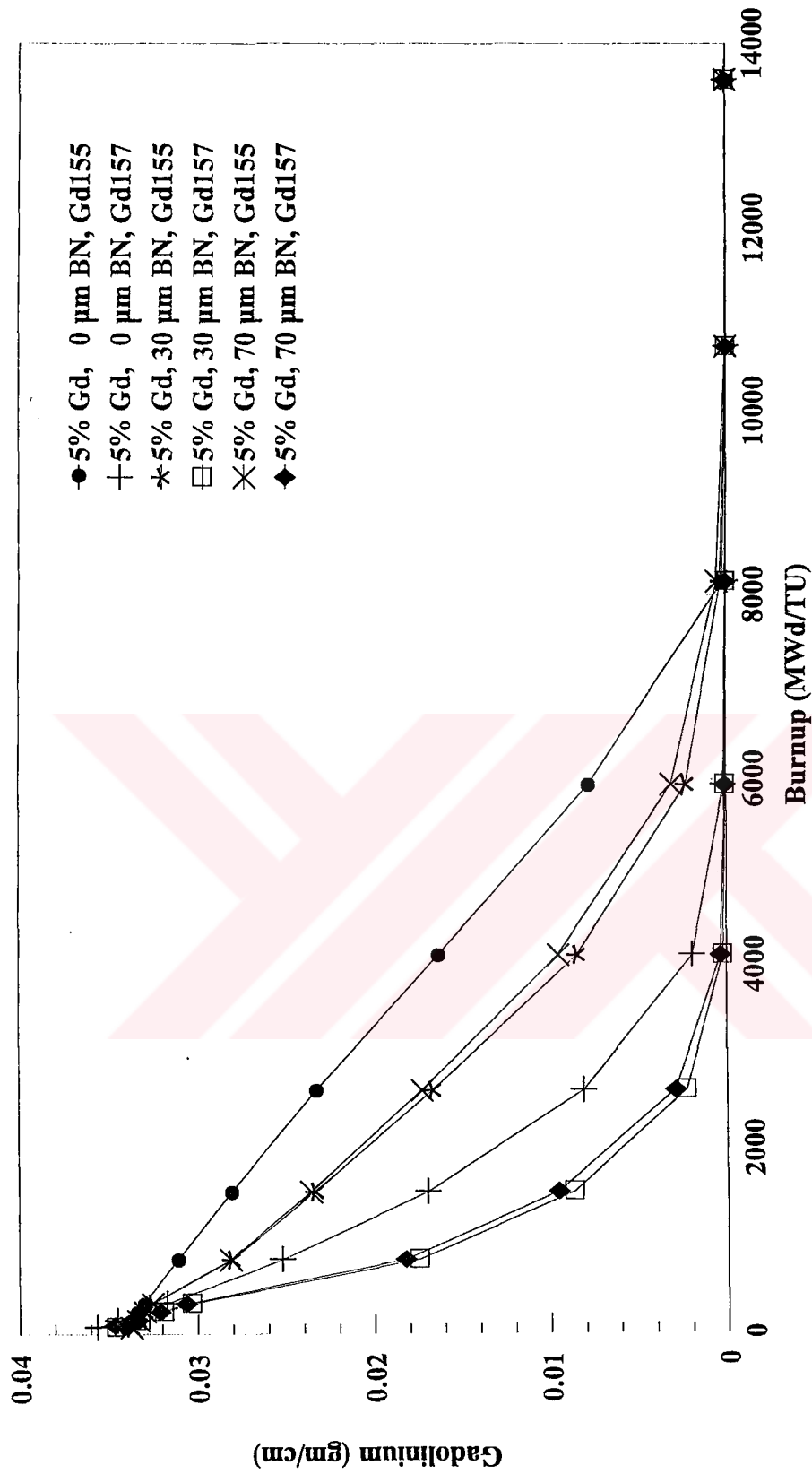


Figure 60. Gadolinium depletion for different types of fuels

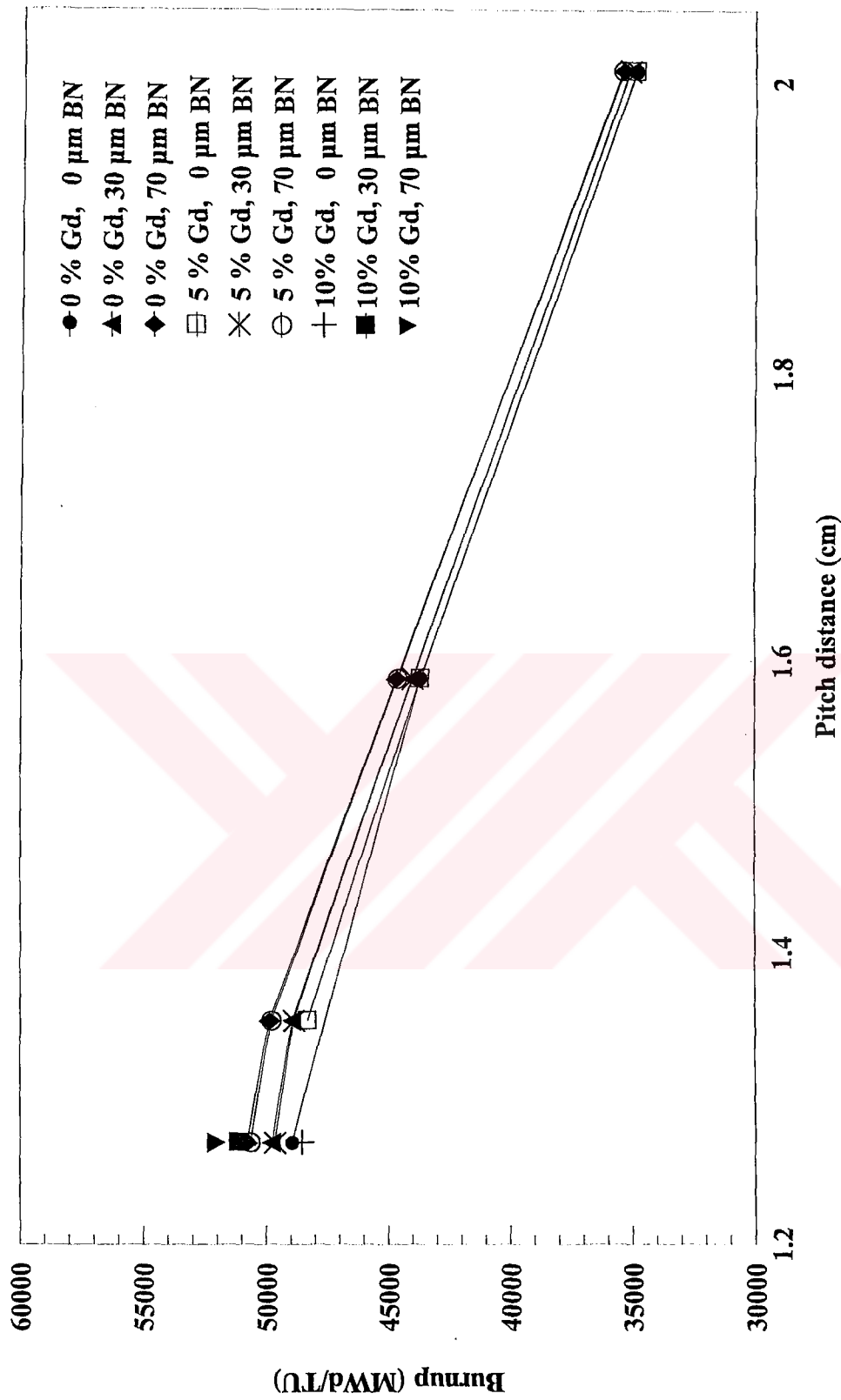


Figure 61. Burnup values when  $k_{\text{eff}} = 1$  for different types of fuels

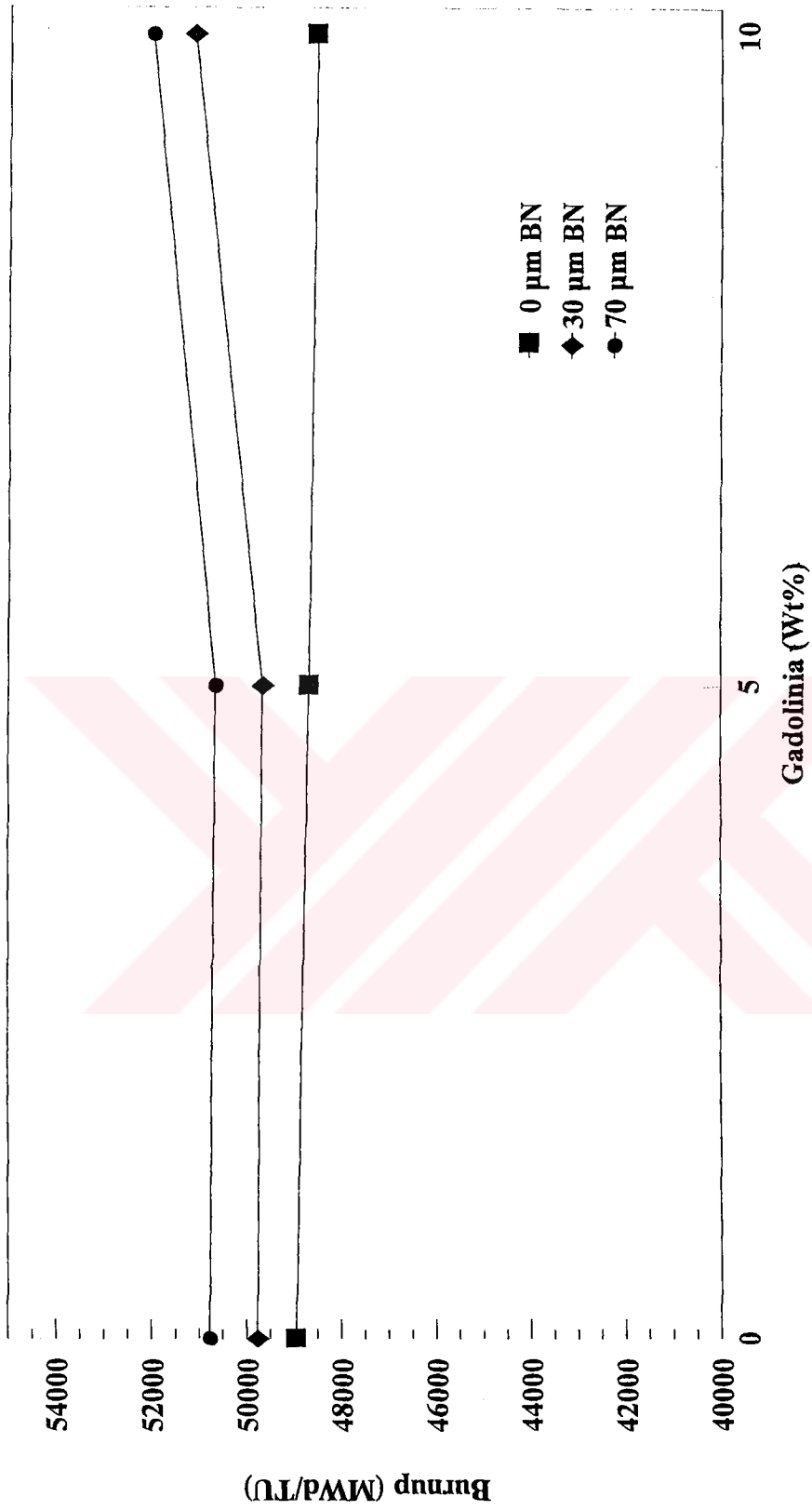


Figure 62 . The effect of BN thickness on burnups  
(pitch distance: 1.27cm)

The main advantage in lowering the pitch distance is to get less moderation (i.e., relatively hardened spectrum) and thus to get higher plutonium production as mentioned earlier in the Section 2.7. However burnable absorbers harden the spectrum and result in the same effect, that is, they cause higher Pu production.

Figures 63 and 64 show the change of Pu-239 concentration for 5% enriched fuel. Pu-239 concentration was given in terms of g/cm as traditionally done. It is the amount of Pu-239 produced per unit length of fuel per unit area (i.e.,  $\text{cm}^2$ ). There is not any significant effect of Gd on Pu-239 production while BN has a significant effect as seen from the upper curves. However, this does not indicate high Pu-239 production due to the presence of BN only. Because gadolinia exists in one out of 25 fuel rods, while BN coating is on all fuels. Pu-239 produced in the fuel undergoes either fission or neutron capture reaction to give Pu-240 which is not fissile but gives Pu-241 on further neutron capture. The fission and capture cross sections of Pu-239 are 741 b and 274 b while those of Pu-241 are 950 b and 425 b, respectively. Pu-241 is also a good fissile material produced in the reactor fuel. As seen from Figures 65 to 67 Pu-239 production remains almost constant in all cases at  $k_{\text{eff}} \sim 1$  which is achieved around 50,000 MWd/TU for most fuels as seen from Fig.57b. The presence of gadolinia and BN does not have any significant contribution on the production of other isotopes. The depletion of U-235 was shown in Fig. 68. There is a slight difference in the amount of residual U-235 between  $\text{UO}_2$ -only fuel and others. The relatively high Pu-239 production in burnable absorber fuels leads slightly higher residual U-235.

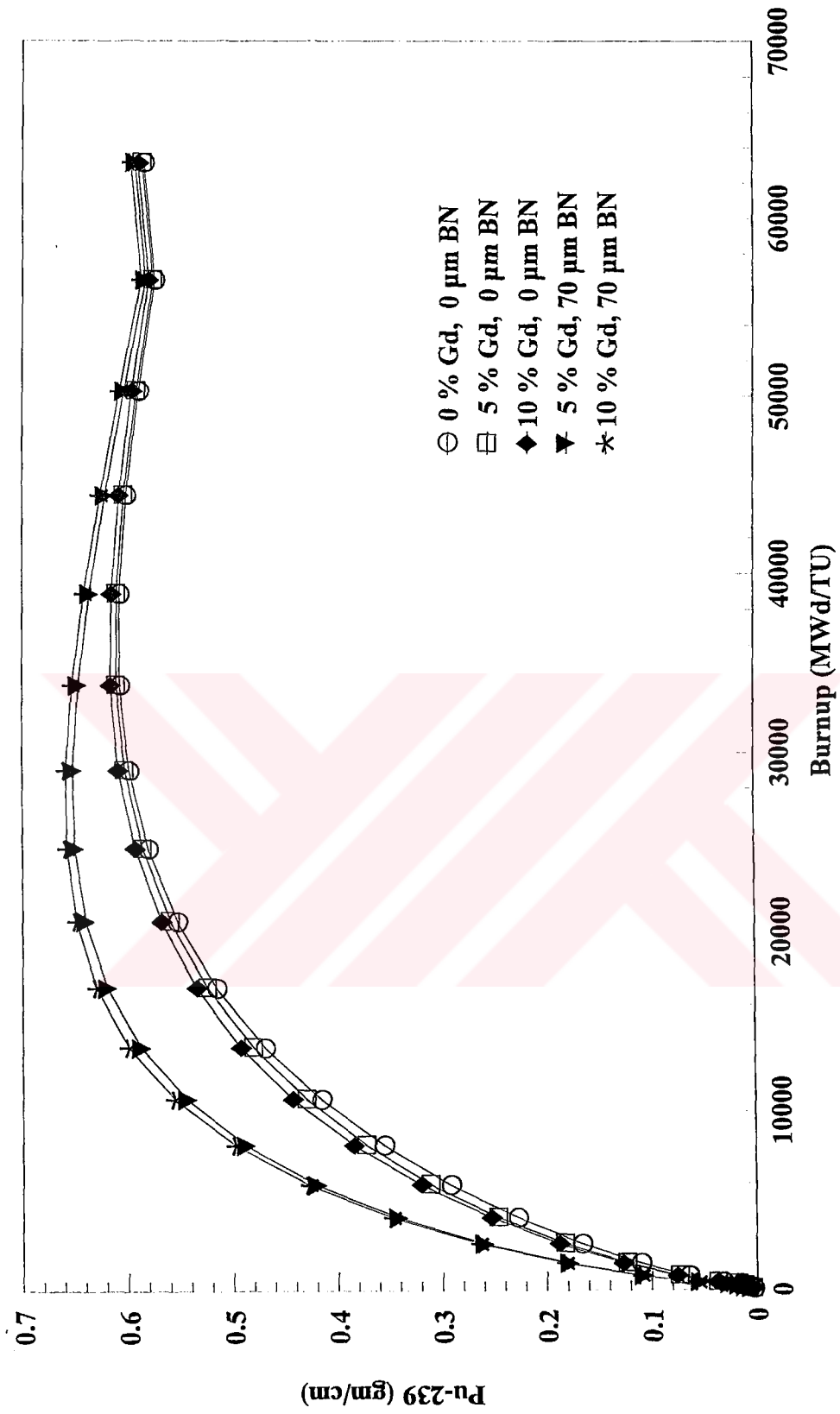


Figure 63 . Gadolinium effect on plutonium production  
(enrichment:5%, pitch distance:1.27 cm)



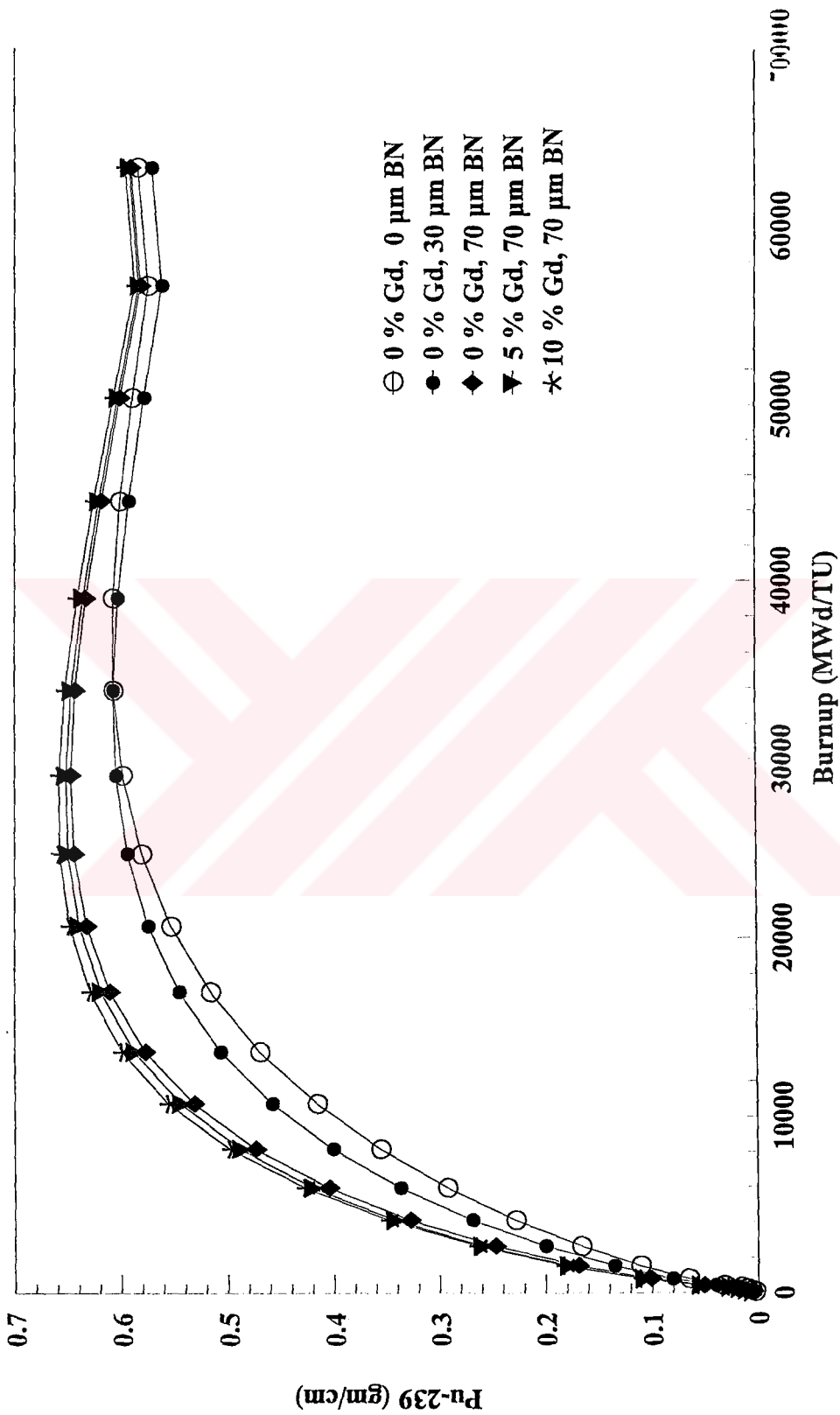


Figure 64 . Boron effect of plutonium production in different fuels  
(enrichment: 5%, pitch distance: 1.27 cm)

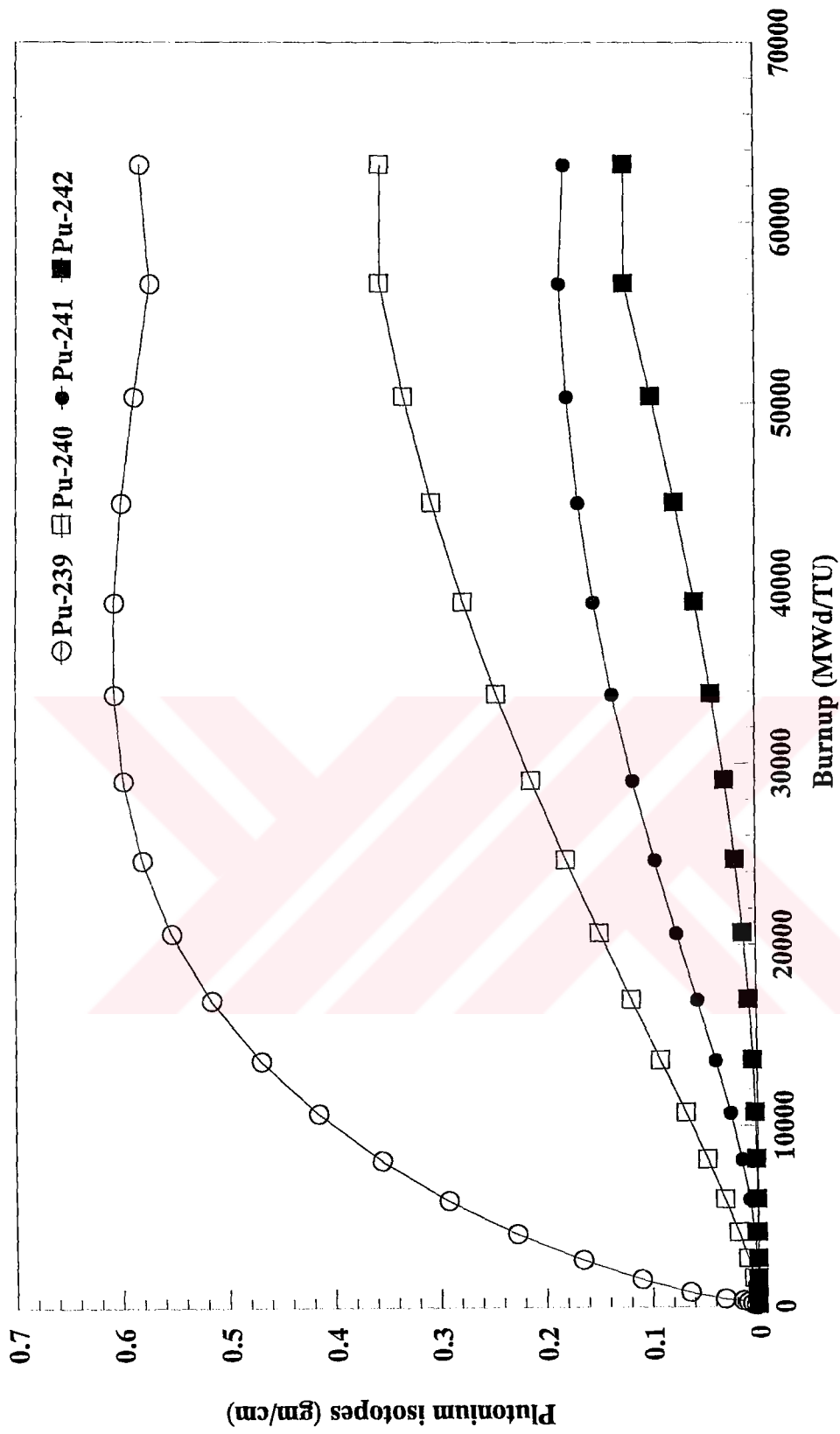


Figure 65. Production of plutonium isotopes  
 (Gd: 0 %, BN: 0 μm, enrichment: 5%, pitch distance: 1.27 cm)

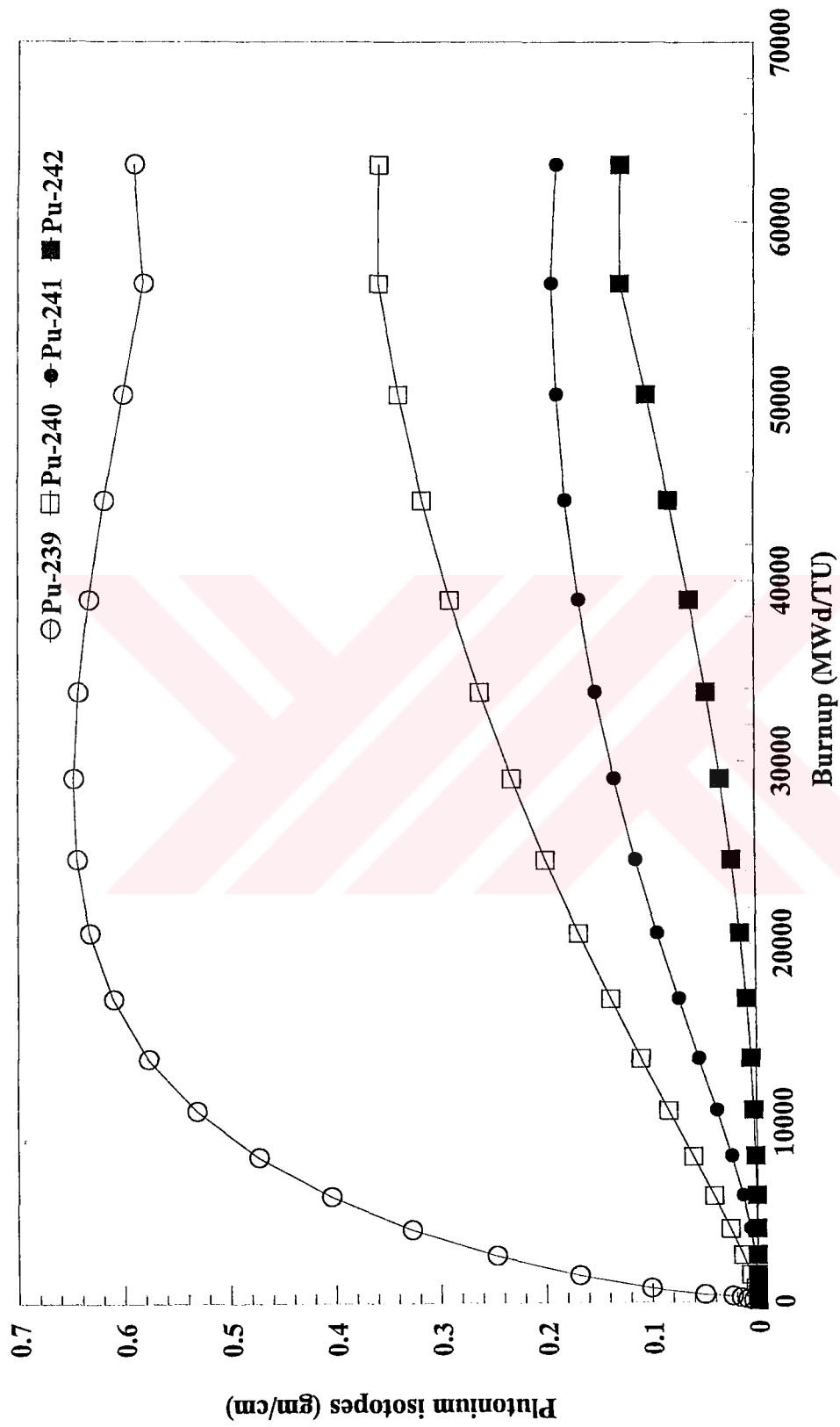


Figure 66 . Production of plutonium isotopes  
 (Gd:0%, BN 70 μm, Enrichment:5%, pitch distance:1.27 cm)

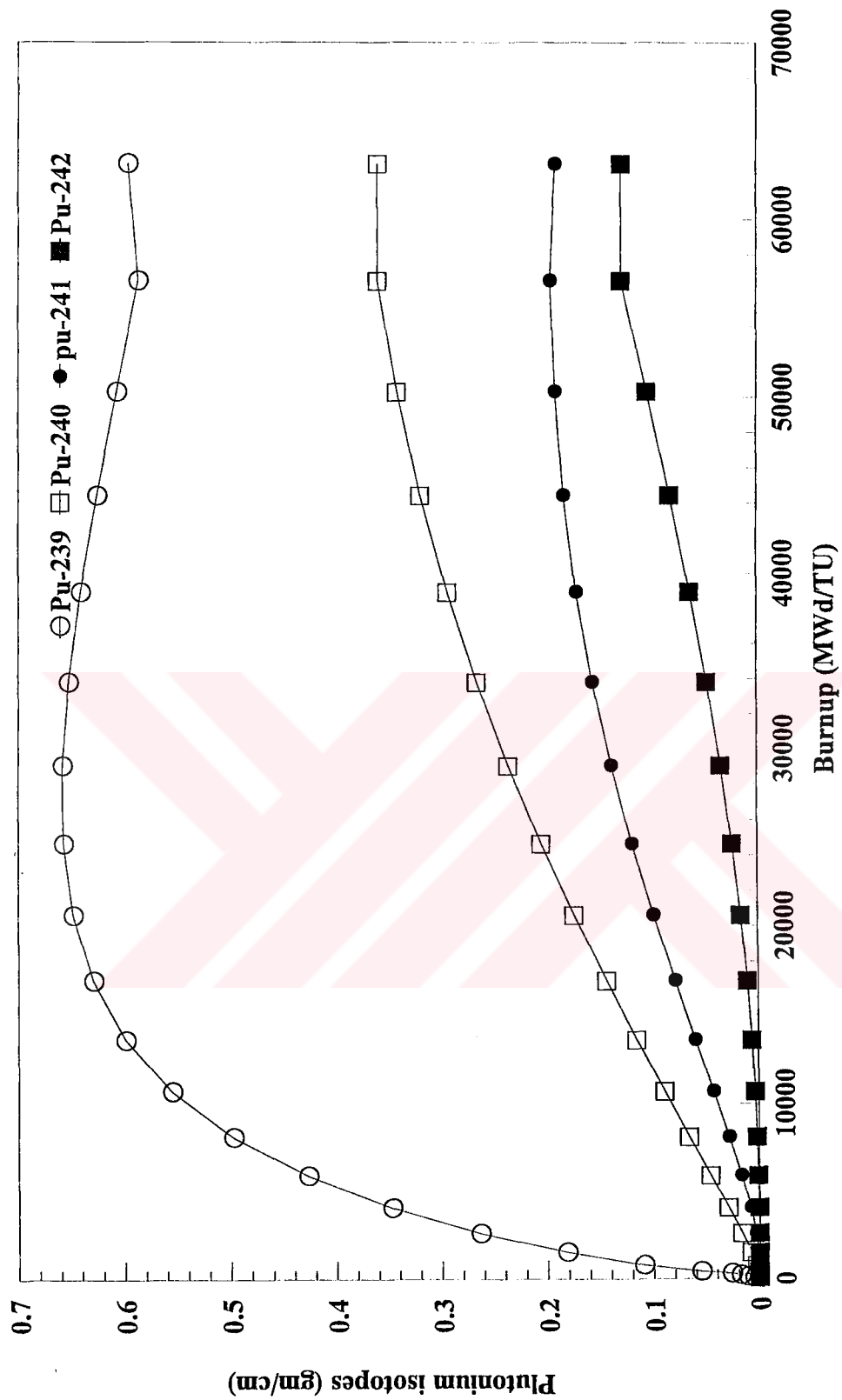


Figure 67. Production of plutonium isotopes  
(Gd:10 %, BN: 70  $\mu$ m, enrichment: 5%, pitch distance:1.27 cm)

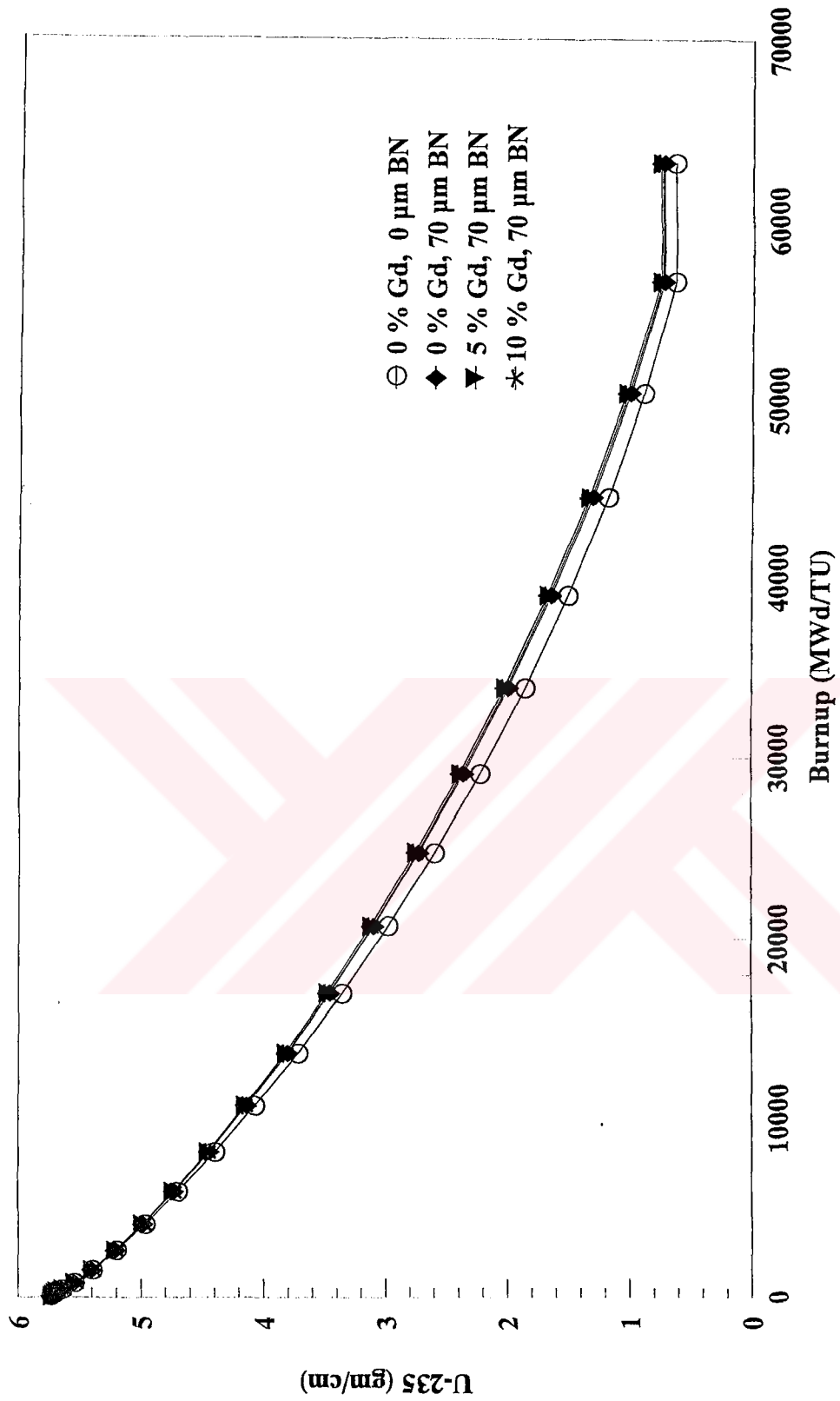


Figure 68 . Depletion of U-235 in different fuels  
(enrichment: 5%, pitch distance: 1.27 cm)

## CHAPTER 11

### CONCLUSIONS

#### Fuel:

1. The addition of gadolinia to urania can be performed successfully by sol-gel method.
2. Green pellet densities are reported to change between 45 to 50 %.
3. PVA decomposes on a wide temperature range and it is more advantageous to use it rather than stearic acid. PVA was used as binder in all other specimens in this research work.
4. At lower compaction pressure gadolinia containing fuel shows larger porosity than  $\text{UO}_2$  -only fuel. However high pressure compaction must be preferred not to reduce pores only but also to reduce voids which cause severe decrease in density.
5. A high reduction temperature of powder yields low pellet density. Therefore the reduction temperature must be taken as 873 K to obtain pellets with high densities.
6. XRD pattern of  $\text{UO}_2\text{-Gd}_2\text{O}_3(5\%)$  and  $\text{UO}_2\text{-Gd}_2\text{O}_3(10\%)$ , have the same characteristic peaks with  $\text{UO}_2$ -only. This means that gadolinia mix with urania homogeneously and they form a single phase.
7. The cumulative pore volume decreases 3.33 times in  $\text{UO}_2$ -only, 3.97 times in  $\text{UO}_2\text{-Gd}_2\text{O}_3(5\%)$ , and 3.12 times in  $\text{UO}_2\text{-Gd}_2\text{O}_3(10\%)$  due to compaction at 200 MPa.
8. The density of  $\text{UO}_2$ -only was found to be 98.01 % of the theoretical density which is a very high achievement; the reported values for the conventional techniques is 94-96%. The observed densities of  $\text{UO}_2\text{-Gd}_2\text{O}_3(5\%)$  and  $\text{UO}_2\text{-Gd}_2\text{O}_3(10\%)$  fuels were found to be 95.3 and 95.9 % respectively.
9. The cumulative pore volume of sintered pellets was decreased almost one order of magnitude (e.g., 10 times) compared to green pellets.  $\text{UO}_2$  fuel has

the minimum porosity while  $\text{UO}_2\text{-Gd}_2\text{O}_3(5\%)$  has larger porosity than  $\text{UO}_2\text{-Gd}_2\text{O}_3(10\%)$ . It is well known that gadolinia retards sintering and thus leads to larger pores in sintered pellets.

10. Surface morphology of the grains of  $\text{UO}_2$  and  $\text{UO}_2\text{-Gd}_2\text{O}_3$  fuel pellets were studied by using scanning electron microscope. It is concluded that the addition of gadolinia does not change the general appearance of grains and their packing mode, but it increases the grain size.
11. The difference in the ruggedness between  $\text{UO}_2\text{-Gd}_2\text{O}_3(5\%)$  and  $\text{UO}_2\text{-Gd}_2\text{O}_3(10\%)$  is not very significant. The grains of pure urania pellets are more rugged than gadolinia containing pellets. Therefore  $\text{UO}_2$  fills the space much more efficiently than gadolinia containing samples.
12. The  $\text{UO}_2\text{-Gd}_2\text{O}_3(10\%)$  sample shows the largest fractal dimension of grain size distribution. The large fractal dimensions of gadolinia containing samples shows that the grain number dependence on grain sizes is more arbitrary in  $\text{UO}_2\text{-Gd}_2\text{O}_3(5\%)$  and  $\text{UO}_2\text{-Gd}_2\text{O}_3(10\%)$  than in  $\text{UO}_2$  only sample.

#### **BN Coating:**

13. The IR spectrum analyses of BN powder was found to be in agreement with the ones given in the literature [30,31]. A strong absorption peak was found at  $1400\text{ cm}^{-1}$  and a weaker one appeared at about  $800$  and  $880\text{ cm}^{-1}$ .
14. X-ray diffraction analyses of powder and sintered BN were found to be in agreement with the ones given in the literature.
15. Platelike and rodlike BN layers formed on fuel pellets. A leaflike BN formation was rarely seen.
16. The side views of the coating showed that BN coating forms only on the surface and has no penetration into the fuel and also there is a very good adherence of BN on the substrate. BN and fuel atoms are not penetrated into each other. BN stays as an inert unpenetrating smooth coating on the fuel.

**Neutronic calculations:**

17. The effects of burnable poisons either gadolinia or BN essentially disappear after 30,000 MWd/TU.
18. At 5% enrichment, “UO<sub>2</sub>+30μmBN” fuel provides criticality at the very beginning since its  $k_{\text{eff}} \geq 1$ . This fuel can be used safely without running into much reactivity problems.
19. Other fuels can be used in the appropriate locations in the core depending on the neutron flux pattern.
20. It is estimated that for any type of pitch distance after 40,000 MWd/TU burnup, the BN concentration goes down to negligible amount.
21. Gadolinium is depleted at much faster rates due to its high absorption cross section.
22. The pitch distance used in commercial reactors (i.e., 1.27cm in KWU) gives the highest burnup. Therefore no core design change is needed.
23. There is no appreciable effect of Gd on Pu-239 production. while BN does have a significant effect. This must be due to their amounts used in the reactor.
24. The amounts of Pu isotopes do not vary with the amounts Gd or BN.



## RECOMMENDATIONS

In future, further work should be done using Plasma Enhanced Chemical Vapor Deposition (PECVD) technique. Such a technique may produce BN thin films with more desirable properties at low substrate temperatures. Deposition and sintering can also be done simultaneously in this process.

Another recommendation is to coat the fuel with boron instead of BN. Here again CVD technique can be used, and  $H_2$  is used instead of  $NH_3$  to produce pure boron film from  $BCl_3$ .



## REFERENCES

- [1] Swisher J. and Wilson D., Energy, **18**, No.5, 437, 1993.
- [2] Rogner H., Nakicenovic N., Grubler A., Energy, **18**, No.5, 461, 1993.
- [3] Marchetti C., Nucl. Sci. Eng., **90**, 521, 1985.
- [4] IAEA, Power Reactors Information Service (PRIS), 1994.
- [5] Radioactive Waste Management, International Atomic Energy Agency (IAEA) Information Series, Division of Public Information, 1993.
- [6] Ayanođlu S.F. and Gündüz G., J. Radioanalytical Chem. **43**, 155, 1978.
- [7] Hepşen T., “Muđla Yatađan Linyitlerinden Uranyum Deđerlendirilmesi”, ITÜ, Mining Engineering Department, October, 1976.
- [8] Projected Costs of Generating Electricity from Power Commission in the period 1995-2000, NEA-OECD, 1992.
- [9] Öner D.D. and Bayraktar B.N., “Nükleer Enerji Raporu”, TAEK-TR-94-1, 1994.
- [10] “WASP Modeli ile Türkiye Uzun Dönem Üretim İncelenmesi”, TEK-APK 352, 1991.
- [11] Ünlü K., Nucl. Eng. Int., 16, January 1995.
- [12] Nucl. Eng. Int., 51, 1994.

- [13] Lamarsh, J.R., "Introduction to Nuclear Reactor Theory", Addison Wiley Pub. Co., Ontario, 1966.
- [14] IAEA Training Course on Safety Review and Assessment for Construction Permit, AECB, Ontario, Canada, 1985.
- [15] OECD and IAEA, "Uranium; Resources, Production and Demand", NEA, OECD, Paris, 1993.
- [16] Durmazucar H., "Uranium Dioxide productivity by Sol-Gel Technique", Master's Thesis, Middle East technical University (METU), 1989.
- [17] Chacrabarti S., and Paul A., "Ceramic Pigments and Enamels through Solution Route:", Trans. Indian. Ceram. Soc., 45, 1, 7, 1986.
- [18] Has P.A. and Clinton S.D., I and EC. Prod. Res. Dev., 5(3) 236, 1966.
- [19] Ferguson D.E., Dean O.C., and Douglas D.A., "Sol-Gel Process for the Remote Preparation of Recycle Fuels", Third Conferance on Peacefull Uses of Atomic Energy, U.S.A., 1964.
- [20] Proc.Symp. "Thorium Fuel Cycle", Gatlinburg, Tennessee, May 3-6, 1966, CONF-660524, U.S. Atomic Energy Commission, 1966.
- [21] Proc.Symp. "Sol-Gel Processes For Ceramic Nuclear Fuels", International Atomic Energy Agency, (IAEA), Vienna, May 6-10, 1968.
- [22] Proc. Symp. "Sol-Gel Processes and Reactor Fuel Cycles", Gatlinburg, Tennessee, May 4-7, 1970, CONF-700502, U.S. Atomic Energy Commission, 1970.
- [23] Une K., J. Nucl. Sci. Tech., 23, 1020, 1986.
- [24] Yamanouchi S. and Tachibana T., J. Nucl. Sci. Tech., 25 528, 1988.
- [25] Manes L., Matls. Chem. Phys., 15 213, 1986.

- [26] Naito K. and Oguma M., J. Nucl. Mater., 149, 341, 1987.
- [27] Tsuji T., Matsui T., Abe M., and Naito K., J. Nucl. Mater., 168, 151, 1989.
- [28] Ho S. M. and Radford K. C., Nucl. Tech., 73, 350, 1986.
- [29] Une K., J. Nucl. Mater., 158 210, 1988.
- [30] Une K., Tanabe I., and Oguma M., J. Nucl. Mater., 150, 93, 1987.
- [31] Yuda R., Une K., J. Nucl. Mater., 178, 195, 1991.
- [32] Riella H.G., Durazzo M., Hirata M., Noguera R., J. Nucl. Mater., 178, 204, 1991.
- [33] Ganguly C., Indian J. Tech., 28, 296, 1990.
- [34] Ferguson D.E., Dean O.C., and Hass P.A., CEND-153 .1, 23, 1961.
- [35] Ganguly C. and Basak U., J. Nucl. Mater., 178, 179, 1991.
- [36] Sengupta K., Majumdar S., Ganguly C., and Roy P. R., Am. Ceram. Soc. Bull., 65(7), 1057, 1987.
- [37] Gündüz G., Önal I., and Durmazuçar H.H., "Çöz-Pel Yöntemiyle Gadolonyum Oksitli Uranyum Dioksit Yakıtı Yapımı", III.Ulusal Nükleer Bilimler Kongresi, 27-29 Eylül, 1989.
- [38] Gündüz G., Önal I., and Durmazuçar H.H., J. Nucl. Mater. 178 212, 1991.
- [39] Gündüz G., "Uranium dioxide-Gadolinium Oxide Fuel Production By Sol-Gel Technique", Final Report, International Atomic Energy Agency (IAEA), Research Contract, Project nu.IAEA-5977/RB1, RB2, 1992.
- [40] IAEA, TECDOC Progress Report on "Technology and Performance of Integrated Burnable Absorbers for Water Reactor Fuel", Presented in Istanbul Meeting, Nov.1-5, 1993.

- [41] Onefrei M., J. Nucl. Mater., 137, 207, 1986.
- [42] Matthews R.B. and Hart P.E., J. Nucl. Mater., 92, 207, 1980.
- [43] Zimmer E., Ganguly C., Borchardt J., and Langen H., J. Nucl. Mater., 152, 169, 1988.
- [44] Hart R.S., Natalizio A., and "CANDU, The Advanced PWR, with Proven Performance", AECL-9963, AECL, Canada, 1989.
- [45] Drumm C.R. and Lee J.C., Nucl.Sci.Eng., 96, 17, 1987.
- [46] Simmons R.L., Jones N.D., Popa F.D., Mueller D.E., and Pritchett J.E., Nucl.Tech., 80, 343, 1988.
- [47] Pritchett J.E. and Mueller D.E., Trans. Am. Nuc. Soc., 55, 117, 1987.
- [48] Srinalta S., Schmidt R.F., and Pritchett J.E., Trans. Am. Nuc. Soc., 55, 124, 1987.
- [49] Arya S.P.S. and Damico A., Thin Solid Films, 157, 267, 1988.
- [50] Paine R.T. and Narula C.K., Chem.Rev., 90, 73, 1990.
- [51] Rand M.J. and Roberts J., J. Electrochem. Soc., 115, 423, 1968.
- [52] Murarka P., Chang C.C., Wang D.N.K., and Smith T.E., J. Electrochem. Soc., 126, 1951, 1979.
- [53] Hirayama M. and Shohn K., J. Electrochem. Soc., 122, 1671, 1975.
- [54] Steele S.R., Feist W. and Getty W., "Research On Thin Film Tunnel Cathodes, Recombination Cathodes and Similar Cold Cathodes", Final Report, (Contract DA 28-043-AMC-0035(E)), September, 1966.

- [55] Steele S.R., Pappis J., Schilling H., and Simpson J., "Chemical Vapor Deposited Materials For Electron Tubes". 1st.Triannu.Rep.,(Contract DAA 1307-68-C-0156), June 1986.
- [56] Baronian W., Mater. Res. Bull., 7, 119, 1972.
- [57] Sano M. and Aoki M., Thin Solid Films, 83, 247, 1981.
- [58] Motojima S., Tamura Y., and Sugiyama K., Thin Solid Films, 88, 269, 1982.
- [59] Takahashi T., Itoh H., and Takeuchi A., J. Cryst. Growth, 47, 245, 1979.
- [60] Takahashi T., Itoh H., and Kurdoda M., J. Cryst. Growth, 53, 418, 1981.
- [61] Gebhardt J.J., Proc. 4th.Int. Conf. On "Chemical Vapor Deposition", Boston, MA, Electrochemical Society, Princeton, NJ, 460 1973.
- [62] Clerc G. and Gerlach P., Proc. 5th.Int. on "Chemical Vapor Deposition", Slough,.Electrochemical Society, Princeton, NJ., 777, 1975.
- [63] Zunger A., Katzir A., and Halperin A., Phys. Rev. B, 13, 5560, 1976.
- [64] Powell C.F., Oxley J.H., and Blocher J.M., "Vapor Deposition", Wiley, New York, 663, 1966.
- [65] Hanigofsky J.A., More K.L., Lackey W.J., Lee W.Y., and Freeman G.B., J. Am. Ceram.Soc.74[2], 301, 1991.
- [66] Lee W.Y., Lackey W.J., Freeman G.B., Agrawal P.K., and Twait D.J., J. Am. Ceram. Soc., 74[9], 2136, 1991.
- [67] Matsuda T., Uno N., Nakae H., and Hirai T., J. Mater. Sci., 21, 649, 1986.
- [68] Pierson H.O., J.Compos.Mater., 9, 228, 1975.
- [69] Naslain R., et al., J. Am. Ceram. Soc., 74[10], 2482, 1991.

- [70] Constant G. and Feurer R., J. Less-Common Met., 82, 113, 1981.
- [71] Hyder S.B. and Yep T.O., J. Electrochem. Soc., 123, 1721, 1976.
- [72] Chayahara A., Yokohoma H., Imura T., Osaka Y., and Fujisavan M. Applied Surface Science, 33/34, 561, 1988.
- [73] Miyomoto H., Hirose M., and Osaka Y., Jpn. J. Appl. Phys., 22, L216, 1983.
- [74] Yuzuriha T.H., Mlynko W.E., and Hess D.W., J. Vac. Sci. Tech., A.3 2135, 1985.
- [75] Yuzuriha T.H. and Hess D.W., Thin Solid Films, 140, 199, 1986.
- [76] Gafri O., Grill A., Itzhak D., Inspektor A., and Avni R., Thin Solid Films, 72, 523, 1980.
- [77] Komatsu S., Moriyoshi Y., Kasamatsu M., Yamada K., J. Appl. Phys., 70(11), 7078-7084, 1991.
- [78] Alexander J.H., Joycte R.J., Sterling H.F., "Extended Abstracts", Can. Meet. of The Electrochemical Society, Montreal, Electrochem. Society, Princeton, NJ, Abstract 462 (October, 1968).
- [79] Schmolla W. and Hartnagel H.L., J. Phys. D, 15, 195, 1985
- [80] Schmolla W. and Hartnagel H. L., J. Electrochem. Soc., 129, 2637, 1982.
- [81] Adams A.C. and Capio C.D., J. Electrochem. Soc., 127, 399, 1980.
- [82] Adams A.C., J. Electrochem. Soc., 128, 1379, 1981.
- [83] Dana S.S. and Maldonado J.R., J. Vac. Sci. Technol, B,4, 235, 1986.
- [84] Nakamura K., J. Electrochem. Soc., 132, 1757, 1985.

- [85] Gashtold V.N., Kutol'n S.A., Bielova L.F., and Komarova G.M., Eletron. Tekh., 12, 58, 1970.
- [86] Noreika A.J. and Francombe M. H., J. Vac. Sci. Technol., 6, 722, 1969.
- [87] Wiggins M.D., Aita C.R. and Hickernell F.S., J. Vac. Sci. Technol., 2, 322, 1984.
- [88] Davidse P.D. and Maissel L.I., J. Appl. Phys., 37, 574, 1966.
- [89] Weissmantel C., Bewilogua K., Dietrich D., Erler H.J., Hinnerberg H.J., Klose S., Nowich W., and Reisse G., Thin Solid Films, 72, 19, 1980.
- [90] Weissmantel C., Bewilogua K., Breuer K., Dietrich D., Ebersbach U., Erler H.J., Rau B., Reisse G., Thin solid Films, 96, 31, 1982.
- [91] Rother B., Zscheile, Weissmantel C., Heiser C., Holzhtuter G., Leonhardt G., and Reich P., Thin Solid Films, 142, 83, 1986.
- [92] Weissmantel C., Vac. Sci. Technol., A.1, 179, 1981.
- [93] Miyoshi K., Buckley D.H. and Spalvins T., Vac. Sci. Technol, A.3, 2141, 1985.
- [94] Halverson W. and Quinto D.T., J. Vac. Sci. Technol., A.3, 2141, 1985.
- [95] Sokolowski M., J. Cryst. Growth, 46, 136, 1979.
- [96] Sokolowski M., Sokolowski A., Rusek A., Romanowski Z., and Gajewska M., J. Cryst. Growth, 52, 165, 1981.
- [97] Sokolowski M., Sokolowski A., Michalski A., Romanowski Ż., Rusek A., and Wronikowski M., Thin Solid Films, 80, 249, 1981.
- [98] Chopra K. L., Agarwal V., Vankar V.D., Deshpandej C.V., Bunshah F., Thin Solid Films, 126, 307, 1985.



- [99] Hamilton E. J. M., Dolan S.E., Mann C.M., Colijn H.O., McDonald C.A., Shore S.G., Science, 260, 659, 1993.
- [100] Lin P., Deshpande C., Doerr H.J., Bunshah R.F., Chopra K.L., and Vankar V.D., Thin Solid Film, 153, 487, 1987.
- [101] Schmolla W. and Hartnagel H. L., Solid State Electronics, 26, 10, 931, 1983.
- [102] Paciorek K. J. L., et al., Inorg. Chem, 27, 2432, 1988.
- [103] Maya L. and Richards H. L., J. Am. Ceram.Soc., 74, 406, 1991
- [104] Nakamura, K.J. Electrochem. Soc., 132, 1757, 1985.
- [105] Gafri O., Grill A., Itzhak D., Inspektor A., and Avni R., Thin Solid Films, 72, 523, 1980.
- [106] Ringel H.D. and E. Zimmer, Nucl. Tech., 45, 287, 1979.
- [107] McBride J.P., "Preparation of UO<sub>2</sub> Microspheres by a Sol-Gel Technique, Oak Ridge National Laboratories", ORNL 3874, 1966.
- [108] Banister M.J. and Buykx W.J., J. Nucl. Mat., 64, 57, 1977.
- [109] Das P. and Chowdhury R., J.Nucl.Mat., 158, 261, 1988.
- [110] Lamarsh J.R., "Introduction to Nuclear Engineering", Addison-Wiley Publishing Comp., 1983.
- [111] Duderstad J .J. and Hamilton L. J., "Nuclear Reactor Analysis", John Wiley & Sons, New York, 1976.
- [112] Walker F. W., Miller D. G., and Feiner F., "Chart of Nuclides", General Electric Company, 1984.
- [113] Meghreblian R.V., "Reactor Analysis", McGraw.Hill Book Comp., 1960.

- [114] Power W.L. and Tullis T.E., J. Geophys. Res. **96**, 415, 1991.
- [115] Freisen W.I., Laidlow W.G., J. Coll. Inter. Sci., **160**, 226, 1993.
- [116] Kolb M., J. Non.Cryst.Solids, **121**, 227, 1990.
- [117] Costa J.M., Sagues F. and Vilarrasa M., Corr. Sci., **32**, 665, 1991.
- [118] Korcak J., Bull.Inst.Int. Stat., **3**, 294, 1938.
- [119] Gelleri B. and Sernetz M., Analytica Chimica Acta, **163**, 17, 1984.
- [120] Friedlander G. and Kennedy J.W., "Nuclear and Radiochemistry", John Wiley and Sons, Inc., 1956.
- [121] Mandelbrot, B.B., "The Fractal Geometry of Nature Freeman, San Francisco, 1982.
- [122] Moskovits M., Cem. Conc. Res. **20**, 449, 1990.
- [123] Avnir D., Farin D., and Pfeifer P., J. Coll. Inter. Sci., **103**, 112, 1985.
- [124] Friesen W.I. and Mikula R.J., J. Coll. Inter. Sci., **120**, 263, 1987.
- [125] Roth M.J., Macgoudal J.D., and Kemshell P.B., "The Preparation of input data for WIMS, General Reactor Division, AEE, Winfrith, Dorchester, 1967.
- [125] "Nuclear Fuel", NPP Akkuyu for the Turkish Electricity Authority (TEK), Kraftwerk Union, KWU, 1983.
- [125] Belle J., "Uranium Dioxide :Properties and Nuclear Application, Naval Reactors", Division of Reactor Development, U.S. Atomic Energy Commission, 1961.
- [126] Tempest P.A., Tucker P.M., and Tyler J.M., J. Nucl. Mater., **251**, 1988.

- [127] Fukushima S., Ohmichi T., Maeda A., and Watanabe H., J. Nucl. Mater., 105, 201, 1982.
- [128] M.Hirai and Ishimoto S., J. Nucl. Sci. Tech., 28, 995, 1991.
- [130] C.Miyake, Kanamaru M., and Imoto S., J. Nucl. Mater., 137, 256, 1986.
- [131] Une K. and Oguma M., J. Nucl. Mater., 131, 88, 1985.
- [132] Massih A.R., Persson S., and Weiss Z., J. Nucl. Mater., 188, 323, 1992.
- [133] Hirai M. and J. Nucl. Mater., 173, 247, 1990.
- [134] Ho S.M. and Radford K.C., Nucl. Tech., 73, 350, 1986.
- [135] Gündüz G., Uslu İ., Önal I., Durmazuçar H.H., Öztürk T., Akşit A.A, Kopuz B., Özeş F., Can Ş., and Uzmen R., Nucl. Tech., (to be published in July 1995).
- [136] Wada T., Noro K., and Tsukui K., "Behaviour of UO<sub>2</sub>-Gd<sub>2</sub>O<sub>3</sub> Fuel", Proc.Int.Conf., BNES "Nuclear Fuel Performance", London, UK, p.63.115-19 Oct. 1973.
- [137] Sampath S., Chadha A., and Chakraborty D.M., "O/M variations in uranium oxides by X-Ray Diffractometry", Bhabha Atomic Research Centre, B.A.R.C.-1140 1981.
- [138] Manzel R. and Dörr W.O., Ceram.Bull., 59, 601, 1980.
- [139] Kogai T., Twasaki R., and Hirai M., J. Nucl. Sci. Tech., 26, 744, 1989.
- [140] Littlechild J.E., Butler G.G., and Lester G.W., Proc.Int.Conf.Nuclear Fuel Performance, BNES, London, paper 65, 1973.
- [141] Une K. and Kashibe S., J. Nucl. Mat., 189, 210, 1992.

- [142] Uslu İ. and Gündüz G., “Nükleer Yakıtlarda Fractal Boyut”, Dinamik Sistemler Sempozyumu, ODTÜ Uludağ Tesisleri, Bursa, 16-17 December 1994.
- [143] Lin P., Deshpandey C., Doerr H.J., Bunshah R.F., Chopra K.L., and Vankar V., Thin Solid Films, 153, 487, 1987.
- [144] Chopra K.L., Agarval V., Vankar V.D., Desphadey C., and Bushah R.F., Thin Solid Films, 126, 307, 1985.
- [145] Montasser K., Tamano J., Hattori S., and Morita S., Plasma Chemistry and Plasma Processing, 4, 251, 1984.
- [146] Komatsu S., Moriyoshi Y., Kasamatsu M., and Yamada K., J. Appl. Phys. 70, 7078, 1991.
- [147] Saitoh H. and Yarbrough W.A., Appl. Phys. Lett. 58, 2482, 1991.
- [148] Godet C., Schmirgeld L., Zuppiroli L., Sardin G., Gujrathi S., and Oxorn K., J. Mater. Sci., 26, 6408, 1991.
- [149] Bath A., van der Put P.J., Becht J.G.M., Schooaman J., and Lepley B., Am. Inst. Phys., 70, 4366, 1991.
- [150] Maya L. and Richards H.L., J. Am. Ceram. Soc., 74, 406, 1991.
- [151] Kessler G., Bauer H.D., Pompe W., and Scheibe J., Thin Solid Films, 147, L45, 1987.
- [152] Andrews L., Hassanzadeh P., Burholder T.R., and Martin J.M.L., J. Chem. Phys., 98, 922, 1993.
- [153] Paine R.T. and Narula C.K., Chem. Rev., 90, 73, 1990.
- [155] Matsuda T., Uno N., Nakae H., and Hirai T., J. Mater. Sci., 21, 649, 1986.

[156] Thomas J., Weston N.E., and O'Conner T.E., J.Am. Chem. Soc., 84, 4619, 1963.

[157] Jeronice M., Gilpin R.K., and Choma J. Carbon, 31, 325, 1993.



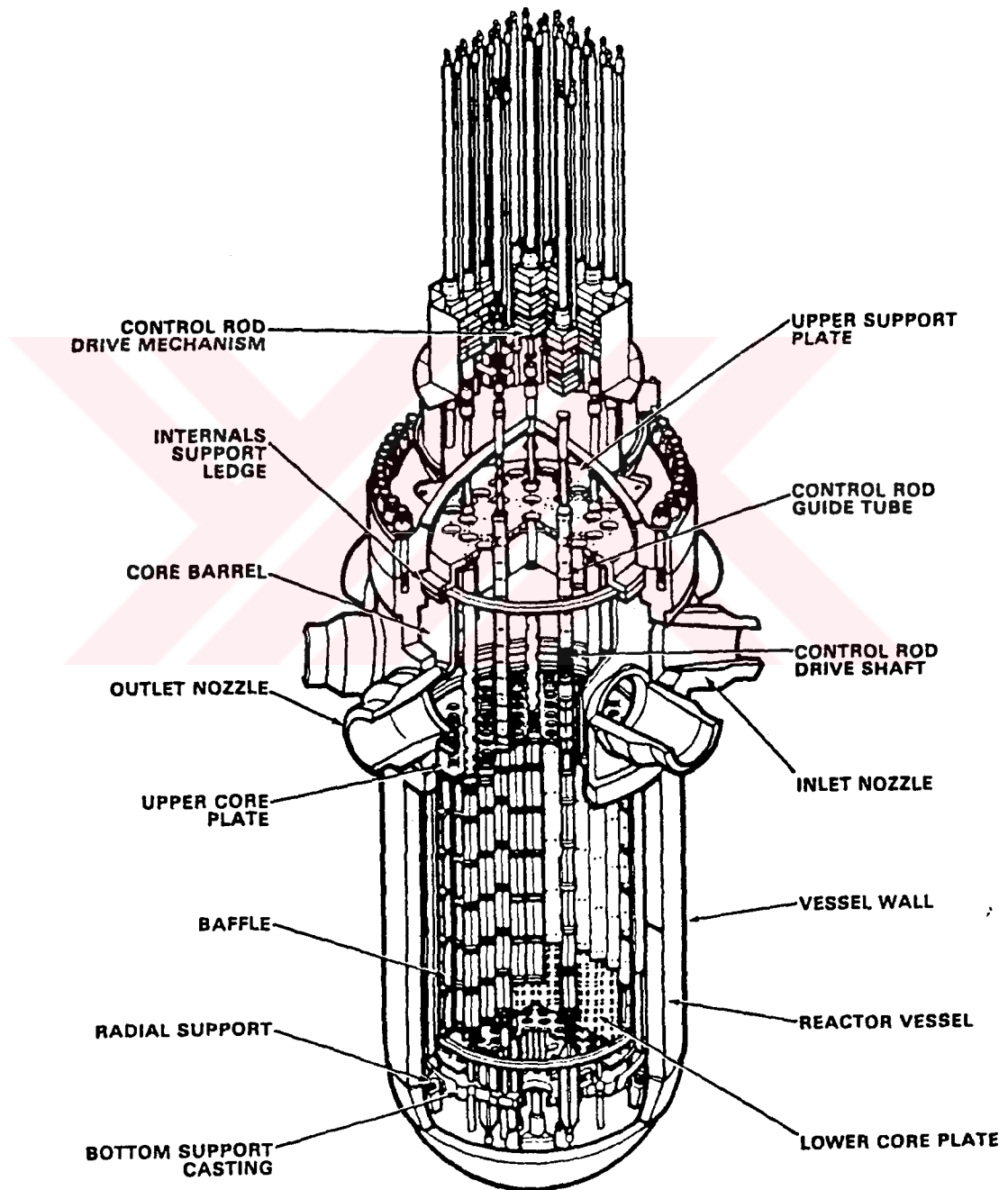
## APPENDIX A

### ELECTRICAL ENERGY DEMAND OF TURKEY[9]

Years	Peak power (MW)	Power Increase (%)	Energy (GWh)	Energy Increase (%)
1995	14065	8.9	87205	9.2
1996	15235	8.3	94605	8.5
1997	16505	8.3	102500	8.3
1998	17880	8.3	111050	8.3
1999	19375	8.4	120310	8.3
2000	20990	8.3	130350	8.3
2001	22610	7.7	140850	8.0
2002	24360	7.7	151720	7.7
2003	26240	7.7	163430	7.7
2004	28260	7.7	176040	7.7
2005	30445	7.7	189630	7.7
2006	32710	7.4	203680	7.4
2007	35145	7.4	218835	7.4
2008	37760	7.4	235130	7.4
2009	40570	7.4	252615	7.4
2010	43590	7.4	271450	7.4

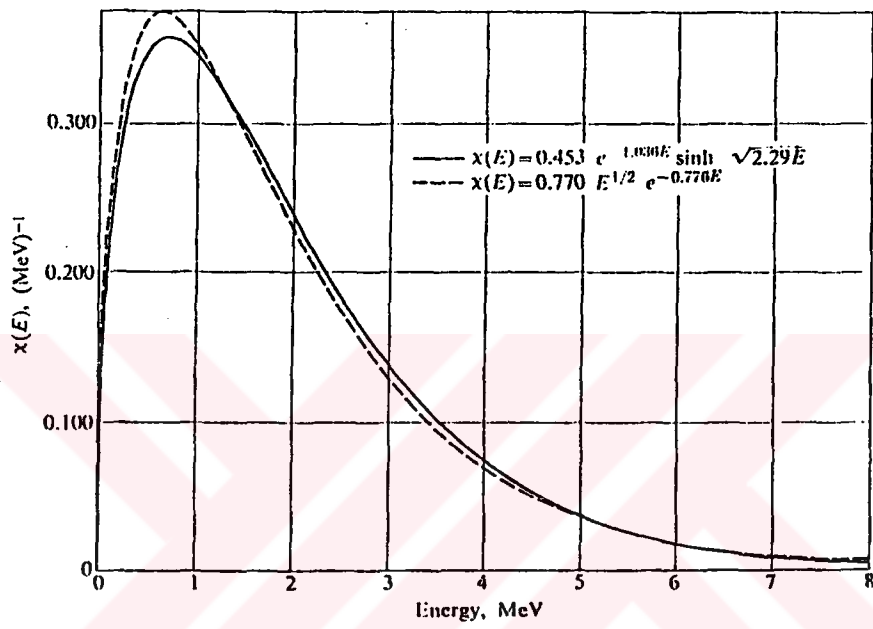
## APPENDIX B

### SCHEMATIC OF PWR REACTOR VESSEL INTERNAL STRUCTURE



## APPENDIX C

### THE NEUTRON SPECTRUM





## **VITA**

Date of Birth: December 4, 1955.

Place of Birth: Bodrum, Mugla, Turkey.

Citizenship: Turkish.

Current position: Chemical Engineer.

### **Education**

B.S., Middle East Technical University, (METU) 1980,

M.S., Middle East Technical University, (METU) 1983.

### **Honors and Awards**

Nazilli Teacher Training High School, Honor student.

Middle East Technical University, Honor Student as

3rd year student (1979) and 4th year student (1980).

### **Experience**

Student Assistant in Chemical Engineering Department, Middle East Technical University (METU), 1980-1982.

Research Assistant in Chemical Engineering Department, Middle East Technical University (METU), 1982-1985.

Associate Editor of the Journal of Thermal Sciences and Technology, January 1984 to January 1985.

International Atomic Energy Agency Training Course on Safety Review and Assessment for Construction permit, Turkish atomic Energy Authority, Ankara, Turkey, September 9 to October 4, 1985.

Training Course on Waste Management given by Sinai Eğitim ve Geliştirme Merkezi (SEGEM) (Industrial Education and Development Center), Ministry of Industry and Trade of Turkish Republic, Ankara, 5 to 9 May, 1986.

Visiting scientist, Oak Ridge National Laboratory (ORNL), Fellowship by International Atomic Energy Agency (IAEA), Oak Ridge, Tennessee, 2 May 1987 to 2 May 1988.

Consultant, (Waste Management) Martin Marietta Energy Systems, Inc., Oak Ridge National Laboratory, Health and Safety Research Department, (Subcontract No. 95X-SC275V), Oak Ridge, Tennessee 37831, 1988.

Associate Director, International Energy Agency (IAEA) Project TUR/9/007, Radioactive Waste Disposal in Turkey, Implementation of a Low-Level Waste Management System, Supported by IAEA, 1985-1989.

30-hour training program, conducted by the East Tennessee Chapter of the Health Physics Society to assist chapter members in preparing for the National Registry of Radiation Protection Technologist Examination, December, 1987.

Private student, Gazi University, Completed satisfactorily the lectures named as "Advanced Process Control" and "Distillation of Multicomponent Mixtures", in 1991 Spring Semester.

Chief Scientific Investigator, IAEA Project "The safety Assessment of Near Surface Radioactive Waste Disposal Facilities (NSARS)", (IAEA-6546/CF) 1991-1995.

Lecturer, Course on "Safety Evaluation and Licensing of Nuclear Installations", organized by Turkish Atomic Energy Authority, Beşevler, Ankara, 14-25.9.1992,.

Scientific Investigator, IAEA project "Production, Characterization and Performance of Boron Nitride Coated Uranium and Gadolinium Oxide Fuel" (IAEA-5977/R2/RB), 1994.

One Month Training Program, Interregional Training Course on "Safety Assessment Methodologies for Near Surface Radioactive Waste Disposal Facilities" , organized by IAEA, Argonne National Laboratory (ANL), Argonne, Illinois, USA, 14 February - 4 March 1994.

Scientific Investigator, IAEA project "Technology and Performance of Integrated Burnable Neutron Absorbers for Reactor Fuel" (IAEA-5977/R3/RB), 1995.

Lecturer, "Radiation", organized by Turkish Atomic Energy Authority, High Schools of Bodrum, Yatağan, Muğla, Marmaris, Fethiye, 14-18 October 1994.

## Publications

I. Uslu, P. Özler, and B. Kısakürek, "Dynamic Analysis of a Distillation Column", Published in the Proceedings of the International Federation of Automatic Control, Workshop on Computer Aided Design of Projects and Development Policies, Middle East Technical University (METU), pp. 147, June 22-24, 1982.

I. Uslu, "Transient Response of a Distillation Column", Master of Science Thesis, Middle East Technical University (METU), 1983.

I. Uslu, B. Kısakürek, and A. Sümer, "Geçici-Durum Şartlarını Minimal Duruma Getiren Bir Dinamik Destilasyon Kolon Modeli", 1st National Computer Aided Design Symposium", Ege University, Published in the Proceedings, pp. 335, April 25-27, 1984.

I. Uslu, "Biogas is Applicable for Turkey", Journal of Thermal Sciences and Technology, v. 7.1, pp. 45, May 1984.

I. Uslu, Heat Transfer Studies in 1982 (review paper), Journal of thermal Sciences and Technology, v. 7.1 pp. 42, May 1984.

A. Sümer, B. Kısakürek, and I. Uslu, "Dolgulu Destilasyon Kolonlarının Bilgisayar Yardımı ile Tasarımı", Published in the Proceedings of the 1st National Computer Aided Design Symposium, Ege University, pp. 346, April 25-27, 1984.

I. Uslu and G. Gündüz, "Nuclear Waste Vitrification Using Colemanite", Waste Management Research Abstracts No.16, International Atomic Energy Agency (IAEA), Vienna, IAEA/WMRA/16, pp.326, 1985.

F. Gözbebek, A. Kahraman, and I. Uslu, Radyoaktif Artıkların Yönetiminde Son Gelişmeler, Published in the Proceedings of the International Symposium on Environmental Management, Environment'87, Istanbul, pp. 265, June 1987.

I. Uslu, D. E. Fields, and M. G. Yalçintas, "Low-Level Waste Studies in Turkey", 32nd Annual Meeting of the Health Physics Society, Salt Lake City, Utah, July 5-9, 1987.

D. E. Fields, I. Uslu, and M. G. Yalçintas, "Evaluation of Proposed Shallow-Land Burial Sites Using the PRESTO-II Methodology and Code", Published in the Proceedings of the Oak Ridge Model Conference, volume I, Waste Management, Part 3, pp. 305-311, Oak Ridge, Tennessee, October 14-16, 1987.

I. Uslu, D. E. Fields, and M. G. Yalçintas, "Studies Involving Proposed Waste Disposal Facilities in Turkey", Published in the Proceedings of 1987 Winter Meeting of the American Nuclear Society (ANS), Los Angeles, California,

- TANSAD 55 1-760, pp. 114-115, CONF-871101-31, November 15-19, 1987, (Radioactive Waste Management, DOE/RWM-88/1, pp. 13, January 1988).
- I. Uslu, D. E. Fields, and M. G. Yalçintas, "Comparison of the PRESTO-II and DRASTIC Methodologies for LLW Site Selection", Annual Meeting of the Tennessee Academy of Science, November 20, 1987.
- I. Uslu, D. E. Fields, and M. G. Yalçintas, "Prediction of Radiation Effects from Proposed Low-Level Waste Disposal Sites in Turkey", Annual Meeting of the Tennessee Academy of Science, November 20, 1987.
- M. G. Yalçintas, I. Uslu, and D. E. Fields, "Correlation Between Soil Sample Concentration and Gamma Reading for Th-232 in FUSRAP Sites in New Jersey", Annual Meeting of the Tennessee Academy of Science (TAS), November 20, 1987.
- I. Uslu, D. E. Fields and M. G. Yalçintas, "PRESTO-II Computer Code for Safety Assessment on Shallow Land Disposal of Low-Level Wastes", Published in the Proceedings Waste Management '88, the 14th Annual WM Symposium, Tucson, Arizona, CONF-880201-2, February 28-March 3, 1988. (Radioactive Waste Management, DOE/RWM-88/3, pp. 25, March 1988)
- D. E. Fields and I. Uslu, "Selected Approaches to Pathway Analysis", International Workshop on Radiological Protection in Mining, Darwin, Australia, April 4-8, 1988.
- D. E. Fields and I. Uslu, "Application of Pathway Analysis", Invited presentation to Roana State Community College, May 5, 1988.
- D. E. Fields, I. Uslu, and M. G. Yalçintas, "Evaluation of Human Doses and Health Effects from Shallow-Land Disposal of Radioactive Wastes", invited presentation to the Pittsburgh Energy Technology Center's Seminar Series on Fossil Energy, September 17, 1987.
- Ö. Özerden, İ. Uslu, and M. Saygın, "Radyasyon Erken Uyar Sistemi ile İlgili Özet Bilgiler", Report, Turkish Atomic Energy Authority, August 19, 1988.
- M. G. Yalçintaş, M. S. Uziel, J. A. Roberts, and I. Uslu, "Radiation Exposures from a Cesium-Contaminated Field", Oak Ridge National Laboratory Report, Oak Ridge, Tennessee 37831, ORNL/RAP,-46, September, 1988.
- I. Uslu, "Sarayköydeki Arazimizde Çaydaki Radyonüklidlerin Yeraltı Sularıyla Taşınması Hakkındaki Rapor", Report, Turkish Atomic Energy Authority (TAEA), October 10, 1988.
- I. Uslu, "Management of Low-Level and Intermediate Level Radioactive Wastes", Invited presentation to the Middle East Technical University (METU), October 11, 1988.

I. Uslu, M. G. Yalçintas, and D. E. Fields, TRANFOOD; "Radionuclide Transport via Terrestrial Foodchain", Oak Ridge National Laboratory (ORNL) Report, (RSIC Newsletter, ORNL, No.290, pp. 7, January 1989) Oak Ridge, Tennessee 37831, ORNL/TM-10782, October 1988.

I.Uslu, D. E. Fields and M. G. Yalçintaş, "Studies on Disposal of Low-Level Radioactive Wastes in Turkey", Oak Ridge National Laboratory (ORNL) Report, Oak Ridge, Tennessee 37831, ORNL/TM-10700, August 1989.

I. Uslu, G. Aksüt, and G. G. Yülek, "Radiological Considerations of the Nuclear Ship Visits", Turkish Journal of Nuclear Sciences, Turkish Atomic Energy Authority, V. 16, no.1-2, p.43, December 1989.

I. Uslu, N. Özlođlu, F. Gözbebek, G. Buyan, and G. Aksüt, "1986 ürünü kontamine Çayların Yakılması veya Gömülmesi ile ilgili Teknik Rapor", Turkish Atomic Energy Authority, 24 October 1989.

I. Uslu, Safety Analysis Report of the Low Level Waste Treatment Facility at the Cekmece Nuclear Research and Treatment Facility, 1989.

Muammer Saygın, I. Uslu, G. Aksüt, "Radyasyon Erken Uyarı Sistemi 1989 Yılı Verilerini İçeren Teknik Rapor", Turkish Atomic Energy Authority, 4 December 1989.

I. Uslu and D. E. Fields, "Selection of Low-Level Radioactive Waste Disposal Sites Using Screening Models vs. More Complex Methodologies", Journal of Tennessee Acedemy of Science 68(4) p. 106-108, October 1993.

G. Gündüz, İ. Uslu, C. Töre, and E. Tanker, "Boron Nitride Coated  $UO_2-Gd_2O_3$  Fuel", Technical Committee Meeting on Water Reactor Fuel Element Modelling at High Burnup, Windermore, England, 18-23 September 1994.

İ. Uslu and G. Gündüz, "Nükleer Yakıt Üzerine Bor Nitrür Kaplanması" Birinci Ulusal Kimya Mühendisliği Kongresi, ODTÜ, ANKARA, 13-16 Eylül 1994.

İ. Uslu and G. Gündüz, "Nükleer Yakıtlarda Fractal Boyut", Dinamik Sistemler Sempozyumu, ODTÜ Uludağ Tesisleri, Bursa, 16-17 Aralık 1994.

G. Gündüz, İ. Uslu, et al. "Effects of Different Parameters on the Densities of  $UO_2$  and  $UO_2-Gd_2O_3$  Fuel Produced by Sol-Gel Technique", Nuclear Technology, (will be published on July 1995).